ABSTRACT

Title of Dissertation:	STRUCTURAL PERFORMANCE ASSESSMENT ON PREVENTIVE MAINTENANCE/REHABILITATION OF STEEL GIRDER BRIDGE SYSTEMS
	Yifan Zhu, Doctor of Philosophy, 2022
Dissertation directed by:	Research Professor, Chung C. Fu, Department of Civil and Environmental Engineering, University of Maryland

Bridge maintenance, including preventive maintenance, rehabilitation, and replacement keeps the structure safe in its service life. Bridge maintenance methods have developed and expanded to bridge inspection, bridge condition assessments, structural health monitoring technologies, service life prediction, and maintenance with new materials or technologies. This dissertation proposes two structural performance assessments, (1) a rapid machine learning assessment classifying whether the design is under an acceptable range; and (2) comparing the structural health monitoring data with engineers' predictions to evaluate the current structural performance. The first part of this dissertation focuses on preventive maintenance evaluation. This part discusses and plans a specific topic to instrument a newly constructed link slab system on a multiple simply-supported bridge. Before any simulation and field test of the general steel I-girder bridge model was conducted, literature regarding bridge maintenance, performance assessment, the durability of bridges, structural health monitoring method, current condition

assessment methods, and research on the material and structural behavior of link slabs were reviewed and investigated. Then comprehensive experimental programs on the new materials HPFRC and ECC were conducted, and the extensive hands-on laboratory results update the nonlinearity and accuracy of the structure model. Moreover, a series of data analyses of the current steel bridge in the United States was conducted for further database establishment. Two sets of simulation-based finite element parametric analyses of the bridge with protective maintenance or structural repairing were introduced to generate preferred designs and further be used for rapid performance assessment. The inputs are the configuration of the bridge and the proposed work or deteriorated location, which generate the dataset for the training, validating, and testing of the evaluation model. The resulting regression model allows for quick assessment of the function developed by taking advantage of machine learning. This research verifies the assessment's results using the Maryland Transportation Authority (MDTA) pilot HPFRC link slab system on the bridge overpass I-95 as a case study by comparing the prediction and actual structure health monitoring data after the assessment's results were verified, and its performance was evaluated.

This dissertation also examines one case from the Maryland State Highway Administration (MDSHA) bridge over the Patapsco River, which has several frozen expansion rocker bearings. This restrained the longitudinal movement of the superstructures due to thermal expansion and contraction. It has partially recovered to its normal condition after repairing and strengthening the pier under this bearing. In this study, we combined the finite element analysis and monitoring data to simulate structural behavior, and evaluate repair work using the proposed methods.

Finally, This research evaluates the repaired bridge with partially strengthened structural components (i.e., deck, girders, or piers) and forecasts its wear and tear. In this study, the original and deteriorated bridges were numerically modeled first and simplified to 3D grid models. Then, the current condition rating process was used to determine the structural performance at the element level. After establishing the evaluation criteria and investigating the corresponding condition ratings, the rapid assessment models for the repaired bridges were carried out. The condition prediction relied on historical ratings and (if any) monitoring data.

STRUCTURAL PERFORMANCE ASSESSMENT ON PREVENTIVE MAINTENANCE/REHABILITATION OF STEEL GIRDER BRIDGE SYSTEMS

by

Yifan Zhu

Dissertation submitted to the Faculty of the Graduate School of the
University of Maryland, College Park, in partial fulfillment
of the requirements for the degree of
Doctor of Philosophy
2022

Advisory Committee:
Professor Chung C. Fu, Chair
Professor Sung W. Lee, Dean's representative
Professor Amde M. Amde
Professor Mohamed Sherif Aggour
Professor Yunfeng Zhang

Dedication

To my family.

Acknowledgements

I would like to express my sincere gratitude to Dr. Chung C. Fu, who had been continuously supporting, advising, and guiding me through the development of this dissertation. His endless encouragement and inspiration made me continue this research work and present this dissertation. He also provides invaluable advice on this topic and any research topics during my Ph.D. This work would not have been possible without his support.

Further, I would like to express my deepest gratitude to my parents, Prof. Yanpeng Zhu and Prof. Xiuli Wang, who gave all their love, patience, guidance, understanding, and unconditional support to me and encourage me all through these years. I love you more than I expressed here.

I also thank my committee members, Dr. Yunfeng Zhang, Dr. Amde M. Made, Dr. Mohamed Sherif Aggour, and Dr. Sung W. Lee. Your knowledgeable, thoughtful, and detailed feedback throughout this dissertation helped me to expand and explore more possibilities and fulfill this research work. It is an honor to learn from all these professors.

Many thanks to all the members of the department of Civil and Environmental Engineering for their kind support during my Ph.D. study. Especially, I am deeply indebted to my group members: Yunchao Ye, Kuang-yuan Hou, Xinya Liu, Chaoran Xu, and Naiyi Li, for their immense support and help during my Ph.D. You are always ready for any discussion and help without hesitation when I need you. I am fortunate to be a part of the Bridge Engineering Software & Technology (BEST) Center.

I also acknowledge the generous support from the University of Maryland, the Maryland Transportation Authority (MDTA), and the Maryland State Highway Administration (MDSHA). I also had the pleasure of conducting lab experiments in the lab of the National Ready-Mix Concrete Association (NRMCA) and the Federal Highway Administration (FHWA). And I enjoyed working with our consultants and experts for bridge design, modification, rehabilitation, and structural health monitoring system development. I am grateful to everyone I've collaborated with. A special thanks to the team from Rensys LLC, for their technical support in sensor adjustments and validation.

Last but not least, I greatly appreciate my family and friends. Thank you so much for your tremendous support and continuous encouragement. Yun, Kevin, Xiwei, Gengwen, Hua, Linjia, Shuaiyi, Franklin, and Zhou, thank you so much for being supportive throughout my time here and helping me in many aspects.

Table of Contents

List of Tables

List of Figures

List of Abbreviations

AASHTO: The American Association of State Highway and Transportation Officials

ADE: agency developed elements

ANNS: Artificial Neural Networks

BME: Bridge Maintenance Element

CDF: cumulative distribution function

DT: Decision tree

ECC: Engineered Cementitious Composite

FL: Fuzzy Logic

FNR: false-negative rate

FRP: Fiberglass-Reinforced Plastic

GCR: General Condition Ratings

HPFRC: High-Performance Fiber Reinforced Concrete

HRWR: High Range Water Reducer

iCDF: inverse cumulative distribution function

KNN: k-nearest neighbors algorithm

LHS: Latin Hypercube Sampling

LSTM: Long-short term Memory method

NBE: National Bridge Element

NBI: National Bridge Inventory

PDF: probability density function

RC: Regular Concrete

RMSE: root means squared error

RNN: Recurrent Neural Network

SVM: Support vector machines (SVMs)

TFHRC: Tuner-Fairbank Highway Research Center

TPR: true positive rate

UHPC: Ultra-High-Performance Concrete

VTRC: Virginia Transportation Research Council

Chapter 1: Introduction

1.1 Background and motivation

According to the data from the National Bridge Inventory (NBI, 2021), about 619,622 bridges in the US are under their service life. Federal, states, local agencies, and other owners are all facing challenges with the increasing needs of their aging structures and limited funds (Federal Highway Administration, 2018). Thus, these agencies have developed bridge asset management and maintenance programs to preserve the mobility of the infrastructures cost-effectively while extending their service life. Typically, agencies prioritize repairing or replacing the structure under the "worst-first" strategy. This scenario caused the maintenance needs of bridges defined as "good" or "fair" to be ignored with only periodic inspections. However, the total maintenance cost is much higher if bridges are only repaired or replaced when they have severe damage. Hence, a more efficient bridge management system requires balancing bridge rehabilitation/ replacement and protective maintenance.

This research started from data collected from the National Bridge Inventory (NBI) official database. Then data cleaning and data processing were conducted to filter the individual bridge data with invalid information. After the initial dataset is generated, This research calculates the statistical distribution for each attribute. In order to conduct the performance assessment, this research proposes a method based on the selected bridge configurations and parametric studies' results using finite element analysis with refined materials and structural models. Coupled with the cost-benefit analysis in the assessment system, the preferred design sets could also be found by an input feature in the database. After the data processing, labeling, and classifying, machine learning techniques have been used to train the assessment models and find the best model for the system. When this is applied to any individual project, the rapid assessment for the bridge repair recommendation would be given by the assessment system. Furthermore, if the structure is equipped with a structural health monitoring system, the behavior forecasting model using a deep learning LSTM network can be applied to forecast the behavior of the monitoring location in a short period by using the monitoring data. Combined with engineering judgment, the structural performance would be evaluated. The alert can be generated if the prediction is far from the actual data or an engineer's estimation.

This research firstly investigated the performance of the steel I girder bridge before and after bridge preventive/ protective maintenance. In particular, three items might contribute to the change of structural performance within the large index items of bridge preventive maintenance: joint elimination, bearing replacement, and adding an additional overlay. Although joint elimination and adding overlays are not considered changing or adding additional structural function to existing bridges in traditional structural analysis, they are critical to reach the target for both extending the structure's service life and reducing the long-term maintenance cost.

An example of this research is to investigate the design, construction, and performance after the instrument of link slabs, which is a combination of joint eliminations with bearing modifications. Previous studies showed that it did not meet the original design idea to reduce maintenance costs and extend the service life of the structure. Still, it triggered the additional question that the structure needs to be repaired.

Therefore, optimal link slab design was also investigated in this research for further use in performance assessment.

To investigate the optimal design of the newly constructed link slab on the steel I girder bridge, the lab test was conducted for material testing and sensor validation, then a modified stress-strain relationship of the high-performance cementitious composite was carried out for further model establishment. Then a series of parametric studies about the behavior of the bridge with newly constructed link slabs is performed and recorded. Coupled with the cost estimation of link slab systems, the preferred design of the link slab system under a typical multi-span simply supported bridge is defined and labeled. And the performance of each design is evaluated in the trained model.

The first case study for this approach is to test the design of the Maryland Transportation Authority (MDTA) pilot HPFRC (UHPC and ECC) link slab system. The refined finite element model was cross-validated with the actual structural health monitoring data from the diagnostic load test. Then a method is proposed to evaluate the structure's current condition by comparing the structural health monitoring data with the predictions.

Furthermore, after the methodology has been proven to be successfully applied and the model shows its effectiveness, the rapid assessment system has been expanded to steel bridges in the database, which might need to be repaired. The process of database establishment is similar to the previous one, while the evaluation of bridge-repaired recommendations was generated from a trained fuzzy logic system. Then the database was expanded with a more random dataset to build a more extensive database with noise to avoid overfitting. Then a more detailed recommendation was introduced into the system, and the updated machine learning model remained effective in the performance assessment.

The second case study is the performance analysis and forecasting of the Maryland State Highway Administration (MDSHA) bridge over the Patapsco River. This dual bridge system has been equipped with a structural health monitoring system for an extended period. During the monitoring period, the bridge had undergone several series of bridge inspections, protective maintenance, and rehabilitation. In particular, the bridge had installed a 'strong back support system' on the pier, encountered the bridge rocker bearing partially or fully freezing, steel stringer section loss, and deck replacement, and proposed to install the link slab system to eliminate expansion joints. This dual bridge system has covered major bridge preventive maintenance and rehabilitation works and was selected as an example for the time series data forecasting and evaluation.

1.2 Overview

This research focused on the bridge structural performance assessment after the bridge preventive maintenance work of typical I girder steel bridges and the general assessment of steel bridges after rehabilitation. A structural performance assessment method has been proposed in two scenarios, (1) the rapid assessment to classify if the design is under an acceptable range using machine learning methods; and (2) Comparing the structural health monitoring data with the predictions to evaluate the current condition of the structure.

To reach the goal that truly reflects the condition assessment after preventive maintenance or rehabilitation of steel bridges, the proposed assessment system integrates into the decision-making model that combined with database establishment, database expansion, evaluates the effectiveness of repair work, rapidly assesses the repaired structure, and forecasts bridge behavior using structural health monitoring data. A flowchart (Figure 1-1) shows the general assessment process of this research.

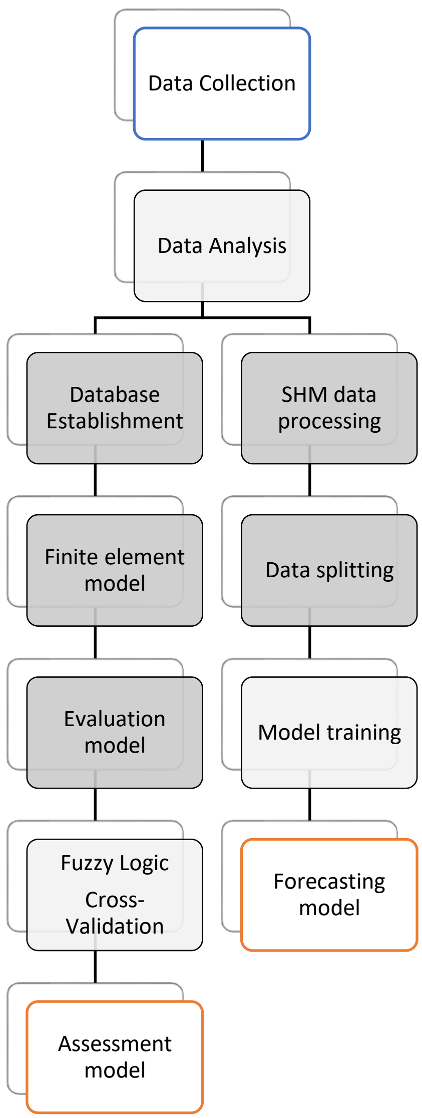

Figure 1-1 Flowchart of the performance assessment methods proposed in this research.

Establishing the assessment and prediction models requires a large batch of data. Thus, this research starts with data collection and analysis of all steel bridges in the United States. After collecting data from the National Bridge Inventory (NBI) database, a series of data categorizing, processing, and analysis has been done to build the initial evaluation database. Then two parametric studies using the Finite Element (FE) method are conducted to simulate the performance before and after bridge preventive maintenance or rehabilitation. Combining the bridge configuration, the output performance, and repair costs, a set of rules to evaluate the bridge's repair needs is described and converted into the fuzzy logic system. Then the repair recommendation is generated and sent to the database of performance assessment. The new database has deleted all output values from finite element models to simulate the rapid assessment condition. Then performance models are trained using a series of machine learning classification techniques. Moreover, when any long-term structural health monitoring data is available, the performance forecasting model can be trained and updated with those datasets. Combined with engineered judgment and the forecasting output, the performance of the bridge at the monitoring point could be evaluated.

Chapter 2 introduces literature on current bridge management and maintenance systems, including the definition and scope of bridge preventive maintenance, rehabilitation, and replacement. Routine inspection and structural assessment standards, new technologies on bridge inspection and condition rating, evaluation, and forecasting, are also covered. Then a typical bridge protective maintenance work, which installs the link slab system to the existing multiple simply supported bridge, is introduced as a special case that partially changes the performance of the bridge despite theoretically having no structural function to the original bridge. In order to perform the assessment using machine learning techniques, some general information is introduced in this chapter.

Chapter 3 shows the methodology of this research. At the beginning of this research, a series of data collecting, processing, and analysis of the bridge inventory data from the National Bridge Inventory (NBI) database is conducted. After finding the distribution for each required feature, the simulated database is generated for analysis using finite element (FE) modeling. In particular, the input configuration is generated using Latin Hypercube Sampling (LHS, Stein, 1987) based on the distribution of these features. Then the fuzzy logic system is introduced to establish the condition assessment database. Moreover, performance assessment models developed using machine learning (ML) techniques are conducted and compared, and the LSTM time series forecasting method is also covered in this chapter.

Chapter 4 describes the material for the bridge protective maintenance work. Then several types of high-performance cementitious composites are selected, and lab tested for their performance under compression and bending. The phenomenon of strain-hardening is observed and recorded during the lab test. After the data processing for each type of material, the stress-strain relationship is modeled and refined. Combined with regular concrete models from other references, the theoretical material models for bridge maintenance works are generated. Moreover, a test sample of the time series forecasting model is introduced by training the monitoring data of a beam under cyclic loading.

Chapter 5 constructs a general I girder steel bridge model using 3D finite element analysis and extends it to a parametric study for the optimal design for the newly constructed link slab. The material models are analyzed, selected, and established from Chapter 3 to demonstrate five types of joint fillings. Then several sets of the parametric study, which include the span length, skew angles, length, and depth of link slabs, are conducted as the original input for the optimal design. Next, this research draws the standard line for any link slab design in the bridge assessment as "Preferred" "Acceptable" and "Warning" by taking advice from engineers and experts. After that, this research uses regression methods to find the optimal design for bridges with specific geometry. Combining the features of eligibility, prioritization, and cost estimation, this research uses machine learning techniques to identify and enhance the structural assessment system.

The first case study described in Chapter 6 is the pilot UHPC/ECC link slab system installed in the state of Maryland. An introduction for the case is firstly given, and the monitoring and finite element analysis are conducted to cross-check its design. Then the configuration of this bridge was input into the trained evaluation model to test the estimation of maximum stress and deformation, as well as the assessment of this design.

Chapter 7 presents an expanded database of the repaired bridge analysis by generating a large set of parametric three-dimensional finite element models. As the configuration of those bridges is generated using LHS from the distribution of the original database, the input features are considered reliable to represent the actual condition of the steel bridges. Then a fuzzy logic system is introduced and evaluated for the recommendation of bridge repair. After the second batch of the bridge condition and repair recommendation database develops, the structural performance assessment models are trained using machine learning classification techniques. Finally, a comparison of these models is discussed.

Chapter 8 introduces the second case study. This proposed project covers major bridge preventive maintenance and rehabilitation work done over the past two decades with an instrumented long-term structural health monitoring system. This chapter mainly focused on structural performance analysis with expansion rocker bearing freezing, structural health monitoring data forecasting, and bridge performance evaluation.

Chapter 9 summarizes the current work done in this dissertation. Discussions on the findings and conclusions of this research have also been included in this chapter. Recommendations for future works are proposed with potential topics.

Chapter 2: Literature Review

2.1 Bridge maintenance

Bridge maintenance, which is a critical component of the bridge assets management plan, is a series of works to keep the transportation system to be continuously functional in the operational phase (FHWA, 2016). It is a general response to specific issues about the potential for transportation networks to be disconnected. Preventive and routine maintenance would be grouped into a well-designed maintenance strategy.

Asset management (23 U.S. Code 101(a)(2)) is defined as a “strategic and systematic process of operating, maintaining, and improving physical assets, with a focus on both engineering and economic analysis based on quality information, to identify a structured sequence of maintenance, preservation, repair, rehabilitation, and replacement actions that will achieve and sustain the desired state of good repair over the life cycle of the assets at a minimum practicable cost.”(FHWA, 2018). A general example of bridge assets management plan is described in Figure 2-1

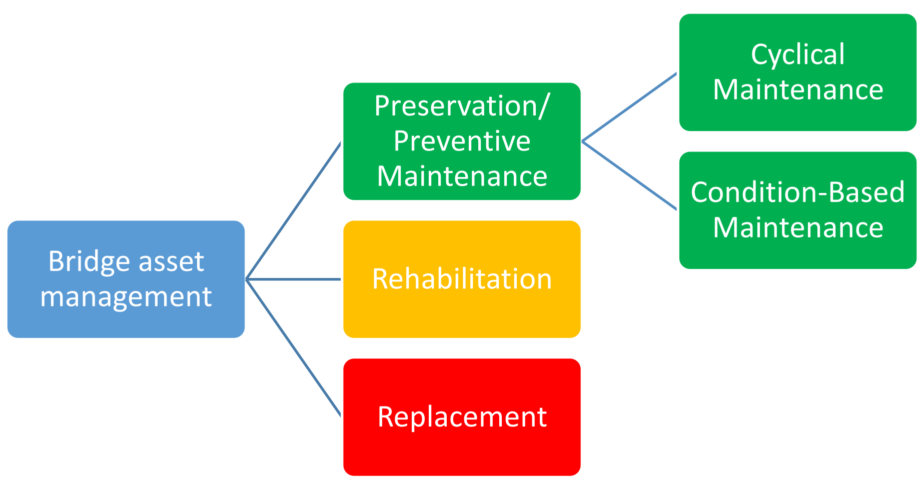

Figure 2-1 Bridge action categories (FHWA 2018)

2.1.1 Preventive maintenance of bridges

Bridge preventive maintenance, also called protective or preservation maintenance, is a strategy for bridge asset management systems that reduces the long-term maintenance cost and extends the service life of the structure. The definition of bridge preservation is given by the Federal Highway Administration (FHWA, 2016) that “Preservation consists of work that is planned and performed to improve or sustain the condition of the transportation facility in a state of good repair. Preservation activities generally do not add capacity or structural value, but do restore the overall condition of the transportation facility.” Under the National Highway Performance Program and the Surface Transportation Program, bridge protective maintenance work is eligible and recommended owing to long-term sustainability and safety issues. The best practice of this cost-effective strategy includes the following (FHWA, 2018):

(1) A basic identification method that will work for all of the management system's structures and will be repeatable. It will most likely contain element-level condition data and also thorough inspection and scopes. The method of inspecting bridge components with condition ratings based on the National Bridge Inventory (NBI) is a generalized example. (2) the preservation work must acquire prioritization and commitment from the owner during the decision-making process. And (3) Verification and feedback on work completed. Some general preventive maintenance activities are listed in Table 2-1:

Table 2-1 Examples of maintenance activities (source from FHWA, 2018)

Activities		Bridge Component
Cyclical Maintenance	Clean/ Wash Bridge	Deck and/or Super/Substructure
	Clean Joints	Deck
	Deck/ Parapet/ Rail sealing and Crack sealing	Deck
	Seal Concrete	Super/Substructure
Condition-based Maintenance	Joint Seal Replacement	Deck
	Joint Repair/Replace/Elimination	Deck
	Concrete Deck Repair (see halo effect below) in Conjunction with Overlays, CP Systems or ECE Treatment	Deck
	Deck Overlays (thin polymer epoxy, asphalt with waterproof membrane, rigid overlays)	Deck
	Repair/Replace Approach Slabs	Approach
	Seal/Patch/Repair Superstructure Concrete	Superstructure
	Protective Coat Concrete/Steel Elements	Superstructure
	Spot/Zone/Full Painting Steel Elements	Superstructure
	Steel Member Repair	Superstructure
	Fatigue Crack Mitigation (pin-and-hanger replacement, retrofit fracture critical members)	Superstructure
	Bearing Restoration (cleaning, lubrication, resetting, replacement)	Superstructure
	Patch/Repair Substructure Concrete	Substructure/Culvert
	Protective Coat/Concrete/Steel Substructure	Substructure/Culvert
	Pile Preservation (jackets/wraps/CP)	Substructure

2.1.2 Bridge rehabilitation

Bridge rehabilitation, which means major construction work that recovers the structural integrity of the bridge, is an essential procedure that corrects major safety defects of the structure after inspection and evaluation. Bridge rehabilitation work might include but is not limited to repair of bridge components with structural damage, and the partial or total replacement of bridge components, etc.

2.1.3 Bridge replacement

The decision to replace a bridge with a new facility while maintaining the same general traffic corridor is known as bridge replacement. The replacement work must comply with structural, geometric, and construction requirements. Before deciding on bridge replacement or rehabilitation, a life cycle cost-benefit analysis must be performed.

2.2 Current bridge condition assessment methods

2.2.1 National Bridge Inventory general condition ratings

National Bridge Inventory (NBI) general condition ratings (GCRs) is an assessment and rating system at the element level (FHWA, 1995). The general bridge is separately evaluated as bridge decks (NBI item 58), bridge superstructure ((NBI item 59), bridge substructure (NBI item 60), and culverts (NBI item 62) with the number scaling from 0 (failed condition) to 9 (excellent condition). A classification (23 CFR 490.409) of a bridge is defined by the minimum rating of all elements of the structure. When the minimum rating of the structural elements is equal to or more than 7, this structure is classified as a “Good” condition. When the minimum condition rating of any item is equal to or lower than 4, the structure is classified as a “Poor” condition. If the minimum rating is either 5 or 6, the structure is under the “Fair” condition classification.

The GCRs provide a general classification of bridge status and help users understand when a bridge needs to be preserved, repaired, or replaced. This rating system, on the other hand, is far too coarse. Before executing the project's final activity, a complete set of bridge inspections, a full appraisal, and a plan of work activities with cost estimates are required.

2.2.2 Current AASHTO guidelines for bridge inspections and condition evaluation

Generally, bridges in the United States that are owned by the state DOTs will conduct inspections at the element level, which is mostly based on the guidance of The American Association of State Highway and Transportation Officials (AASHTO) Manual for Bridge Element Inspection. Depending on the state manuals that are developed, the different elements defined could be from different sources in an attempt to meet the specific needs of each state. These elements could be categories such as (a) national bridge elements (NBEs); (b) bridge management elements (BMEs); and (c) agency-developed elements (ADEs), including ADE-NBE or ADE-BME, and ADE alone (Lin at. Al, 2019). The Manual defined the element with a measure of 4 condition states, which are Good (CS1), Fair (CS2), Poor (CS3), and Severe (CS4). The majority of state DOTs have adopted this type of elemental level bridge inspection and management technique, which was developed in the early 1990s. Detailed bridge element condition data allows for a more accurate depiction of the severity and scope of bridge conditions. (FHWA 2014). The collection and processing of inspected condition data could perform a national wide reporting, analysis, and forecasting under risk-based data-driven methods. Additionally, based on the Manual for Maintenance Inspection of Bridge (AASHTO), each highway bridge should be rated at two load levels by the load and capacity evaluation, which is referred to as operating ratings and inventory ratings.

Moreover, current standardized procedures for performing existing bridge condition assessments start from bridge load rating by structural analyses; and load testing might be conducted when met with an unsatisfactory result or missing design document or information. The load rating process is described in the American Association of State Highway and Transportation Officials (AASHTO) Manual for Condition Evaluation of Bridges.

Bridge design specified by AASHTO based on Allowable Stress Design (ASD, before 1994) and Load Factor Design (LFD, after 1994) by establishing the structural bearing capacity not to exceed the allowable limit and adjusted with a factor that shows relative uncertainties, and the LRFD specifications, published starting from 1998 and enforced in 2007, integrated modern design principles of structural reliability and the probabilistic and statistical models of load and resistance in design (Wang et al. 2010). The AASHTO published Manual of Maintenance Inspection of Bridges contains guidance of allowable stress rating (ASR), load factor rating (LFR), and load and resistance factor rating (LRFR), respectively. At present, all three methods (ASR, LFR, and LRFR) of bridge rating are in use by the US State DOTs.

The load rating equation in both ASR and LFR is determined by (AASHTO MBE 2017):

$$RF = \frac{C - A_1 D}{A_2 L(1+L)} \qquad \text{Equation 1}$$

Where:

RF: Rating factor for the live load capacity; C: capacity of the structural member

D: dead load effect on the member

L: live load effect on the member

A_1: factor on dead load

A_2: factor on live load

Both ASR and LFR methods load rate bridges at Inventory and Operating levels. The Inventory rating considers the existing bridge condition with material deteriorations, while the Operating level describes the maximum permissible live load of the bridge. Although ASR and LFR use the same equation, the parameters of capacity (C) and load factors (A1 and A2) might be different.

The AASHTO LRFR Guide Manual is the first bridge load rating method in the United States based on modern principles of structural reliability and limit states design. And the rating equation using the LRFR method is (AASHTO MBE 2017):

$$RF = \frac{C - \gamma_{CD} DC - \gamma DW \pm \gamma_p P}{\gamma_L LL(1 + IM)} \qquad \text{Equation 2}$$

Where:

C: structural capacity, defined as $C = \phi\phi_C\phi_S R_n$; And $\phi_C\phi_S \geq 0.85$

R_n: nominal member resistance

DC: dead load effect of structural component

DW: dead load effect of wearing surface and utilities

P: Permanent load other than dead load

LL: live load effect

IM: dynamic load allowance

The LRFR method evaluates bridges at all three limit states described in the LRFD Bridge Specifications, i.e., the strength-limit state (flexural or shear capacity), the service-limit state (deflection and rotation), and the fatigue-limit state. The LRFR methods simplified the rating process by using the HL-93 design load as the initial evaluation criteria and then checking all other legal loads specified by AASHTO or States in the US.

2.2.3 Fuzzy mathematical approach

The true condition of the bridge is rarely known to the designers and owners due to uncertainties and approximations that are hidden in the design (Yao, 1985). And it is not feasible to determine the absolute condition of a bridge during each inspection. Also, the condition rating is difficult to quantify or model mathematically because it will greatly be influenced by the inspector's judgment. Thus, a high degree of ambiguity in the rating of major components is unavoidable. The application of fuzzy mathematics to bridge condition assessment (Tee, 1988a, 1988b) was proposed based on the background that the bridge will be decomposed to the element level and the cumulated rating function will be used to evaluate the bridge condition, which involves the uncertainty in describing an event or result using natural language.

The fuzzy set theory was developed by Zadeh (1965), who believes that a human's ability to make accurate and significant statements will decrease with the increasing system complexity. Therefore, the theory was developed as a tool for decision-making problems under complex systems. Tee (1988) found that the condition ratings and the importance coefficients are best represented by fuzzy sets.

The fuzzy weighted average technique is selected to combine the subjective condition ratings.

The fuzzy logic approach would be particularly useful for remedying the uncertainties and imprecision in bridge inspectors' observations (Sasmal 2006). A general structural or pavement damage rating scheme according to the local, global, and cumulative conditions can be evolved with a weighted average approach (Bertero & Bresler, 1977; Arliansyah et al., 2003; Sasmal et al., 2004a, 2004b) called Fuzzy Weighted Average (FWA) technique and could be expressed as:

$$R = \frac{\sum_{i=1}^{p}(w_i \times r_i)}{\sum_{i=1}^{p} w_i} \qquad \text{Equation 3}$$

Where: R is the fuzzy set that represents the final assessment of the condition (global rating); r_i is the local rating of the i^{th} component, and w_i is the importance coefficient, respectively.

2.2.4 Structural health monitoring (SHM)

The process of implementing an autonomous damage detection strategy for aerospace, civil, and mechanical engineering infrastructure is referred to as SHM (Figueiredo et al., 2013). Bridges are susceptible to environmental-induced and traffic-induced deformation and vibrations. Remote sensing uses in situ, on-site, or air-bone sensors to test and monitor sensitivity to these loads, such as vehicles, wind, earthquake, and thermal loads. Strain gauges, displacement transducers, velometers, and accelerometers are commonly used (Fu et al., 2019). The structural health monitoring (SHM) system that consists of these sensors is widely used in monitoring for complex structures or diagnostic load testing for bridges as a damage detection or characterization strategy for real-time assessment of structural conditions. A successful SHM system should be capable of determining and evaluating the serviceability, reliability, and durability of structures (Sousa, 2011). The SHM system consists of both a proper design and implementation of SHM based on a multidisciplinary team and decision-making supported by the monitoring data (Housner et al. 1997; Sousa et al. 2013). Many researchers have investigated the application and knowledge extraction from the SHM system (Swartz et al., 2009; Karbhari et al., 2009; Catbus et al., 2013; Tan et al., 2009; Figueiredo et al., 2013), and some have developed integrated assessment scenarios taking advantage of the processed data from the SHM system (Comisu et al. 2017).

Wei et al. (2014) introduced a bridge condition evaluation system based on SHM data without data processing. The researchers believe that the processing of data could cause delayed alarms. By ignoring the index limit, these researchers evaluate the structure with its own variation and weight. Monitoring data from the response of superstructure, substructures, and vehicle indexes were analyzed for bridge condition assessment. The superstructure evaluation index includes lateral and vertical nature frequencies of superstructure, accelerations, displacement, and corresponding section stress and strain of the structure. The pier top displacement and tilt angle, the displacement of bearings are also widely focused on the SHM system. Coupled with vehicle parameters, which might include but are not limited to the derailment coefficient, wheel load reducing rate, track force, the moving load and acceleration of the car, etc., the structure evaluation index was generated without classifying the type and detail configuration of the structure.

2.2.5 Bridge preservation program

Bridges deteriorate, lose function, and eventually reach the end of their service life if no maintenance is performed (Tee, 1988; FHWA, 2018). For safety and economic reasons, bridge asset management, including inspections and maintenance, is required. The preservation, restoration, and replacement of bridges are all covered under this scheme throughout the duration of the structure's service life life (Figure 2-2). These programs include condition-specific exercises as well as cost-benefit assessments.

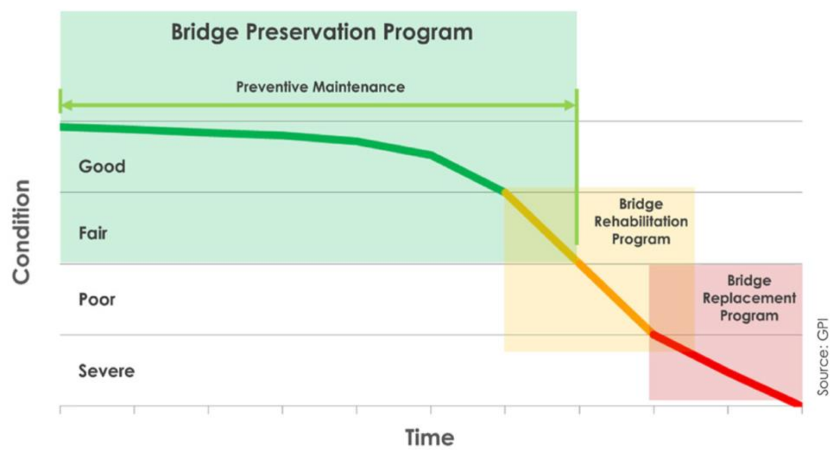

Figure 2-2 Bridge classification under its condition rating (FHWA 2018)

The Bridge Preservation Program is a set of condition-based activities that are applied to the bridge in a good or fair rating (FHWA 2014). This program aims to extend the service life (Figure 2-3) of the bridge by identifying potential damage or deterioration, as well as taking actions to maintain the bridge before any rehabilitation activities are needed under the net benefit of programs.

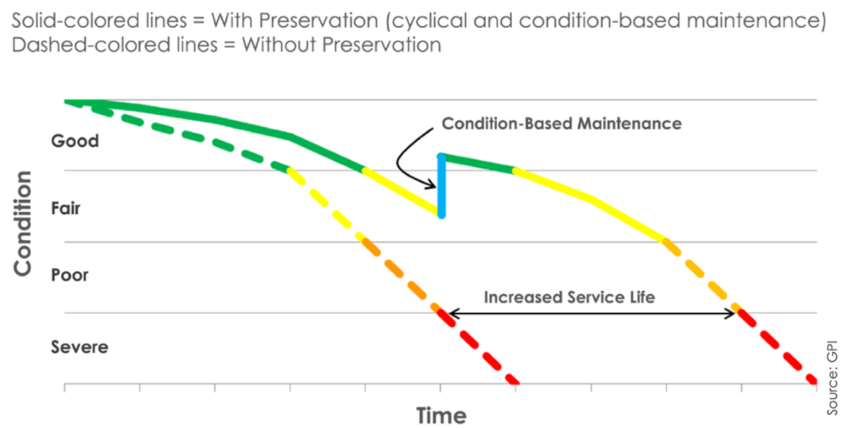

Figure 2-3 A comparison of bridge conditions over time with and without bridge preservation (FHWA 2018)

2.3 Analysis, design, and construction of link slabs, a strategy for performance improvement

Before the extensive use of computer-aided design, conventional bridges were designed as single or multiple simply supported bridges rather than continuous bridges (Ulku et al. 2009). These bridges, however, are the most commonly utilized and are currently suffering aging issues such as corrosion and fatigue, which might lead to partial structural failure. One of the most prevalent issues of highway bridges is joint failure, which can result in leakage and corrosion of bridge girders and substructures (Alampalli et al., 1998). As an alternative to the expansion joint, integrating the newly constructed link slab system to the existing multiple simply supported bridge structures is one of the joint elimination options under bridge protective maintenance that helps to prevent joint failure. Figure 2-4 illustrates a common link slab design.

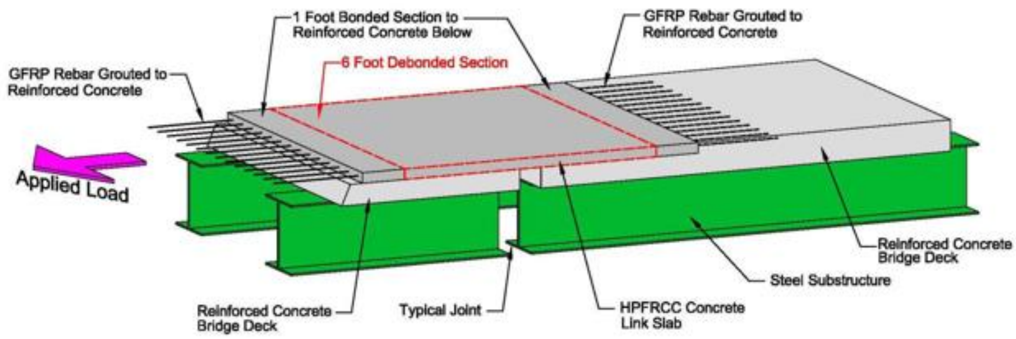

Figure 2-4 Typical design of link slabs (Larusson et al. 2013)

The concept of link slab was proposed by Zia and Caner (1995, 1998) that fully connected the adjacent bridge decks of multiple simply supported bridges while keeping the girder of the bridge discontinuous. Therefore, the structure can still be treated as multiple simply supported during structural analysis. This concept was then tested, adopted, and updated in the United States and many other countries.

Because it does not significantly change the structural performance and is treated as simply supported, the link slab system then is analyzed and determined to have adequate stiffness while reaching higher ductility and extended durability (Zhu et al., 2021). To obtain a better performing link slab, the original design is updated factoring in the geometry of the bridge, boundary conditions, and material selection.

In the original design phase of the link slab using regular concrete, Caner and Zia (1995, 1998) proposed and developed the optimal design concept using the full depth of the bridge deck (showed as fully connected), and the length to be the 7% of the adjacent span length, with 5% of the adjacent span lengths from the center of the link slab as the deboned zone. This design was then proven by Alexander Au et al. (2013).

Besides, the changing of support conditions will influence the behavior of the bridge. Beam end stress and deformation will be accumulated under the link slabs with the elimination of the expansion joint. Thus, bearings are recommended to be changed to allow rotation and longitudinal movement (Graybeal, 2014). Furthermore, investigation shows that part of the link slab would be under tension regardless of the support conditions when considering live load (A. M. Okeil and A. El-Safty, 2005). The brittleness and limited durability of concrete material under certain conditions count against its applications in link slabs (Zhong et al., 2019; Hou et al., 2018). In the application of full-depth link slabs with regular concrete, a relief cut (Figure 2-5) is designed at the middle of the link slab and then sealed when the crack width exceeds the limit of AASHTO recommendations (Ulku et al. 2009). Cracks are expected and documented in the following inspection of eight bridges in the state of Michigan (Figure 2-6)

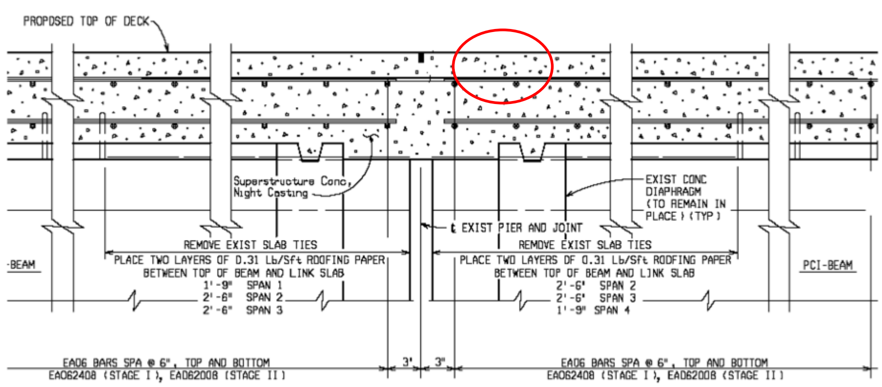

Figure 2-5 Cross-section of a link slab design with relief cut (Ulku et al. 2009)

Figure 2-6 Full-depth crack in link slab that was observed in the inspection (Ulku et al. 2009)

2.4 Durability of steel bridges

The average life of a bridge spans between 50 to 70 years though a typical bridge is designed for a 100-year service life. The durability of the bridge is always a hot topic considering the safety and economic issues.

The aging concrete information system (T. P. Dolen, 2005) shows a highly reduction in material strength and elastic modulus of concrete after 50 years of service life. When the age of the concrete is more than 60 years, a 50% reduction might occur. The main reasons that cause material aging of concrete are due to creep, alkali-aggregate reaction, sulfate attack, delayed ettringite formation, freeze-thaw, etc. (FHWA, 2015). Meanwhile, the deterioration of steel is mainly because of section loss, rust, fatigue, and carbonation-induced reinforcement corrosion.

2.5 Techniques used for bridge condition assessments and prediction

Advanced bridge condition assessment, damage detection, and bridge condition prediction techniques were developed based on data-driven methods and probability theories.

The Markov Chain has been the most commonly used and developed methodology to predict the time-dependent deterioration rate of bridge structures and elements (Jiang et al., 1989; Cesare et al., 1992; Jiang et al., 2005; Fu and Deveraj, 2008; Wang et al. 2008). The core methodology of the Markov Chain is to develop the transition probability matrix as deterioration prediction. These models are developed based on two assumptions: (1) bridge inspections are performed periodically with a fixed time interval, and (2) the future bridge condition depends only on the present condition and not on past conditions. Investigation shows that using the transition probability matrices adjusted for the variation in the inspection period may result in a 22% error in predicting the service life of a bridge deck system (Morcous, 2006). Moreover, Agrawal et al. (2010) used both Markov chains and Weibull-based approaches to develop and verify the deterioration curve based on the data from NYSDOT inspection reports.

Besides, Chang et al. (2019) developed a series of stochastic deterioration models using a combination of methods, including Markov chains, logistic regression, and classification trees, that are more efficient and accurate in condition rating predictions. Furthermore, machine learning and deep learning techniques have been introduced and investigated in bridge condition predictions based on a large dataset, which typically refers to the National Bridge Inventory (NBI) and Bridge Element (BE).

Fiorillo et al. (2019) proposed an application of machine learning techniques for the analysis of NBI and BE, which may improve future predictions of the performance of bridge assets for a more precise evaluation of the condition and correct allocation of management funds to keep bridges in a good state of repair. Vagnoli (2018) presented a machine learning classifier for condition monitoring, and damage detection of bridges is proposed by adopting a Neuro-Fuzzy algorithm. More cases of failure mode recognition could be found by Mangalathu (2018, 2019). Liu and Zhang (2020) developed a data-driven approach by training a Convolutional Neural Network (CNN) model with available NBI data that enables the prediction of future conditions of highway bridge components from historical inspection data with a prediction accuracy of over 85%. An ongoing project by Banaei-Kashani et al. (2021) aims to design hybrid physics-based DL models for bridge deterioration forecasting by incorporating physical knowledge into the learning process.

Chapter 3: Methodology and Statistical Data Analysis

This chapter describes the theories and methodology which are applied to this research. As this research proposed two structural performance assessment methods. The rapid repairing assessment and recommendations rely on machine learning classification techniques. Meanwhile, the evaluation and prediction of structure performance rely on structural health monitoring and LSTM deep learning algorithms. This chapter also introduces LSTM time series forecasting techniques. This research has generated several forecasting LSTM models with real-world structure health monitoring data.

Furthermore, this chapter describes the initial dataset collection using the most recent bridge inventory data from the national bridge inventory (NBI). As of April 2022, a total of 173,839 steel bridges in the US have been input into the initial database. Then, a series of data analyses of steel bridges in the United States has been performed in this chapter.

Lastly, some remarkable findings from the initial data analysis and finite element simulations are described. The Latin hypercube sampling (LHS) was introduced when generating the value of input features of the evaluation model to ensure the sampling and the dataset could represent typical steel bridges in the US. Moreover, the test finite element analysis shows the repaired structure would not change compared with the original model if excluding the aging effect of the structures. These findings provide some basic information and guidelines for further model establishment and assessment. In particular, the effectiveness of repaired work and feature filtering in database selection and FE model simulation has been discussed.

3.1 Methodologies

3.1.1 Condition assessment model using Fuzzy Logic

The application of fuzzy logic (FL) has significantly increased in these years. A general description of fuzzy logic is a multivalued logic that is related to classification (Kaufmann, 1985). Typically, fuzzy logic contains input and output using verbal description with uncertainties and constrained with a series of parallel if-then statements as rules. The primary mechanism in the fuzzy logic is to use these inputs with rules to assign value to the output vector. All inputs and outputs are defined as individual fuzzy sets, which are sets without crisp, clearly defined boundaries (Dubois, 1980).

This research proposed an integrated decision-making model that contains the evaluation of repair recommendations. To develop this evaluation, a fuzzy logic system based on MATLAB (2022) has been developed by defining the input and output features as fuzzy sets, constructing the membership function with shapes and boundary approximation, and generating and adjusting rules to get a reliable logic model for further analysis (Sivanandam, 2007).

Figure 3-1 demonstrates an example using the fuzzy logic system. In this figure, the if-then scenarios are hidden in the logic system. This visualized figure provides clear guidance on how to use the fuzzy logic system. Once the input membership functions (yellow), the rules, and the output membership function (blue) have been determined, the evaluation process will automatically develop by entering the numbers (value) of input for each feature, which are described in the input membership function.

The output will be generated in a vector. Figure 3-2 shows an example of the fuzzy logic surface.

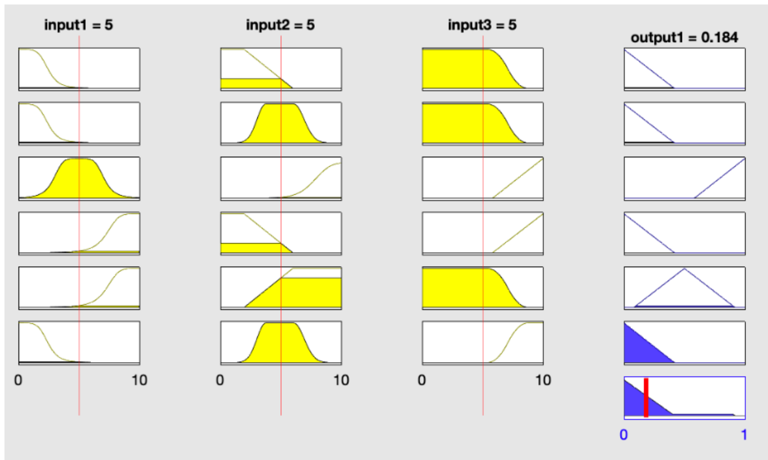

Figure 3-1 Example of rules of fuzzy logic

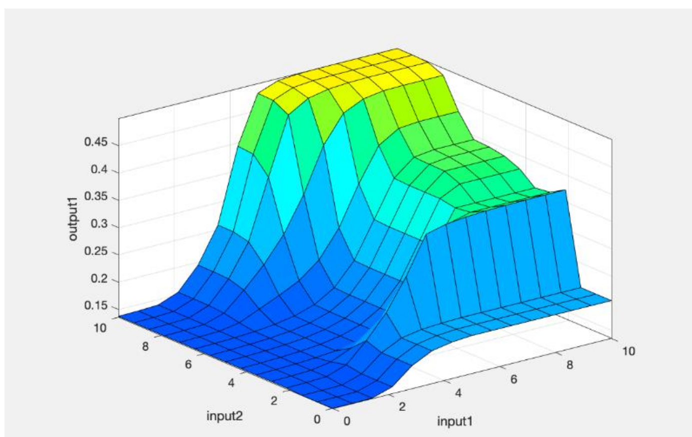

Figure 3-2 Example of fuzzy logic system surface

3.1.2 Optimization

Mathematically, the optimization problem describes as an approach to finding the curve and surface fitting of given data with minimum error.

In the application phase, it can be used to determine specific design parameters that lead to the best system performance while minimizing the costs under given constraints (Sarker, 2008).

The standard form for using software tools for optimization is to denote the optimization variables X as an n-dimensional vector, where the n variables are its components, and the objective function $F(X)$ is searched based on

$$\boldsymbol{X}^* \in R^N \text{ so that } F(\boldsymbol{X}^*) = \min F(\boldsymbol{X}) \qquad \text{Equation 4}$$

Subject to

$$\boldsymbol{X_l} \leq \boldsymbol{X}^* \leq \boldsymbol{X_u} \qquad \text{Equation 5}$$

With the regional constraints: $\boldsymbol{G_i}(\boldsymbol{X}^*) \geq 0 \;\; i = 1,2, \dots, m$

And behavior constraints: $\boldsymbol{H_i}(\boldsymbol{X}^*) = 0 \;\; i = 1,2, \dots, q$

Where: m is the number if inequality constraints; and q are the number of equality constraints.

3.1.3 Machine learning techniques in bridge condition assessment

The advent of knowledge-based expert systems has highlighted the practical value of such known as machine learning. As their name implies, these systems are powered by knowledge that is explicitly represented rather than implied in algorithms. A domain specialist and a knowledge engineer collaborated for a long time to codify the knowledge needed to supply the pioneering expert systems. While this procedure typically illuminates a few rules per man-day, an expert system for a demanding activity may necessitate hundreds or even thousands of rules. The interview method of knowledge acquisition clearly cannot keep up with the growing demand for expert systems; this is referred to as the 'bottleneck' problem by Feigenbaum (1981). This view has inspired researchers to explore machine learning methods for elucidating knowledge.

As this research proposed the rapid performance assessment after the preventive maintenance or rehabilitation work, the idea is to find the optimal design using regression methods in a small dataset and train the assessment model for this particular design by classification methods. Classification refers to the use of the discrimination rule(s) to assign data that were not part of the original training sample to one of the G groups, or to the estimation of probabilities $p_g\ (x)$, $g = 1, \ldots, G$, that the vector x belongs to group g.

Thus, a brief review of various traditional machine learning methods based on the decision theory for classification from statistics is provided in this section. More details that explain these algorithms are directed to Friedman et al. (2017).

Discriminant analysis is a technique that categorizes the dependent variable or criterion and separates objects or events into two or more classes (Wilks, 2019). The term discrimination refers to the process of estimating functions of the training data x_i that best describe the features separating the known group memberships of each x_i.

The methodology of discriminant analysis is to develop discriminant functions that fit the need for categories. Suppose $f_k(x)$ is the class-conditional density of X in class $G = k$, and let π_k be the prior probability of class k with $\sum_{k=1}^{K} \pi_k = 1$. Then the class posteriors $P_r(G|X)$ for optimal classification could be derived:

$$P_r(G = k|X = x) = \frac{f_k(x)\pi_k}{\sum_{l=1}^{K} f_l(x)\pi_l} \quad \text{Equation 6}$$

Then suppose that each class density can be modeled as multivariate Gaussian:

$$f_k(x) = \frac{1}{2\pi^{p/2}|\sum_K|^{1/2}} e^{-\frac{1}{2}(x-\mu_k)^T \sum_k^{-1}(x-\mu_{k)}} \quad \text{Equation 7}$$

Where p is the number of features.

And then, the linear discriminant function (LDA) can be expressed as:

$$\delta_k(x) = x^T \Sigma^{-1} \mu_k - \frac{1}{2}\Sigma^{-1} \mu_k + log\pi_k \qquad \text{Equation 8}$$

And the quadratic discriminant function (QDA) can be expressed as:

$$\delta_k(x) = -\frac{1}{2}\log \ || - \frac{1}{2}(x - \mu_k)^T \Sigma_k^{-1} x - \mu_k + log\pi_k \qquad \text{Equation 9}$$

K-nearest Neighbors Algorithm (k-NN) is a non-parametric method for data classification (Cover, 1967 and Breiman, 1984). In this algorithm, the neighbors are assigned a weight by the location of the data and resampled. For example, the nearest neighbor has the largest weight, while the farthest neighbor has a small weight. Generally, KNN assigns the largest possibility to the nearest class for the observation. The conditional probability for x in category n can be expressed as:

$$P_l(x) = P_r(Y = n|X = x) = \frac{1}{K}\sum_{n \in N_K} I(y_i = n) \qquad \text{Equation 10}$$

Where N_K represents the K points in the training data are close to the observation x which means the K-nearest neighbors had been assigned a weight 1/K and all others have zero weight.

Naïve Bayes (NB) processing the data classification using Bayes theorem. They are one of the most fundamental Bayesian network models, but when combined with kernel density estimation, they can achieve higher levels of accuracy.

Another algorithm to conduct a non-parametric test for the classification problem is called the Decision tree (DT). The trees are generated with a root node, interior nodes, and terminal nodes. The systems are presented with a set of variants relevant to the classification task. The two main steps involved in building the decision tree are:

(1) Dividing the training set space into J non-overlapping and unique regions. The splitting binary can be captured based on the Gini index (GI) that:

$$GI = \sum_{t=1}^{m} \hat{p}_{mt}(1 - \hat{p}_{mt}) \quad \text{Equation 11}$$

Where the $\hat{p}_{mt}$ represents the portion of training observations in the m^{th} region from the t^{th} class. Starting from the root node, the GI for each split will be tested, all the predictors are assembled, and the child interior node will be created with the lowest GI. This process is repeated until the entire training space has been partitioned into J areas. By putting a penalty factor ($\alpha|T|$) on GI, the tree's development can be effectively managed.

(2) The second phase includes taking precautions to avoid overfitting or the formation of a complex tree. Cost complexity pruning, which considers a sequence of trees indexed by a non-negative tuning parameter α, is used to achieve this. The optimal value of α is estimated by a k-fold validation technique such that the GI of the holdout data is minimum. A more detailed explanation of the GI and algorithm to generate the regression tree can be found in Friedman et al. (2001).

Artificial neural networks (ANNs), also known as neural networks (NNs), are computing systems that are modeled after the biological neural networks that compose animal brains (Russell, 2010). Neural networks learn (or are trained) by analyzing events with a known "input" and "output," establishing probability-weighted connections between the two that are stored inside the net's data structure. The difference between predictions and target output is defined as the error. The network then adjusts its weighted associations using this error value and a learning strategy. With each change, the neural network will create more comparable output to the goal output. The training can be ended based on specified criteria when a sufficient number of these improvements have been made.

3.1.4 Time series forecasting

Recurrent Neural Network (RNN, Dorffner, 1996) shows outstanding performance on sequence data. The RNN dynamics can be described using deterministic transitions from the previous to the current hidden states.

The deterministic state transition is a function:

$$h_{t-1} \rightarrow h_t \qquad \text{Equation 12}$$

For classical RNNs, this function is given by:

$$h_t = f(W * h_{t-1}) \qquad \text{Equation 13}$$

Where $f \in \{Sigmoid, tanh\}$

Vanilla RNN (Mikolov. et al., 2010) is a considerable choice in processing sequence data. However, it can only take advantage of the information from the last step rather than learn knowledge from the whole process. This research considers long-short Term Memory (LSTM) which allows it to easily "memorize" information for an extended number of time steps (Zaremba, 2014).

The deterministic state transition is slightly different from Vanilla RNN:

$$h_{t-1}, c_{t-1} \rightarrow h_t, c_t \qquad \text{Equation 14}$$

$$c_t = f \odot c_{t-1} + i \odot g \qquad \text{Equation 15}$$

$$h_t = o \odot \tanh{(c_t)} \qquad \text{Equation 16}$$

The '*long-term*' memory is stored in a vector of memory cells $c_t \in \mathbb{R}^n$, and $h_t \in \mathbb{R}^n$ is the feature representation of the current state, n is the dimension of the hidden state. Here i; f; o; g are gate functions that represent the input gate, forget gate, output gate, and modulation gate, respectively.

Although many LSTM architectures differ in connectivity structure and activation functions, all LSTM architectures have explicit memory cells for storing information for long periods. The LSTM can decide to overwrite the memory cell, retrieve it, or keep it for the next time step. Figure 3-3 illustrates the LSTM equations.

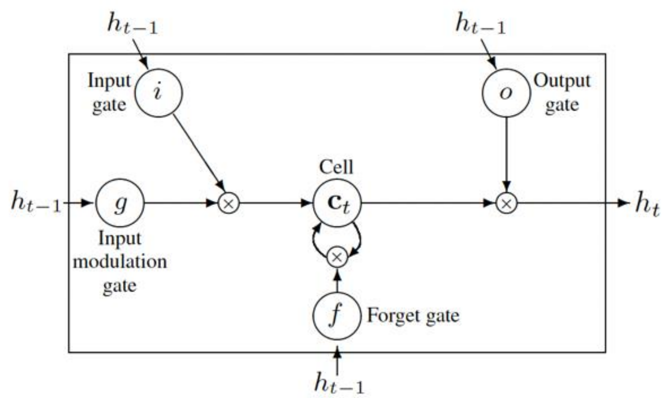

Figure 3-3 A graphical representation of LSTM memory cells used in this research work

3.2 Data analysis of steel bridges in the United States

This section categorizes and analyzes a group of data collected from the National bridge inventory (NBI) database.

3.2.1 Statistics and data categorization

The dataset of steel bridges from the NBI database was collected and evaluated. In this database, 21 features, including state name, structure number, owner's agency, county, year built, main span material, main span design, structure length, features intersected, facility carried, bridge year, deck area, approach spans, approach span design, number of approach spans, skew angle, the maximum length of span, deck width, and bridge condition, were listed without a detailed inspection report. Using the historical record of bridge condition rating is indeed effective for the current bridge condition assessment. However, this method could not cover the detailed performance of the structure and the secondary awareness of the bridge's condition.

Figure 3-4 to Figure 3-11 shows the statistical plot of these attributes and features.

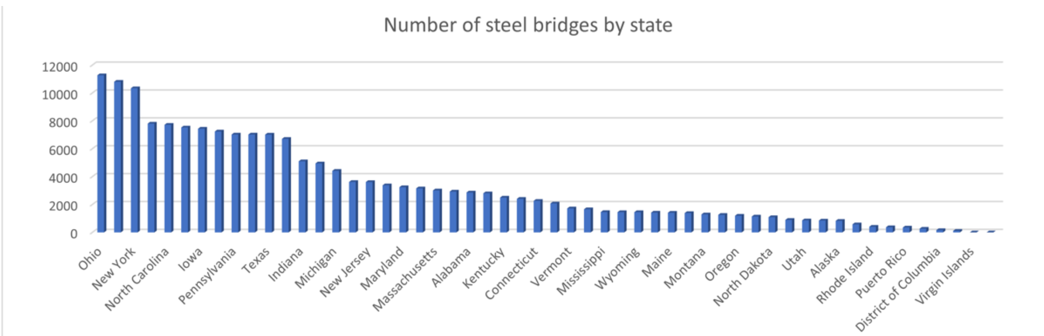

Figure 3-4 Steel bridges' distribution calculated by states.

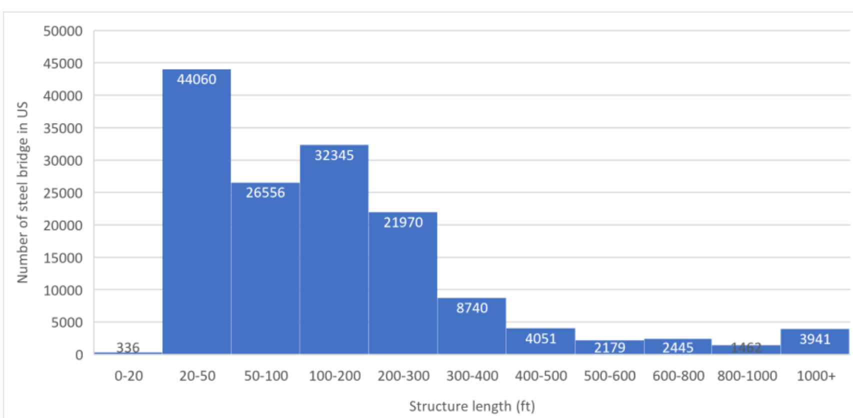

Figure 3-5 Structure length of steel bridges in the US

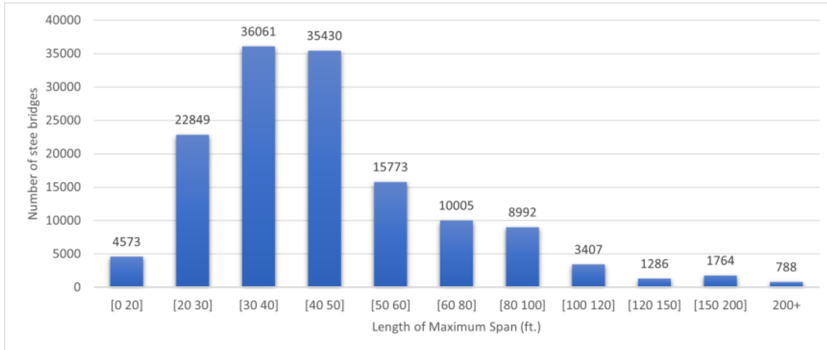

Figure 3-6 Statistics on the length of the maximum span of steel bridges in the United States

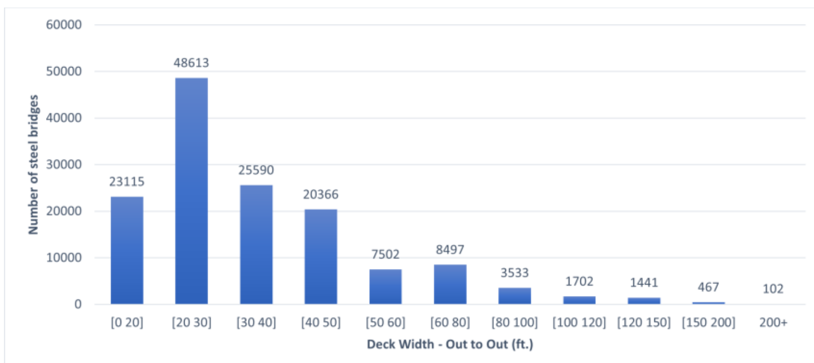

Figure 3-7 Statistics on deck widths of steel bridges

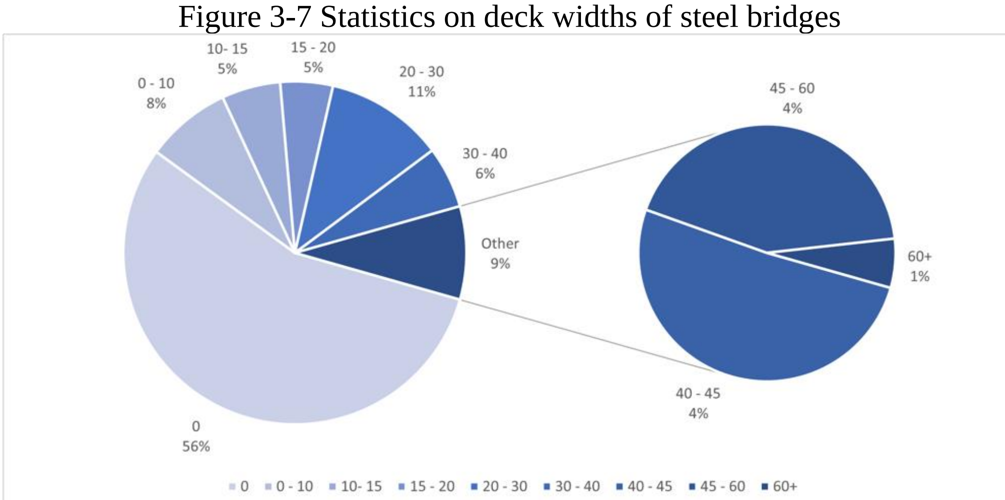

Figure 3-8 A skew angle of all steel bridges (deg)

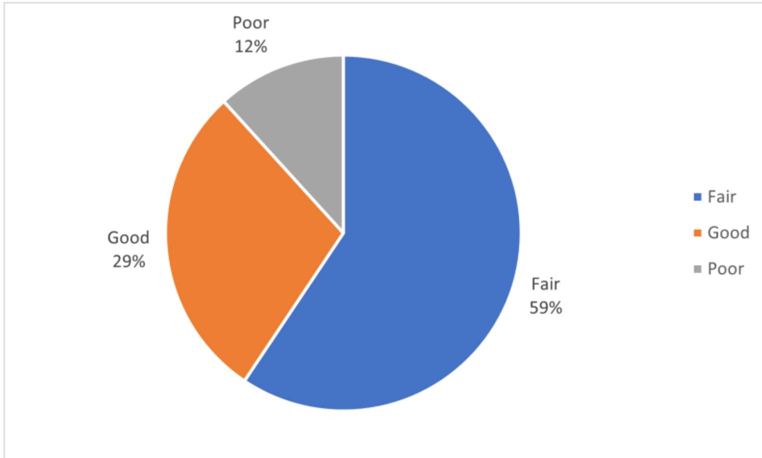

Figure 3-9 Current bridge condition of steel bridges in the dataset

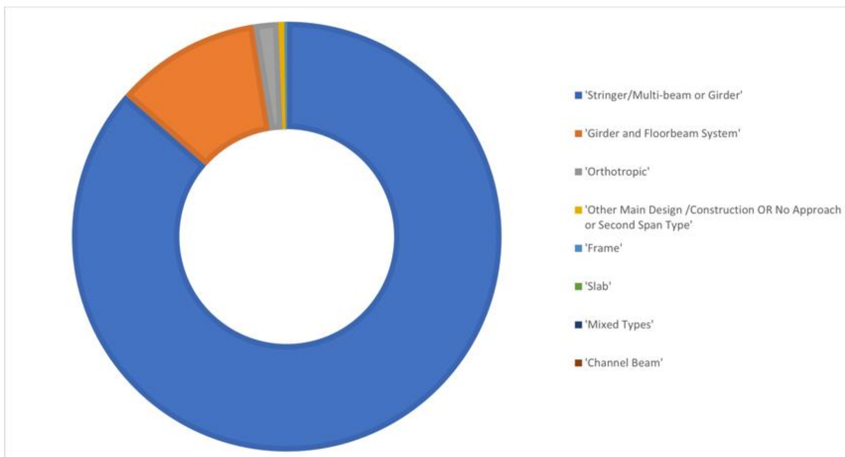

Figure 3-10 Structure types

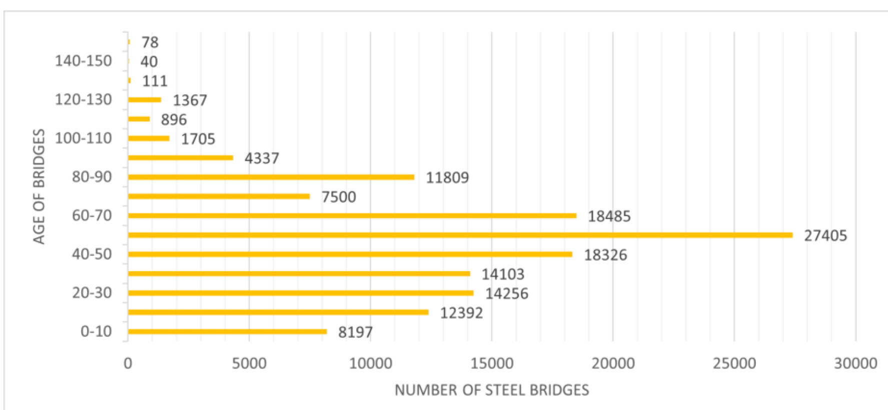

Figure 3-11 Bridge age vs. frequencies

Thus, the dataset was developed and categorized based on the locations (Figure 3-4), configurations (Figure 3-5 to Figure 3-8), previous inspection conditions (Figure

3-9), structure types (Figure 3-10), and age of the bridge (Figure 3-11). From these statistic plots, some trends could be easily found. For example, Ohio has the most steel bridges in the US (detailed number see Appendix); The maximum span length is mainly between 20 ft to 60 ft, while the deck width mainly spans 0 to 50 ft. There are about 56% of the bridges have no skew angles, and 59% of the structures are under the 'Fair' condition.

The previous attributes mainly focus on the change of a single parameter. When we develop the assessment database, all the features are coupled with each other, and the evaluation process uses the weighted average on the condition rating. Thus, the distributions could change when applying any features as a filter. For example, to investigate the relationship between bridge age and condition rating, the bridge condition is first flited, and the bridge year distributions are summarized and plotted (Figure 3-12 to Figure 3-14).

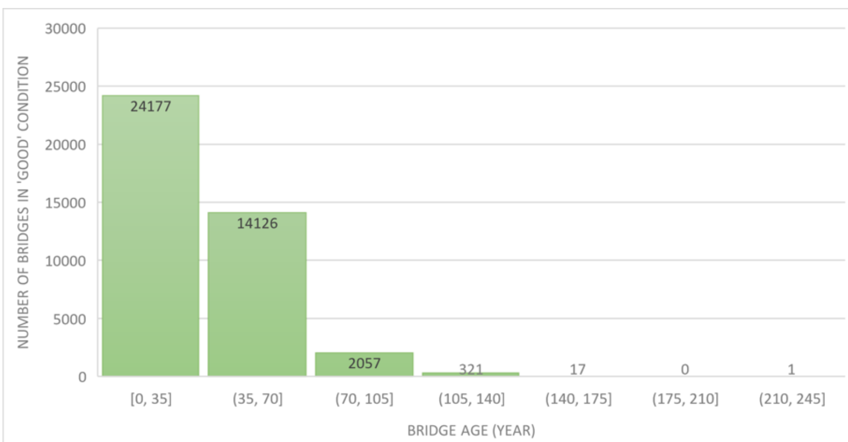

Figure 3-12 Bridge age distribution of the structure under 'Good' condition

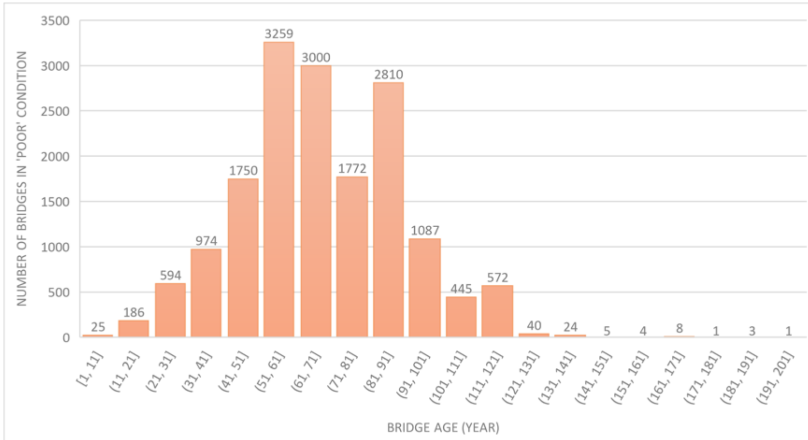

Figure 3-13 Bridge age distribution of the structure under 'Fair' condition

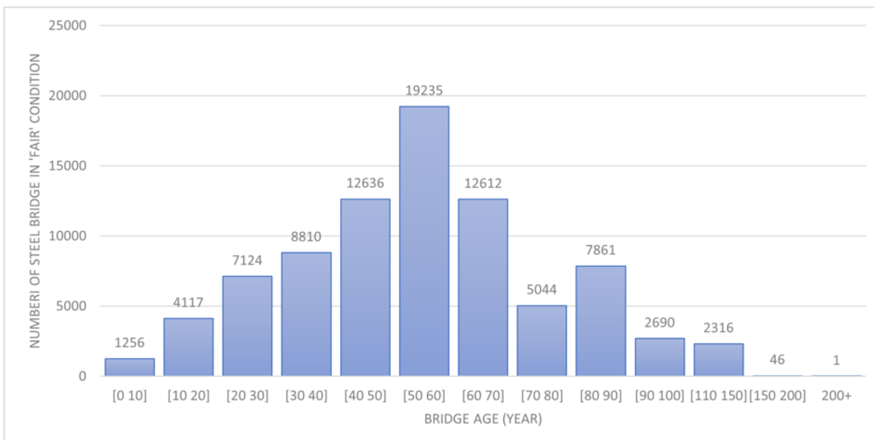

Figure 3-14 Bridge age distribution of the structure under 'Poor' condition

3.2.2 Probability distribution

As the object of this research is to develop the rapid structural performance assessment model, various bridge attributes should be considered based on the probability distribution of the actual data. Thus, statistical data analysis is also conducted in this research to find the probability distribution for attributes of steel bridges in the United States. Furthermore, data cleaning and pre-processing are needed in this research. An example of structure length analysis from the updated database is listed in Table 3-1. After reviewing the database, structures with error information such as 0 span length or 99 deg skew angles were deleted.

Table 3-1 Structure length data analysis

Structure Length (ft.)	
Mean	208.1476537
Standard Error	1.32837875
Median	107.9
Mode	29.9
Standard Deviation	511.1842384
Sample Variance	261309.3256
Kurtosis	2278.969672
Skewness	32.51149854
Range	50794
Minimum	20
Maximum	50814
Count	148085
Confidence Level (95.0%)	2.603595789

The tool MATLAB distribution fitter (2022) is selected in this research to find the best distribution for each attribute. A summary of fitted distribution needed in this research is listed in Table 3-2, and some examples of fitted PDF distribution figures are plotted in Figure 3-15.

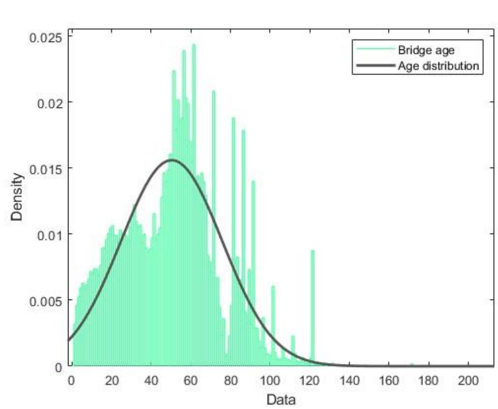

(a) Bridge Age and fitted distribution

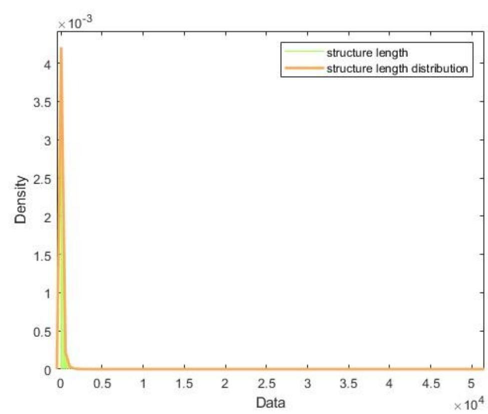

(b) Structure length and fitted distribution

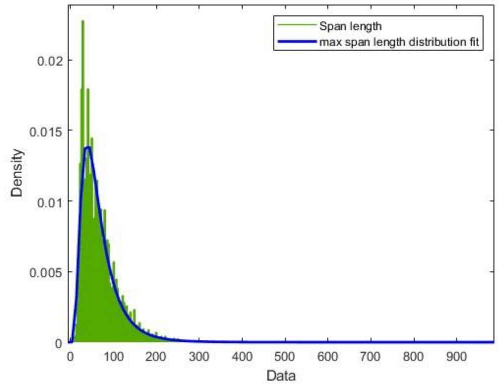

(c) Maximum span length and fitted distribution

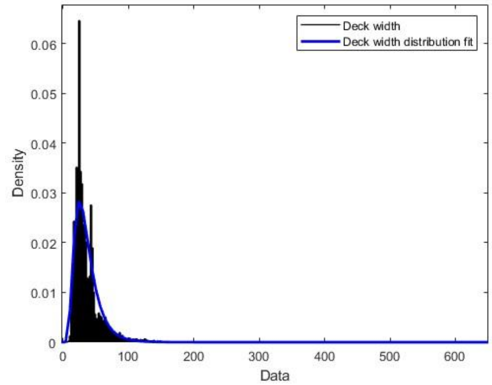

(d) Deck width and fitted distribution

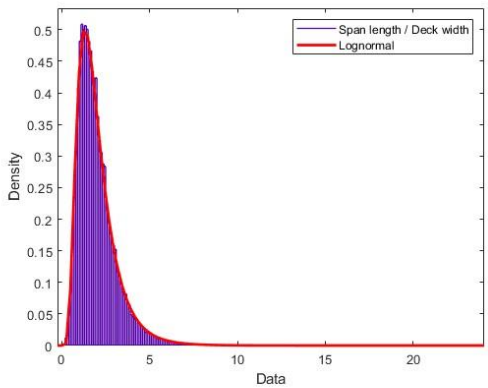

(e) Span length / deck depth distribution

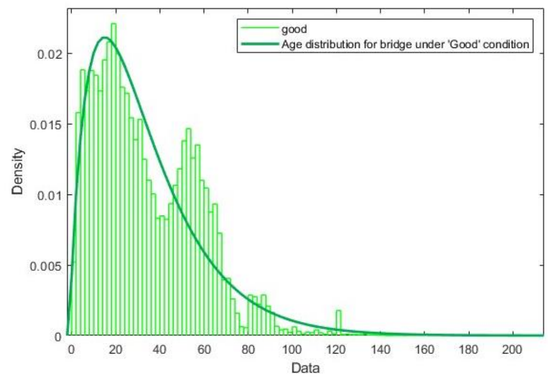

(f) Age for bridge under 'Good' condition’

Figure 3-15 Bridge attribute statistics and its fitted distribution

Table 3-2 Bridge attributes and their assumed probability distribution

Parameters	Type	Parameters	
		Mean μ	Standard deviation σ
Bridge Age (yr.)	Normal	50.3039	25.5445
Structure length (ft.)	Lognormal	4.69309	1.03716
Deck total width (ft.)	Lognormal	4.02351	0.609092
Maximum span length (ft.)	Lognormal	3.47158	0.490804
Span length/ Deck width ratio	Lognormal	0.55193	0.525882
Age for steel bridge under 'Good' condition	Logistic	31.633	13.4206
Age for steel bridge under 'Fair' condition	Logistic	54.2674	12.6455
Age for steel bridge under 'Poor' condition	Logistic	68.3607	12.8911

3.2.3 Machine learning classification using existing bridge data

After the data cleaning, 140933 bridges remain in the database for further assessment. Although the bridge condition assessment might be evaluated and predicted more accurately using the complete history of bridge information, the previous condition is not directly affected in the following repairing recommendation phase. Moreover, this section aims to find the possibility of predicting the bridge's general condition if only using the bridge's available features.

Since the machine learning techniques used in this research mainly focus on assessment classification, a demo model to evaluate the condition rating of a bridge by its general information was investigated. In the training and testing database selection, some relatively irrelevant features, such as structure number, owner agency, county name, intersected features, etc., are not selected for this classification task. Also, redundancy information such as 'year built' is deleted because the feature 'Bridge Age' was already selected. Thus, a total of 13 input features which contain Main Span Material, Main Span Design, Number of Span in Main Unit, Structure Length, Bridge Age, Deck Area, Length of Maximum Span, Deck Width, Approach Spans Material, Approach Span Design, Number of Approach Spans, Skew Angle, and Deck Structure Type has been introduced in the machine learning model and the output feature as Bridge Condition (Table 3-3). After a series of model training, the best performance model with the highest validation accuracy is found to be the decision tree (Fine tree, Figure 3-16) and random forest (Optimizable ensemble, Figure 3-17), which would reach a 67.6% validation accuracy. Moreover, when using the SVM for the model training, all the predictions are classified as 'Fair' while it could still reach relatively high accuracy (more than 50%) compared to Naive Bayes (Figure 3-18) or logistic regression (less than 50%). Thus, this dataset for the condition training is treated as unsuccessful. Comparisons of accuracy are listed in Table 3-4 and Table 3-5.

Table 3-3 Input features for the machine learning model

Input Features
Main Span Material
Main Span Design
Number of Spans in Main Unit
Structure Length (ft.)
Bridge Age (yr)
Deck Area (sq. ft.)
Approach Spans Material
Approach Spans Design
Number of Approach Spans
Deck Structure Type Code
Skew Angle (degrees)
Length of Maximum Span (ft.)
Deck Width - Out to Out (ft.)

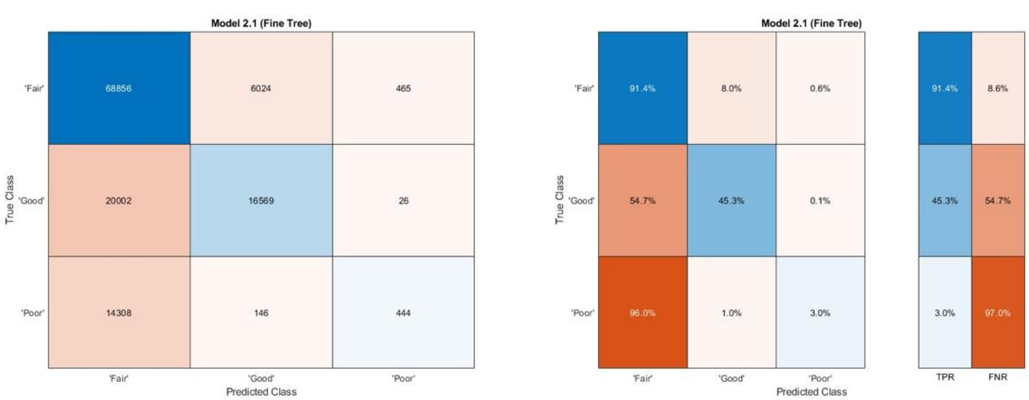

Figure 3-16 Plot of the confusion matrix and True Positive Rate (TPR) & False Negative Rate（FNR) of the decision tree model

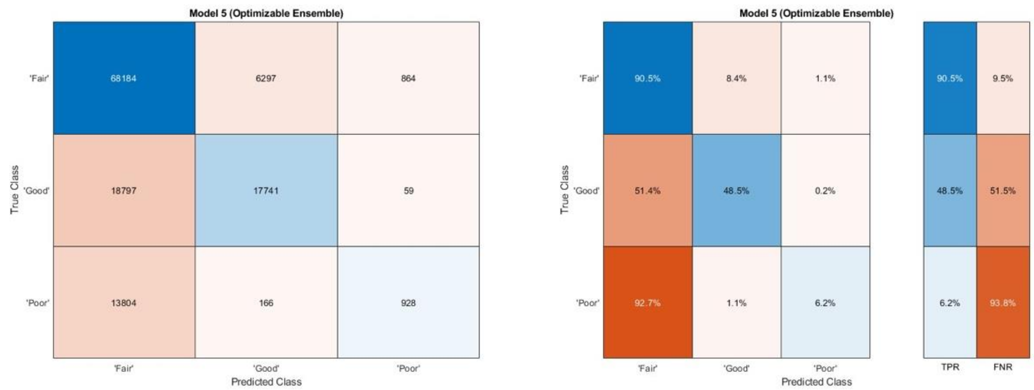

Figure 3-17 Plot of the confusion matrix and TPR &FNR of Random Forest model

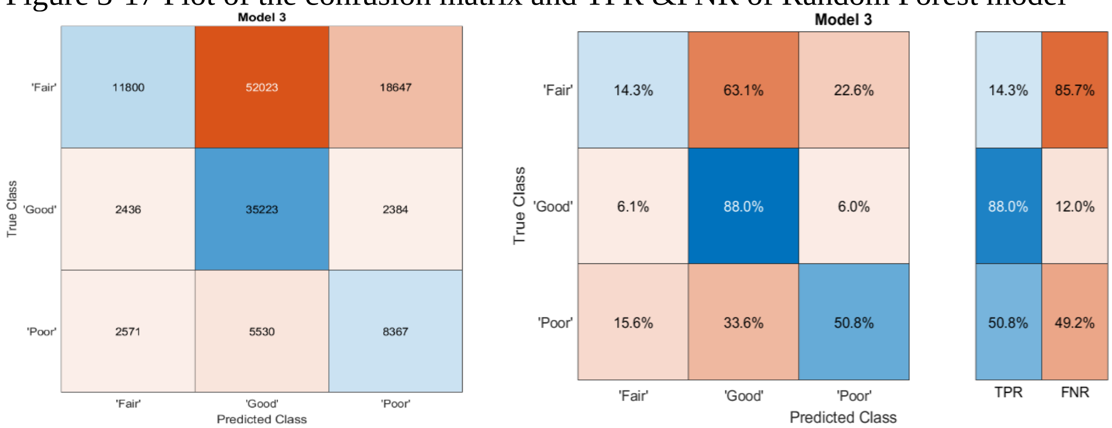

Figure 3-18 Plot of the confusion matrix and TPR &FNR of Naïve Bayes model

Table 3-4 Result comparison of trained models' accuracy using 5-fold cross-validation

Model Name	Accuracy
Fine tree	67.6%
Naïve Bayes	40.6%
Cubic SVM	30.8%
SVM Kernel	67.1%

Table 3-5 Result comparison of trained models' accuracy using 20% Holdout Validation

Model Name	Accuracy
Fine tree	67.7%
Naïve Bayes	39.6%
Linear SVM	66.9%
Logistic Regression	62.4%

3.3 Preparations of the database development

To understand the structural behavior over a long period, detailed inspection reports with sufficient load rating, load tests, and model establishment are needed. Since the initial database from NBI only covers geometry and condition rating, It is not recommended to randomly select a large number of samples from the initial database. Instead, a stratified sampling from features' distribution will be considered to randomly generate and expand the evaluation database.

3.3.1 Assessment database development and expansion

After the distributions of bridges, attributes have been fitted and generated, and the evaluation and assessment database has been established and expanded. The bridge configurations are randomly generated using Latin Hypercube Sampling (LHS) method. In this method, samples are selected randomly from the cumulative distribution function (CDF) by dividing evenly the probabilities and finding the corresponding values. An example of one-dimensional sampling is plotted in Figure 3-19.

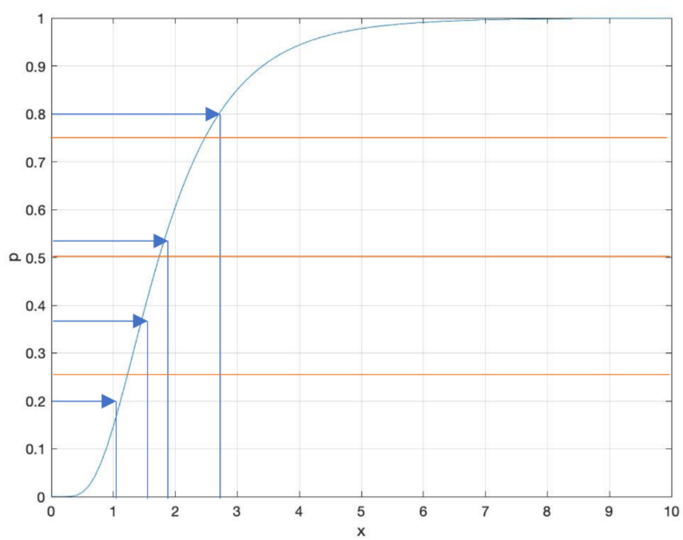

Figure 3-19 Example plot of 1 Dimensional LHS described in CDF

Then find the attribute values based on the inverse CDF (iCDF, Figure 3-20) formula from each individual distribution. The input attributes can be randomly generated based on their distribution and then be used as the configurations and properties of finite element models and expanded evaluation models.

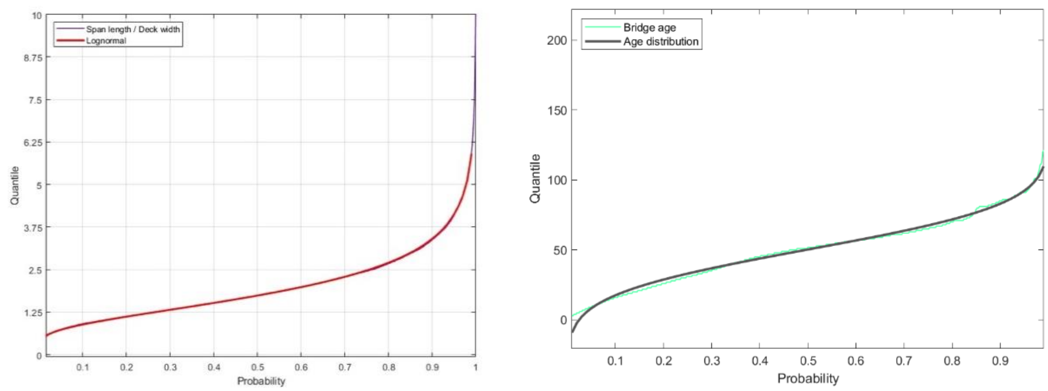

Figure 3-20 Example plot of inverse CDF (icdf) for features' distributions

3.3.2 Testing on repaired bridge finite element model

In this research, the long-term defects of bridges are defined as both material deterioration and structural performance reduction. And a series of sample two-span I girder bridges (Figure 3-21) was firstly generated to find the structural behavior between the original bridge, defected bridge, and repaired bridges.

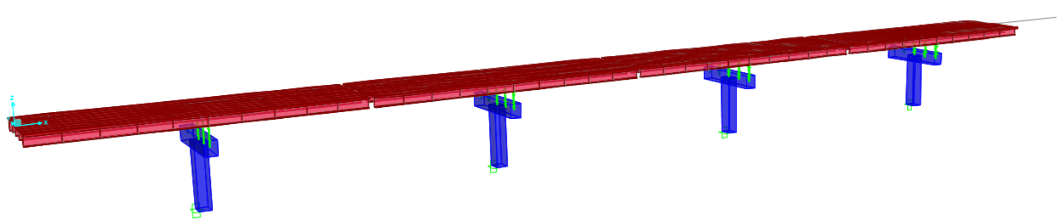

Figure 3-21 General configuration of sample bridges

The sample bridge is described as a 2-span I girder continuous bridge with a 50 ft span length and 375 inches span width. The material properties for concrete are 4000psi regular concrete, and the girders are selected grade 50 structural steel. The bridge was designed to have defects on span 1 (left span) near the bearing of the pier. Thus, a 20% section reduction on steel girders on the defect location is modeled, and a 20% section reduction for the concrete deck on the deteriorated location is also modeled. As of the repaired design, the section loss of steel is designed to be fixed to the original condition, while the deteriorated concrete is removed and replaced with new concrete with higher strength (60000psi) and different modulus (4ksi and 8ksi), respectively. The result of the bridge behavior under vertical load (DL in this case) and thermal load has been shown and compared in Figure 3-22 to Figure 3-32.

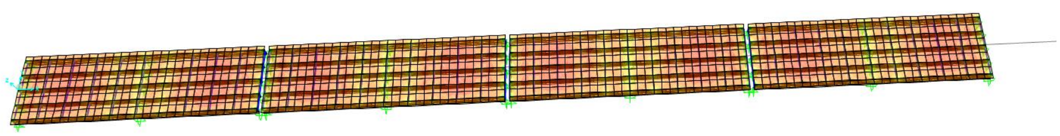

Figure 3-22 Stress plots for the bridge under dead load

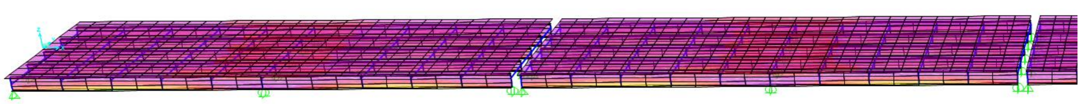

Figure 3-23 Stress plots for the bridge under thermal load

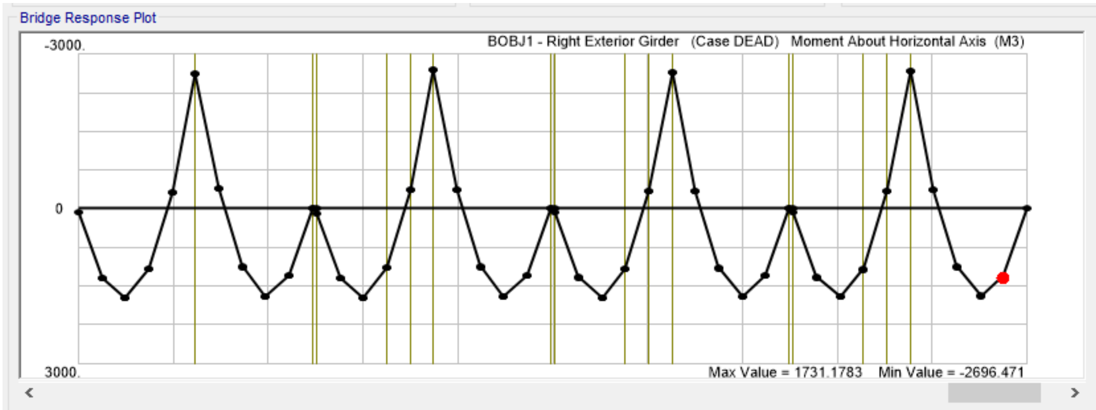

Figure 3-24 Reaction plots for the bridge under dead load

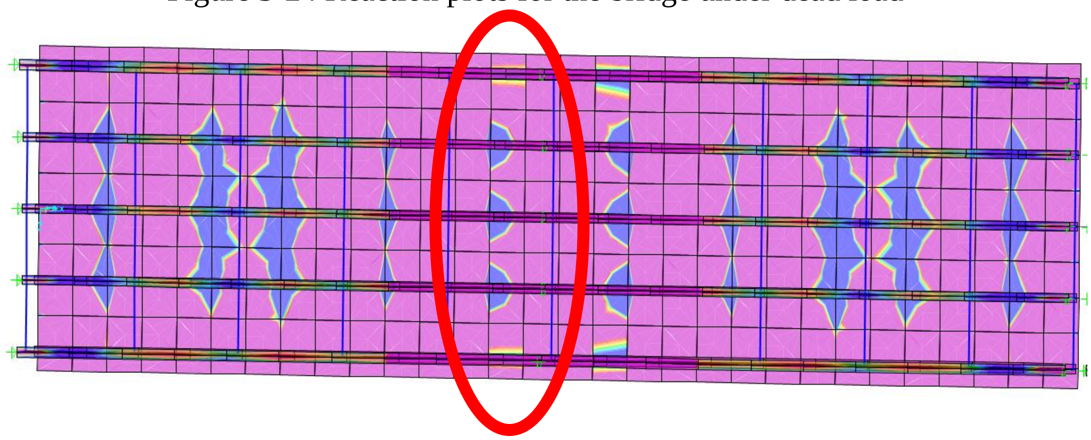

Figure 3-25 Stress plots for the original bridge under thermal load

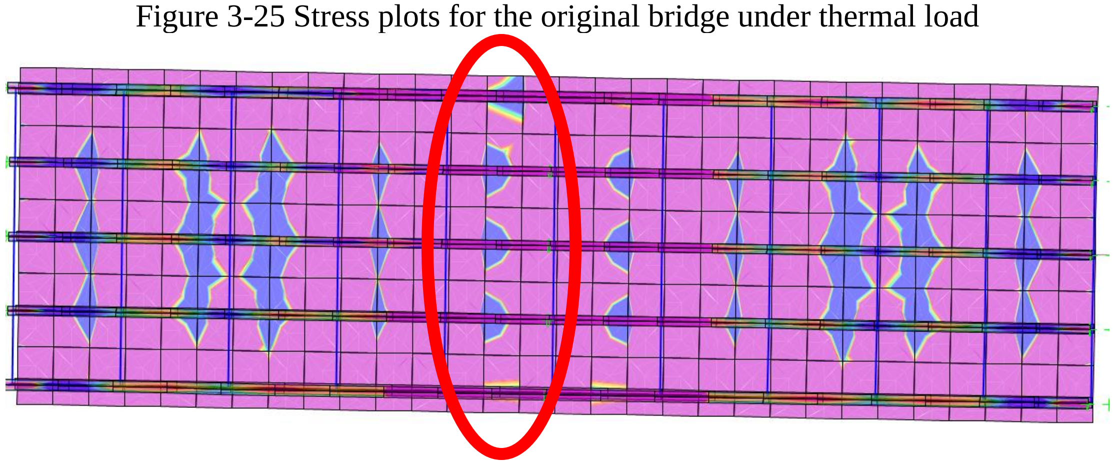

Figure 3-26 Stress plots for the deteriorated bridge under thermal load

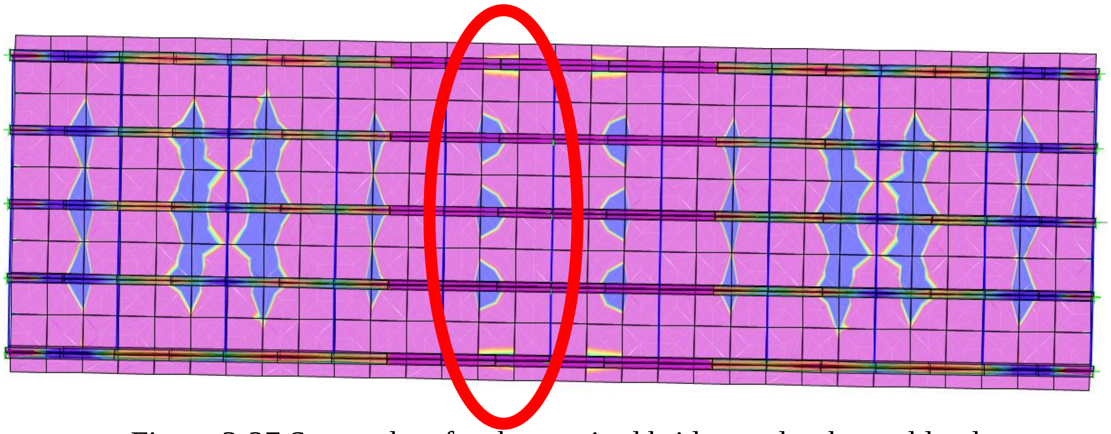

Figure 3-27 Stress plots for the repaired bridge under thermal load

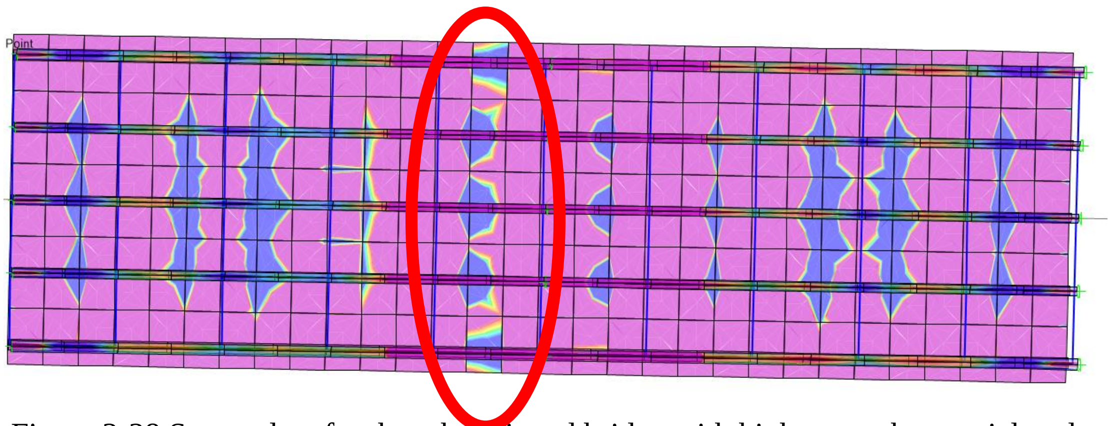

Figure 3-28 Stress plots for the rehabilitated bridge with high strength material under thermal load

It can be found from previous figures that the change in stress distribution is not obvious compared with the original bridge (Figure 3-23), the deteriorated bridge (Figure 3-24), and the repaired bridge (Figure 3-25 shows the repair with regular material, and Figure 3-26 shows the repair with high strength concrete). In particular, the repaired bridge model using the first design shows the same output as the original bridge, while the second design has a stress concentration locally at the repaired location.

Moreover, a series of refined models with fine meshes are also constructed and simulated under the same loading conditions (Figure 3-29 to Figure 3-32). The stress distribution is now obvious that the second design will lead to evenly distributed stress with slightly increasing at adjacent non- deteriorated areas, while the peak stress decreases compared to all other models.

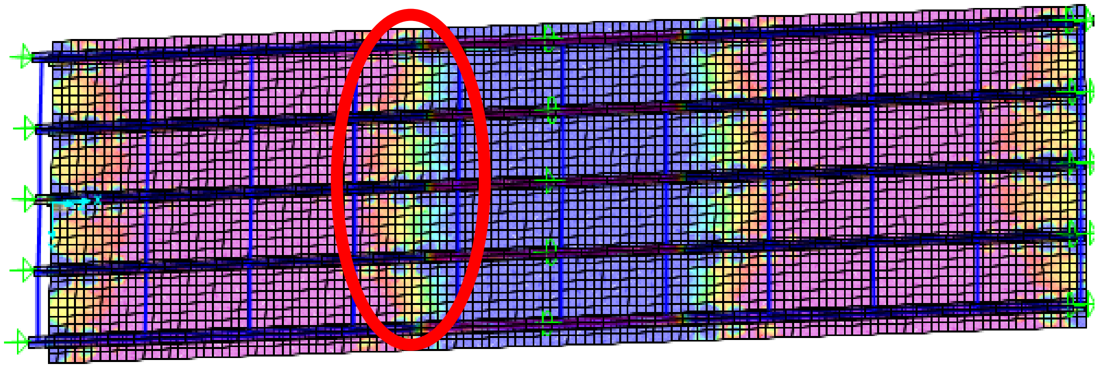

Figure 3-29 Stress plots for the original bridge under thermal load (Refine model)

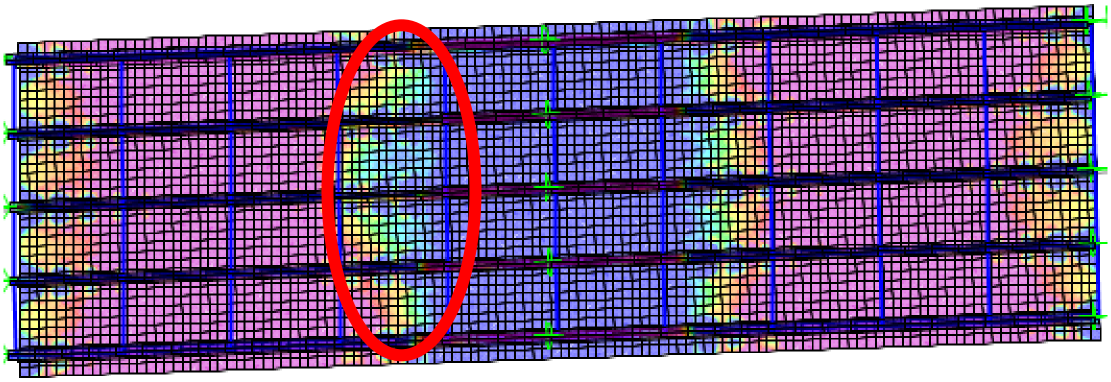

Figure 3-30 Stress plots for the deteriorated bridge under thermal load (Refine model)

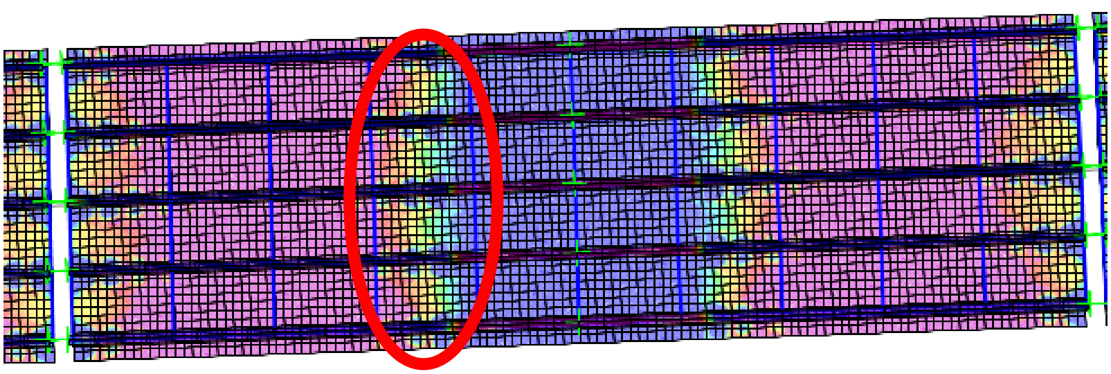

Figure 3-31 Stress plots for the repaired bridge under thermal load (Refine model)

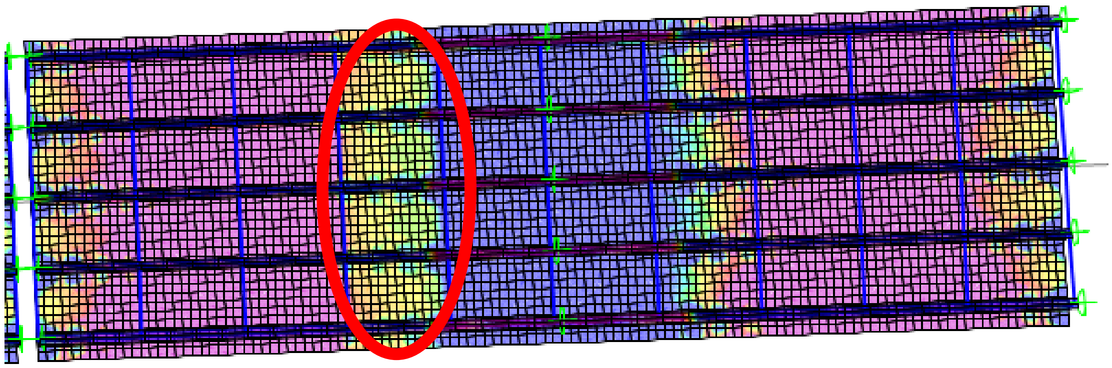

Figure 3-32 Stress plots for the rehabilitated bridge under thermal load (Refine model)

Chapter 4: Lab Test and Data Processing of HPFRC

In this chapter, a series of theoretical models and lab tests have been introduced to investigate the flexure performance of high-performance fiber-reinforced concrete (HPFRC) and cross-verifying a setup of sensors that will be used in the following chapters.

The material properties of fiber reinforced concrete (FRC), including compressive strength, tensile strength, flexure strength, modulus, shrinkage, creep, fracture or plastic damage, etc., could be complicated with a huge variant. Thus, this chapter has introduced some typically theoretical models for the nonlinearity of HPFRC in the first section; tested some self-made and commercial engineer cementitious composite (ECC) for their compressive strength, flexure strength, and young's modulus in the second section; and present some general comment after the data processing from the experiment.

4.1 Mixing design and lab test set-up for various types of HPFRC

Primarily, two types of HPFRC are thoroughly tested in the lab: self-mix ECCs and commercial products. Both had been tested and evaluated under the guideline of ASCE Specifications. Some general information about the design and mixing of the ECC has been introduced below, and the test set-up was also included in this section.

The research team in UMD investigated, selected, designed, and tested for three self-mix ECC based on previous studies that are shown in Table 4-1. Among these selections, Mix 1 is based on VTRC's mix of ECC and Victor Li's research(2013).

* Portions of this chapter previously appeared as: Fu, Chung C., A Pilot Application of Link Slab with Selected Material for MDTA Steel Bridges, Final report, Maryland Transportation Authority, April 2020

Besides, Mix 1 design is similar to ECC M45, which is the most original and widely used mix design formula. Mix 2 design is developed from UCI's (University of California Irvine) lab. This mixture design was the most recent design from the current record for ECC. And Mix 3 is based on Victor Li's publication in July 2013, which was focused on reducing crack sizes of ECC specimens. The research team has focused most on Victor Li's publications since Li's research and design for ECC was initially conducted, and almost all the ECC designs were generated and improved from his work.

Table 4-1 Three self-designed ECC mixes

Mixture		Cement	Sand	Fly ash	Water	Superplasticizer (HRWR*)	PVA Fibers	
Mix 1	lb/yd^3	948	758	1138	6261	12.32	44 (2%)	by vol
	weight fraction	1	0.8	1.2	0.66	0.013	0.04	
Mix 2	lb/yd^3	741	593	1630	519	12	44 (2%)	by vol
	weight fraction	1	0.8	2.2	0.7	0.012	0.06	
Mix 3	lb/yd^3	667	774	1468	567	6.67	44(2%)	by vol
	weight fraction	1	1.16	2.2	0.85	0.01	0.067	

* high-range water reducer

This experiment starts with self-mix ECC to reach more flexibility in observing the behavior of this cementitious composite. The research group performed laboratory tests of various ECC mixes to determine the compression strengths, flexural strengths, and shrinkages of these ECC mixes. Standards, specifications, and references that may involve in the following testing and analysis:

Casting, curing, and fresh concrete tests follow:

- ASTM C192/C192M Practice for Making and Curing Concrete Test Specimens in the Laboratory

- ASTM C138 Standard Test Method for Density (Unit Weight), Yield, and Air Content (Gravimetric) of Concrete
- VTRC Evaluation of High-Performance Fiber-Reinforced Concrete for Bridge Deck Connections, Closure Pours, and Joints
- Victor Li, Concrete Construction Handbook, Second Edition, Chapter 24
- Compressive strength and modulus of elasticity tests follow:
- ASTM C39 Standard Test Method for Compressive Strength of Cylindrical Concrete Specimens
- ASTM C469 Standard Test Method for Static Modulus of Elasticity and Poisson's Ratio of Concrete in Compression

Flexure tests follow:

- ASTM C78 Standard Test Method for Flexural Strength of Concrete (Using Simple Beam with Third-Point Loading)
- ASTM C1609 Standard Test Method for Flexural Performance of Fiber-Reinforced Concrete (Using Beam with Third-Point Loading)

Shrinkage tests follow:

- ASTM C157 Standard Test Method for Length Change of Hardened Hydraulic-Cement Mortar and Concrete

Among the self-mix ECC design and testing periods, 24 specimens were initially planned for testing, with four cylinders and four prisms per combination. However, during the mixing and testing of the existing formula, a large variant of the performance and potential segregation during production were observed. As a result, these designs were adjusted by trial and error. If the fresh concrete shows a sign of segregation or the compressive strength is less than 5000 psi in these serials of mixing, the entire batch is considered unsuccessful.

Thus, a total of 27 batches with 150 specimens were produced and tested within this experimental program by the research team using either a high shear mixer or a regular concrete mixer. During the whole mixing and testing period, there are 23 batches of ECC could be determined as successful with 134 specimens. It is proven that using the high shear mixer could be much easier to reach the required performance of the composite, while the regular concrete mixer needs to adjust the mixing time, the aggregate content, and the HRWR used in the design.

From previous studies, the mixing of HPFRC by the shear mixer was highly recommended, such as the high shear mixer (noted as a “small mixer”) the research team used in the lab. However, considering quantities and the accessibility in the field, the UMD research team focused on the mixing procedure of both types of concrete mixer. These experiments, including design, mixing, and testing, were conducted in the concrete laboratory of the National Ready Mixed Concrete Association (NRMCA). All machines and materials used are shown in Figure 4-3. Test setup and the summary of tested results shows in Figure 4-4, Figure 4-5, and Figure 4-7. The mixing procedures for the ECC are followed by the directions (Figure 4-1 and Figure 4-2):

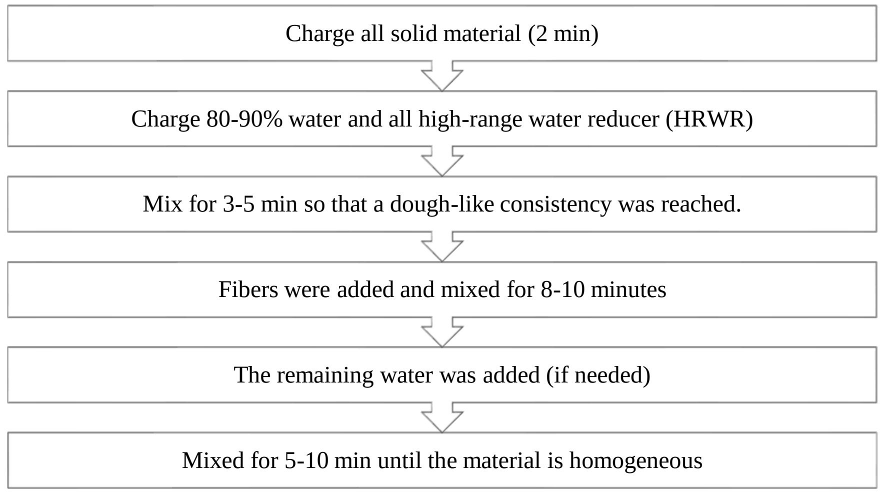

Figure 4-1 Flowchart for mixing ECC using a high shear mixer (small mixer)

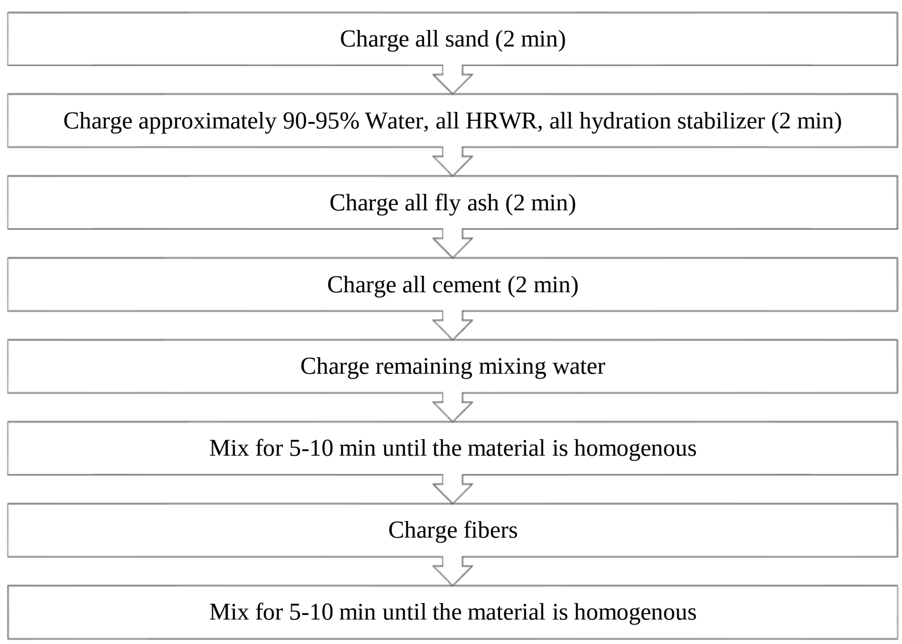

Figure 4-2 Flowchart for mixing ECC using a Regular Concrete Mixer (Large Mixer)

(a) Small Mixer

(b) Large Mixer

(c) PVA fiber

(d) Mixing Material
- Fiber, Cement. Sand, Fly ash, Water reducer (not shown), and Water

Figure 4-3 ECC lab mixes at the NRMCA's Lab in Greenbelt, MD

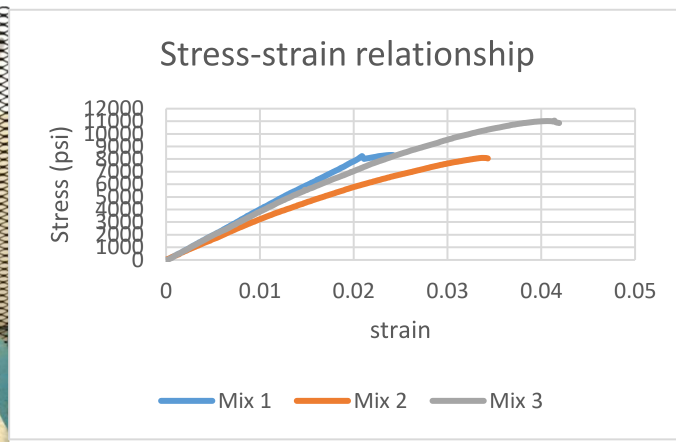

Figure 4-4 Compressive strength or Young's modulus test setup

Figure 4-5 Result of lab flexural test

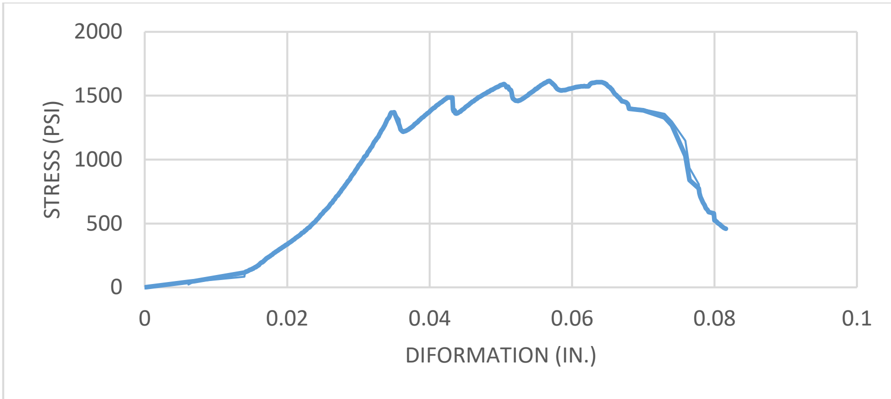

Figure 4-6 Typical ECC flexure performance

Figure 4-7 Room for storing and testing the material shrinkage

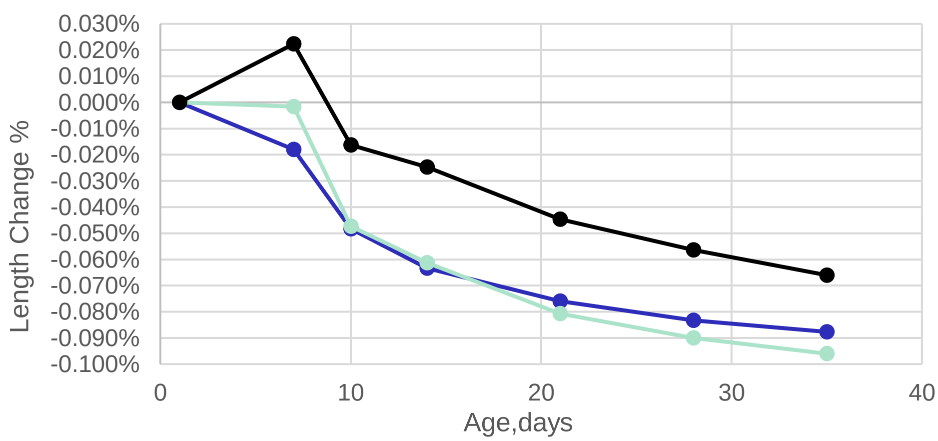

Figure 4-8 Shrinkage performance of three mix designs

Table 4-2 Average shrinkage changes for the 3 mixes

	Mix 1	Mix 2	Mix 3
7 Days	-0.018%	-0.002%	0.022%
7+7 Days	-0.063%	-0.061%	-0.025%
7+28 Days	-0.088%	-0.096%	-0.066%

Since the self-mix ECC shows a large variant during mixing and testing, further investigation was conducted, including sensor instrumentation and searching for commercial FRC. Then the *ductile ECC* (a commercial HPFRC product) was also tested and selected for the field testing to be conservative.

In this phase, three types of sensors, including BDI, strain gauges that are directly attached to the concrete surface, and embedded strain gauges (Figure 4-9), were investigated and tested for effectiveness and serviceability. Moreover, the renovative embedded strain gauges had then been calibrated and adopted for the lab and field tests.

Figure 4-9 Sensor Instrumentation in the Lab Test

4.2 Test results and data processing

In the self-mix ECC results comparisons, all the specimens were made using the regular concrete mixer to simulate the field condition and match the requirement of large quantities. Then chose an average value of each mix and had them listed for comparison.

Furthermore, based on the mixture data from the final full-batch mixes, results were compared with VTRC's results shown in Table 4-3.

Table 4-3 Compressive and flexure strength of self-mix ECC compared with VTRC's results

<table>
<tr><th rowspan="2">Mixture</th><th colspan="2">Compressive (psi)</th><th colspan="2">Flexure (psi)</th></tr>
<tr><th>7 Days</th><th>28 Days</th><th>7 Days</th><th>28 Days</th></tr>
<tr><td>Mix 1</td><td>7757</td><td>7940</td><td>1249</td><td>1508</td></tr>
<tr><td>Mix 2</td><td>6156</td><td>8092</td><td>1196</td><td>1089</td></tr>
<tr><td>Mix 3</td><td>9038</td><td>11214</td><td>1125</td><td>1404</td></tr>
<tr><td rowspan="2">VTRC Batch 1</td><td rowspan="2">4315</td><td rowspan="2">6920</td><td>670 (at first yield)</td><td>895</td></tr>
<tr><td>1070 (peak)</td><td>1440</td></tr>
<tr><td rowspan="2">VTRC Batch 2</td><td rowspan="2">4780</td><td rowspan="2">7865</td><td>645 (at first yield)</td><td>835</td></tr>
<tr><td>1190 (peak)</td><td>1465</td></tr>
</table>

For commercial ECC, which is the Elephant Armor in this section, a total of 15 specimens were used to test for the compressive strength, flexure strength, and Young's modulus. Moreover, four specimens with the configuration of 4 in.× 4 in.× 14in. were used for the calibration of sensors. During this experimental program, loading, deformation, and strain at the mid of the beam were also recorded from the same specimens and comparably discussed with respect to the acquired structural behavior properties.

Results are summarized in Table 4-4, Table 4-5, Table 4-6, and Table 4-7.

Table 4-4 Compression Strength (ASTM C39)

Curing Day	Sample Size (in)	Result (psi)
3	3X6	6926*
7	4X8	6920*
7	3X6	5305
7	3X6	5646
7	3X6	5851
7	3X6	5859
7	3X6	6300
7	3X6	6468
7 Day Moist Cured Avg		5905

*Not moist cured

Table 4-5 Modulus (ASTM C469)

Curing Day	Sample Size (in)	Result (ksi)
7	4X8	1181.3
7	4X8	1087.2
Avg		1134.2

Table 4-6 Flexure Strength (ASTM 1609)

Curing Day	Sample size (in)	Yield Strength (psi)
7	4X4X14	815.0
7	4X4X14	802.5
Avg.		808.8

Table 4-7 EA DOT material property summary

<table>
<tr><th rowspan="2"></th><th colspan="2">7 days</th><th colspan="2">28 days</th></tr>
<tr><th>Dry curing</th><th>Moist curing</th><th>Dry curing</th><th>Moist curing</th></tr>
<tr><td rowspan="2">Modulus</td><td>1181.32 (ksi)</td><td>N/A</td><td rowspan="2">1252.47 (ksi)</td><td rowspan="2">1322.65 (ksi)</td></tr>
<tr><td>1087.24 (ksi)</td><td>N/A</td></tr>
<tr><td>Compression</td><td>6000 (psi)</td><td>5300 (psi)</td><td>7580 (psi)</td><td>6646 (psi)</td></tr>
</table>

Moreover, several interesting phenomena have been discovered through the data processing procedure. As mentioned before, several sets of 4 in.× 4 in.× 14in beams were used to test for both flexure performance and the effectiveness of strain gauges. One of the procedures is to apply cyclic load on these beams using the same configuration of the third point test. The load applied to the specimen was from 0 to 1000 lbs, with the test machine's lowest increasing rate (10 lbs/sec). Then released and repeat with the 1000 lbs loading, and then it increases to 2000 lbs. The loading process follows the trend of 1000lbs, 1000 lbs, 2000 lbs, 2000 lbs, 3000lbs, 3000 lbs, 4000 lbs, 4000 lbs, and to the maximum. Figure 4-10 shows a set of raw data from the system indicating a similar trend of top and bottom sensors with a delay in time. A calibrated example is shown in Figure 4-11. The sensitivity of the top and bottom layer sensor could be re-plotted (Figure 4-12) based on the stress and strain captured from the universal test machine and the strain gauges. It can be seen that the maximum stress under pure bending could reach to 400 psi in the elastic period. And shows their ductility during the plastic deformation and microcracks development under over 600 psi.

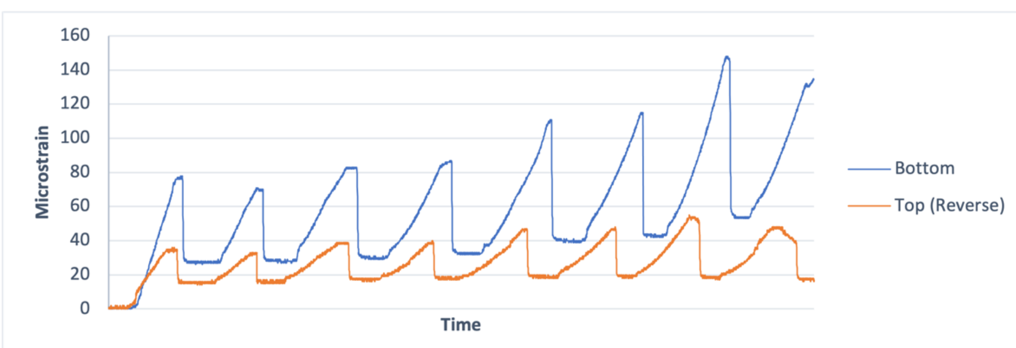

Figure 4-10 Raw data example read from the system

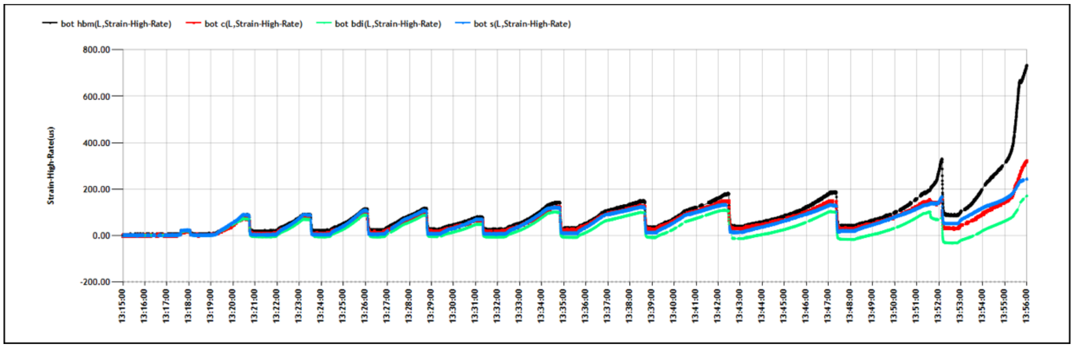

Figure 4-11 Data processing after calibration

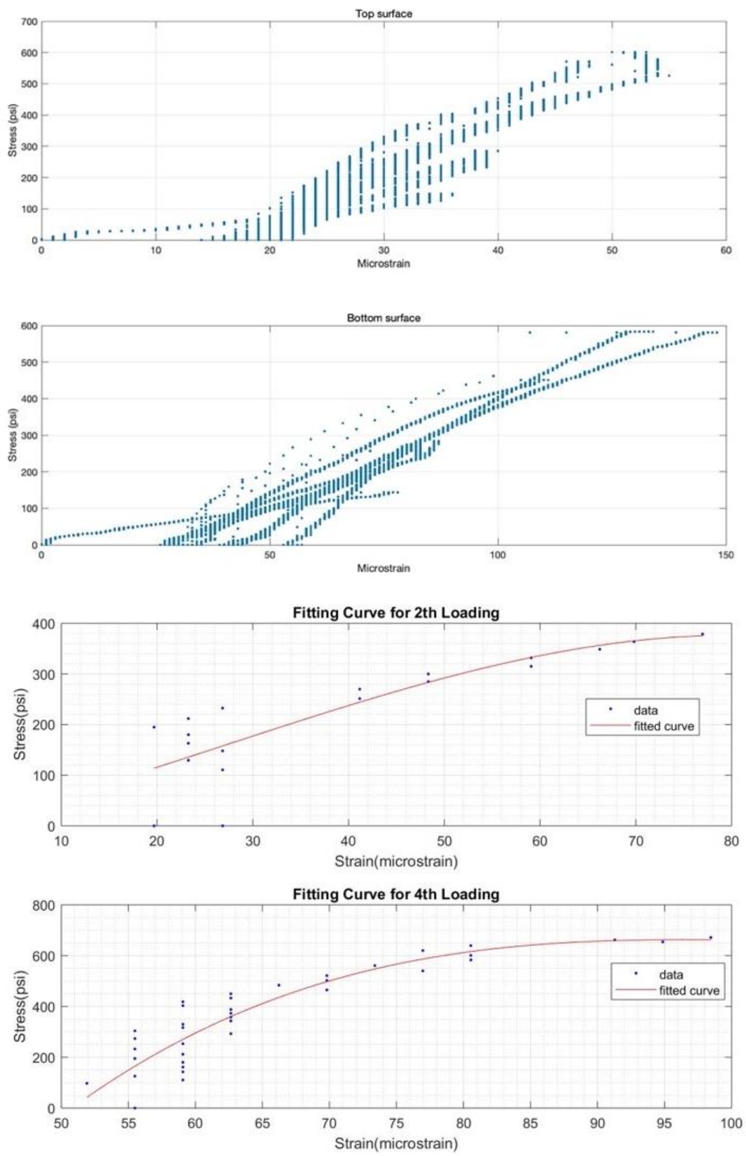

Figure 4-12 Stress-strain relationship under bending

4.3 LSTM model training, updating, and validation

After the sensor validation and data calibration process of these tests, the data captured from the specimen can be treated as original samples that to test the effectiveness of the LSTM deep learning model for short-term forecasting in the long-term structural health monitoring. This chapter selected the cyclic loading testing case as the sample training set. This is because the typical structural health monitoring data for strain, longitudinal displacement, and bearing or pier tilting is expected to show a cyclic trend with small increases or decreases in a long-term manner. Thus, the cyclic loading test for the beam is perfect for performing the cyclic trend through cyclic and increasing applied force and increasing in deformation due to strain hardening.

4.3.1 Specimen behavior forecasting model training with original data

A series of four-point bending tests with cyclic loading added was selected for the model training and evaluation. In this initial model training, the whole period of the experiment was divided into two parts: the first 75% of the original data as the training set and 25% of the data as the testing set (forecast). The model was trained in Matlab using the Adam optimizer with a maximum of 250 epochs. To prevent the gradients from exploding, the gradient threshold was set to 1. the initial learning rate was specified as 0.003, and drop the learning rate after 50 epochs by multiplying by a factor of 0.2.

The initial dataset for the beam strain under the cyclic loading test was established, the first trial of model training was conducted using Matlab (2022), and the behavior was forecasted (Figure 4-13). The comparison between the actual data and forecasting data is plotted in Figure 4-14. From the comparison, we can see that the training model cannot predict performance successfully. Thus, adjustment to the data pre-processing, change of training options, and adding validation set during the model training are essential to improve the effectiveness of the forecasting model.

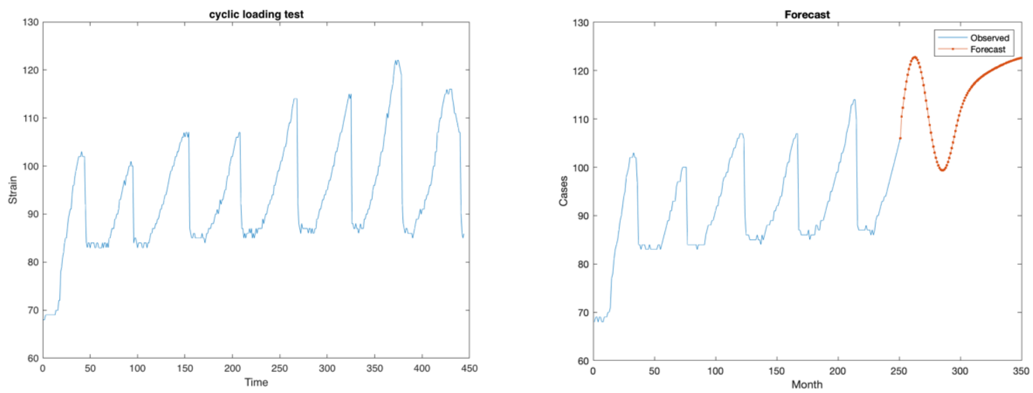

(a) Original data plot (b) Observed data with the last 25% forecasting

Figure 4-13 Strain plots for the specimen under cyclic loading

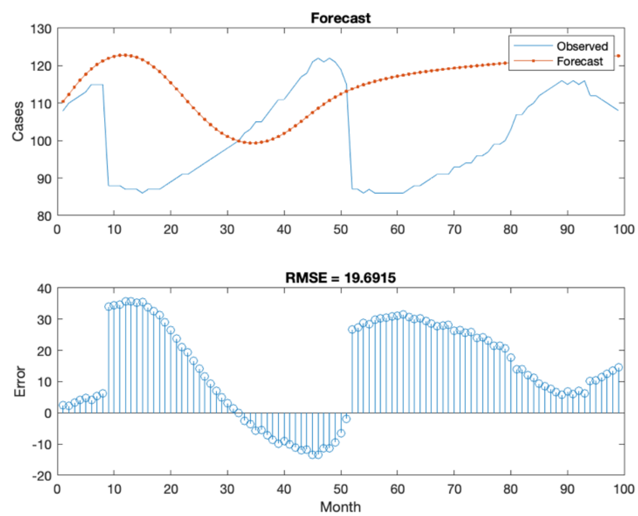

Figure 4-14 Details comparison of the prediction and the actual data

4.3.2 Model updating

The first updates on the training process are to add the validation set and adjust the learning rate dropout period and learning rate drops factor when defining the LSTM network. Then the training process can be evaluated with one more feature, i.e., the loss trend of the validation set (Figure 4-15). This visualized method could help to identify how to update the training model. When the loss trend keeps decreasing by iterations for both the training set and validation set and reaches a relatively low area, the model is under a relatively good performance.

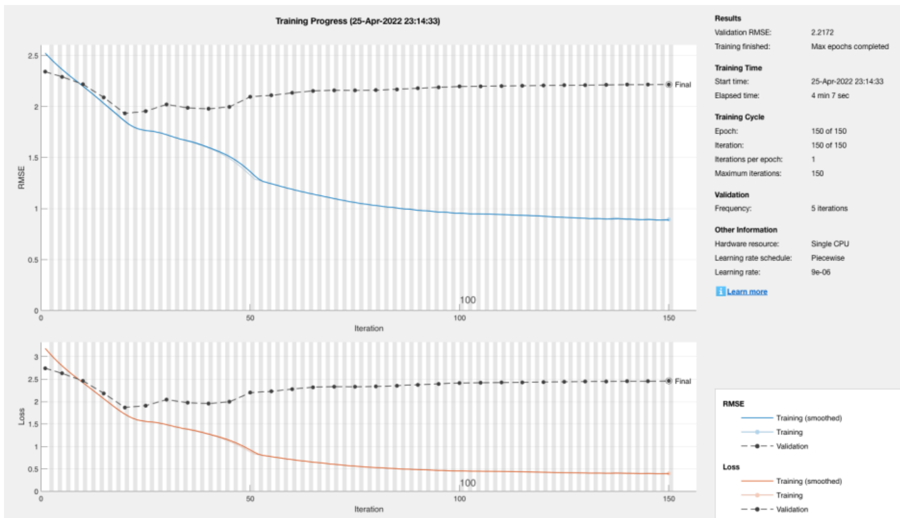

Figure 4-15 Training progress of the updated LSTM network with a validation set

Figure 4-15 shows a trend that the loss of the training set was decreasing while the validation set showed a decrease then increased. Then the prediction model compared to the measured data is plotted in Figure 4-16 and Figure 4-17.

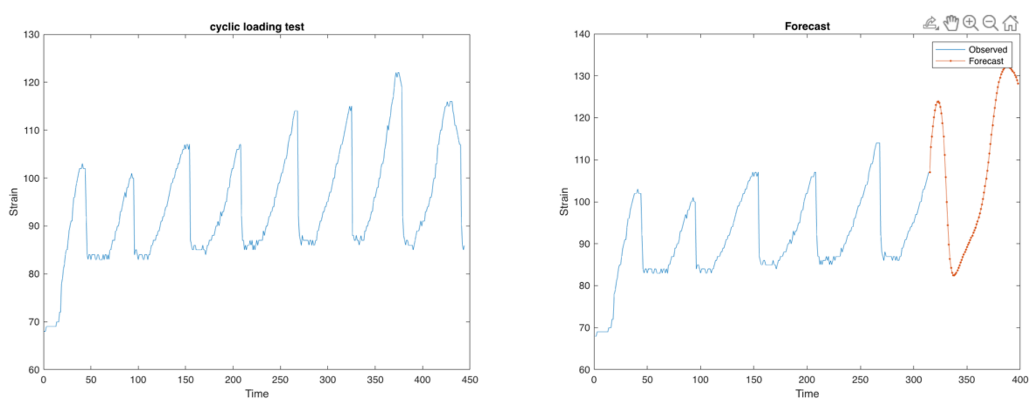

(a) Original data plot (b) Observed data with the last 25% forecasting

Figure 4-16 Strain plots for the specimen under cyclic loading

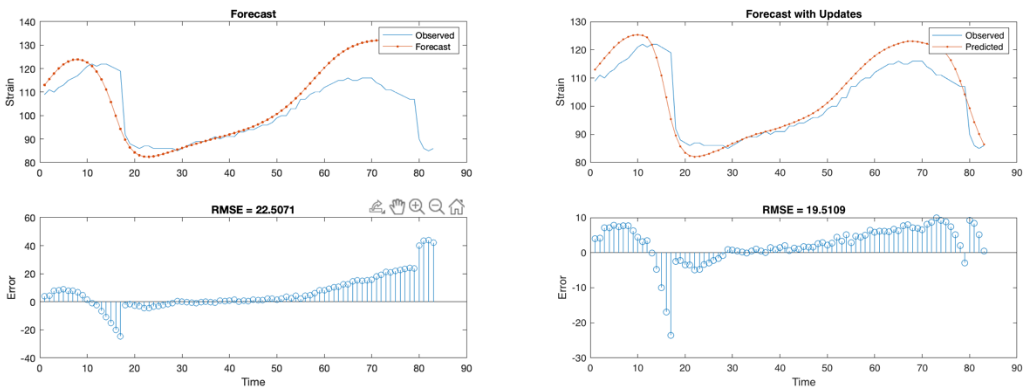

Figure 4-17 Details comparison of the prediction and the actual data

Although the performance has improved by adjusting the maximum iteration epochs, the length of each input data point, the initial learning rate, learning drop period and factor, etc., the trend of the forecast model is still a little bit off at the last 10% range. Thus, the model is updated with data grouping and filtering.

Figure 4-18, Figure 4-19, and Figure 4-20 demonstrate the final version of the updated forecasting model with a relatively low loss in the testing set. Considering the capture rate of the sensor is relatively high, filtered data to develop a new dataset that each point i contains an average value of x points. Thus, the size of the new database was reduced to $1/x$ of the original dataset. However, the performance has been improved, and the final model is generated while the effectiveness of the structure condition forecasting is verified.

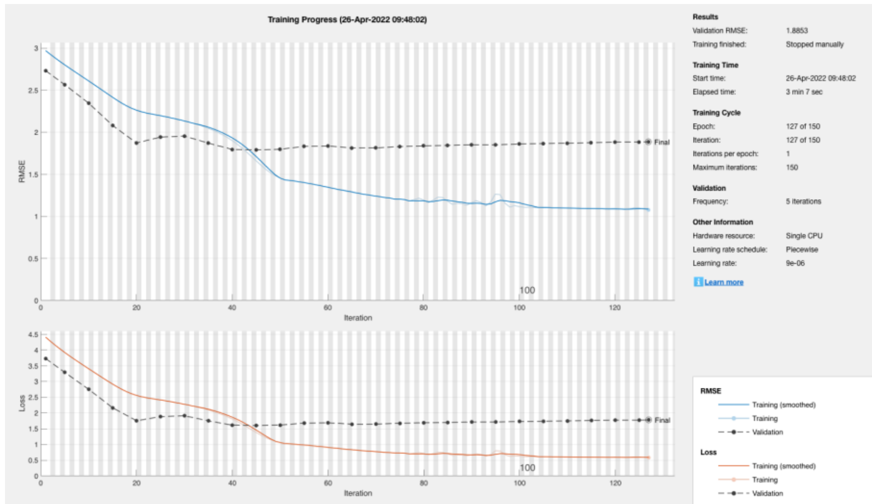

Figure 4-18 Training progress of the updated LSTM network with a validation set

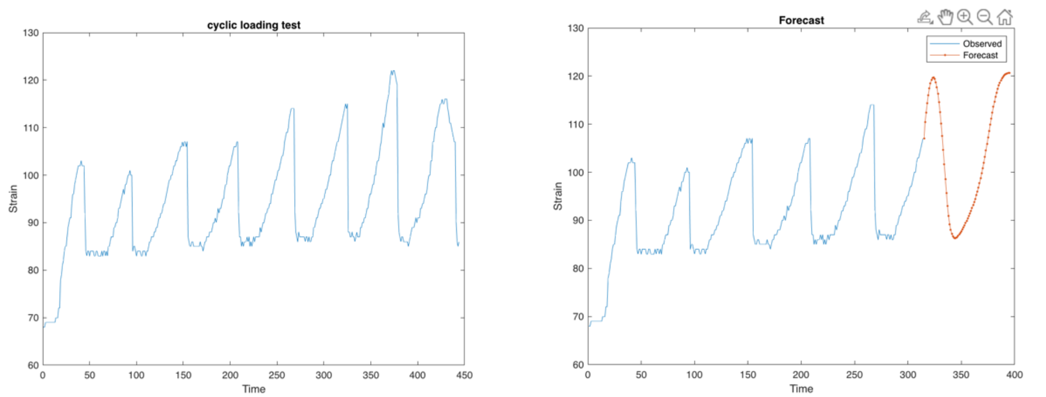

(a) Original data plot (b) Observed data with the last 25% forecasting

Figure 4-19 Strain plots for the specimen under cyclic loading

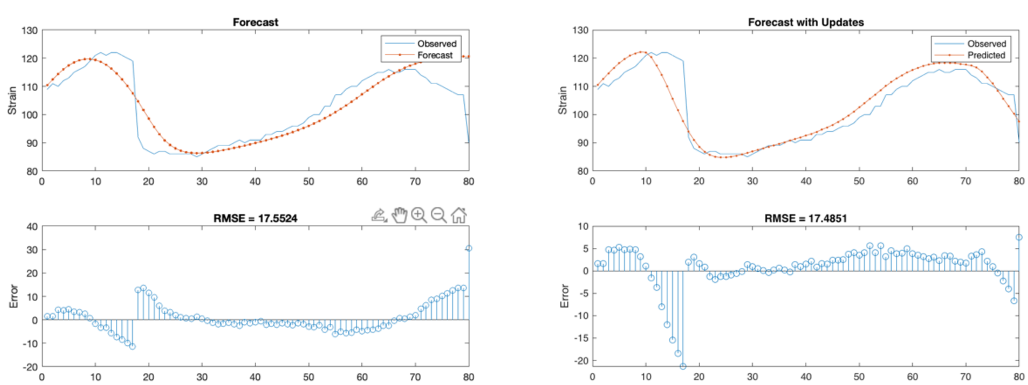

Figure 4-20 Details comparison of the prediction and the actual data

4.4 Discussion on the material selections

For self-mix ECC, all these three mix designs could meet the fundamental requirement of compressive strength (set as 4500 psi) in the first seven days. Considering these FRC would be used as the construction material of the link slab system, which needs higher flexure strength, Mix 1 and Mix 3 are more competitive as the best selection. All these three mixes have lower shrinkage rates. However, self-mix ECC showed a large variation in its performance and highly depended on the material sources, field environments, mixing procedures, and curing methods that cannot be avoided. Moreover, there will be a 25%-30% deduction of compression and flexure in the field due to changes in curing conditions. Thus, self-mix ECC should be carefully applied in the field and for construction.

The commercial pre-mixed ECC shows a better consistency in modulus, compressive strength, and flexure performance. There is not much difference between moist curing and dry curing compared with their performance under axial load, while the flexure performance has slightly increased when moist curing. Besides, Young's modulus that was tested in the NRMCA lab (approximate 1000 ksi) was relatively low as compared to the document shown by the company (2207.5 ksi). Thus, further discussion on material selection should be conducted when applying to the field.

Chapter 5: Structural Behavior Analysis of Prototype Bridges with Link Slabs

5.1 Model selection and establishment

5.1.1 Model and material selection

In this chapter, all the model was established and refined using the commercial finite element analysis software CSiBridge (2017 version). Since the primary goal is to simulate the structural behavior of the entire bridge after constructing the link slab system, finite element models that used in this section are all adopting 3D shell elements for the entire bridge superstructures, which mainly include decks, girders, diaphragms, and the newly constructed link slabs. To simplify this process and only focus on the behavior of the existing bridge and newly constructed link slabs, the two-span simply supported I girder steel bridge was selected as the original model (Figure 5-1).

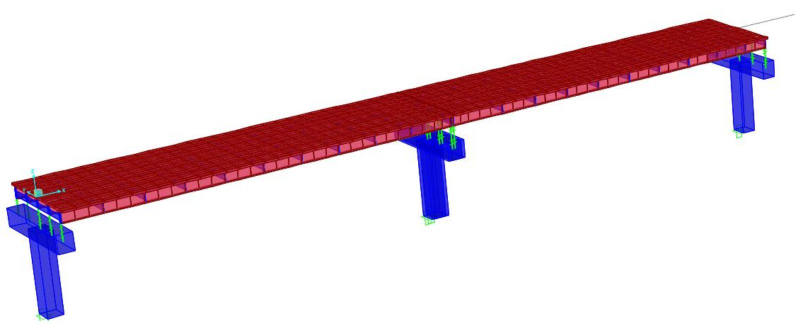

Figure 5-1 General Example of the Original two-span bridge model

In this model, bearings on both abutments are designed as fixed conditions and simplified as pin connections in x, y, and z directions with allowance in rotation.

Bearing at bent (pier in the middle) was designed as expansion bearings and modeled as roller where only restraint on z (vertical) direction.

Moreover, based on previous research and analysis for link slabs, the bearing condition should be changed if the design for the link slabs is proper. Typically, bearings should be replaced with elastomeric bearings with the ability to move along the longitudinal direction and only leave one bearing above the pier at the center of the entire bridge as the fixed condition. To simulate these changes in the analytical models and demonstrate the behavior of the link slab, and show the consistency of the structure, fixed bearings at one abutment were then released to be roller bearings while keeping the mid-span as rollers in order to transfer and release the stress caused by thermal expansion and contraction of the entire bridge.

To simulate the debond zone of the link slab, all the models firstly defined the length of the debond zone and then removed the constraints between the link slab and the girder underneath. Then make these two surfaces as contact only.

The original bridge model was designed as a two-lane, two-span, with the variation in span lengths. The bridge's width is 35 ft, with five equally spacing steel girders supporting the 7-inches concrete decks. The material for the steel girders is Grade 50 structural steel that follows the ASTM standard A709. And the concrete for bridge decks was used regular concrete with the compressive strength $f_c' = 4000$ psi.

The material chosen for constructing link slabs is extended from regular concrete to fiber-reinforced concrete that to employ its ductility and better performance under bending moments. The nonlinear behavior of the link slab material using HPFRC is simulated based on the uniaxial compression stress-strain relationships

(Figure 5-2), and the material properties for the existing bridge were simulated using the value of typical commercial products.

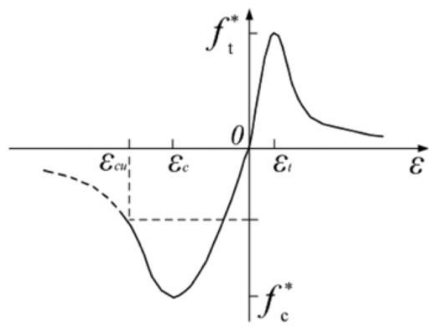

Figure 5-2 Finite Element Model to Simulate the HPFRC used in Link Slabs

5.1.2 Assessments criteria of the bridge with newly constructed link slab

Based on the guidance and intention of the bridge preservative maintenance program, the full assessment of the design will include both the effectiveness of the component (i.e., link slab), the potential negative impact on the existing structure (original bridge), and the cost-benefit analysis that shows the design and construction will indeed reduce the cost in its entire service life while not decrease the safety of the existing structure. Since all the actual designs would follow the codes, standards, specifications, and sometimes the excessive finite element analysis software, respectively. This parametric study would ignore the load combination with the specification requirements and only consider the performance of the structure under a single load type.

5.2 Structural behavior analysis

The failure mechanism was observed and investigated by many researchers, and the general failure type includes but is not limited to: (1) longitudinal displacement of the girder; (2) girder end rotation; (3) upturned of the beam end; and (4) the uneven settlement (Wang et al. 2019). The link slab on a bridge is placed above the beam gap (joint filling) of a simply supported bridge, and because of its installation with relatively weak stiffness, it has unique stress characteristics and failure types (Figure 5-3). These failure types, after investigation, are determined as a result caused mainly by the live load, thermal load, and uneven settlement of the foundation. Some crack prevention and post-processing procedures were typically designed before the installation of the link slabs.

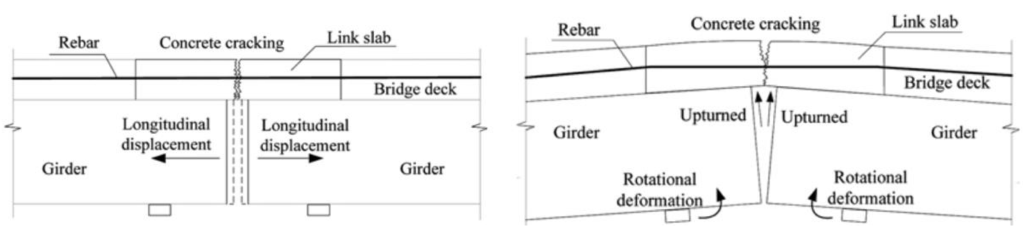

(a) longitudinal displacement of girder (b) upturned of girder end

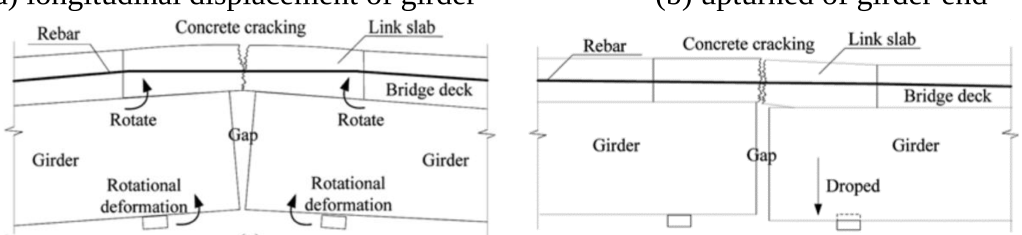

(c) Girder end rotation (d) uneven settlement

Figure 5-3 Typical failure type of link slabs (Wang et al. 2019)

5.3 Parametric study for the preventive maintenance bridge with link slabs

In this section, a series of parametric studies with 90 models are generated to establish the general idea of the structural behavior of the whole bridge with the same cross-section, i.e., a five-girder bridge with equal spacing (Figure 5-4). The initial dataset for the post-repaired bridge assessment is also generated based on these model results. Among these models, some primary parameters, which are the materials used for the link slab system, span lengths of the bridge, skew angles, as well as the lengths and depth of the link slab, are used for the input to see the difference between these models. Besides, the budget for the link slab construction is also included in the final evaluation due to the requirement of the preventive maintenance program. This chapter has defined the performance of the maintenance design plan and labeled all the models with a rating as the output.

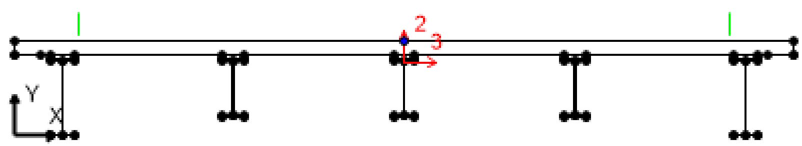

Figure 5-4 Section Model of the Bridge

To simulate the general material used for the link slab system, this study uses three types of ultra-high-performance reinforcement concrete with high ductility and one regular concrete with the same parameters as the original bridge decks. In this study, five bridges with similar configurations are simulated side by side (Figure 5-5), and the joint fillings from left to the right are labeled as the expansion joint; regular concrete (RC) link slab, ECC link slab, UHPC (Type 1) link slab, and UHPC (Type 2) link slab, respectively. Some general material properties used in the ductile link slab design are from the previous lab test result and experiments. And the summary is listed in Table 5-1.

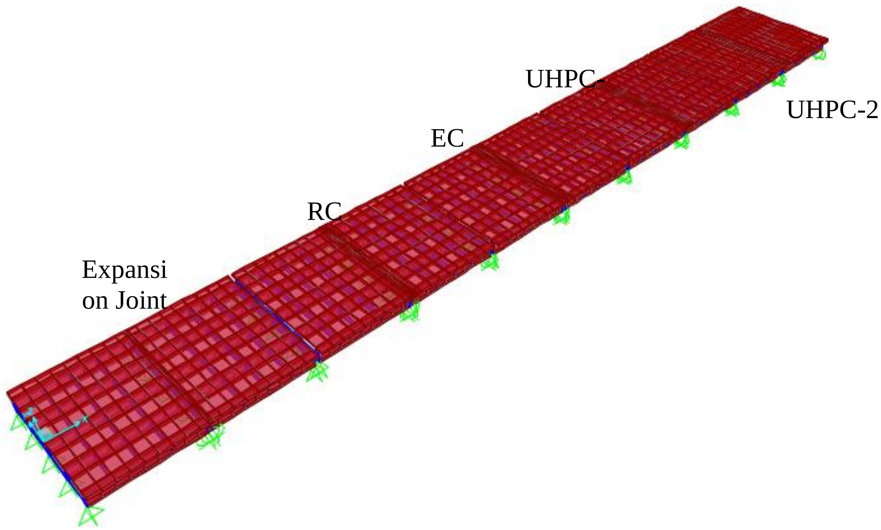

Figure 5-5 One set of parametric studies that used the different materials for link slab

Table 5-1 Summary of Material Properties

Material Type	Compressive strength	Young's Modulus	Coefficient of thermal expansion	Weight per cubic feet
RC	4,000 psi	4,000 ksi	$5.5 \times 10^{-6}/°F$	150 lb
ECC	6,000 ksi	1,000 ksi	$5.5 \times 10^{-6}/°F$	120 lb
UHPC-TYPE 1	20,000 psi	3,800 ksi	$8.2 \times 10^{-6}/°F$	155 lb
UHPC-TYPE 2	20,000 psi	8,000 ksi	$8.2 \times 10^{-6}/°F$	155 lb

Moreover, span lengths from 20 ft to 120 ft are developed for each set of bridges. The skew angles from 0 to 45° are investigated under the same span length of 50 ft., and the change of link slab width (from 4 ft to 10 ft), the link slab depth (partially with 2" or 4" depth) or full depth (7 inches in this design), and the length of debond zone (1/2 of the length of link slab or no debond) were constructed for comparison. Other parameters may be included in this parametric study shortly.

5.4 Result and conclusion of the parametric study

Using the 20ft. span length, for example, the bending moment in the link slab will increase (Figure 5-6) with its material properties, in this case, primarily based on the young's modulus. And the stress distribution due to temperature change and heat transfer has shown in Figure 5-7. From the 2D diagram with the stress of all slabs, it has been shown that the stress distribution in the link slab is uneven, with a large variation in the RC and UHPC link slabs. Thus, the stress contour has been plotted to demonstrate the distribution more clearly (Figure 5-8 and Figure 5-9).

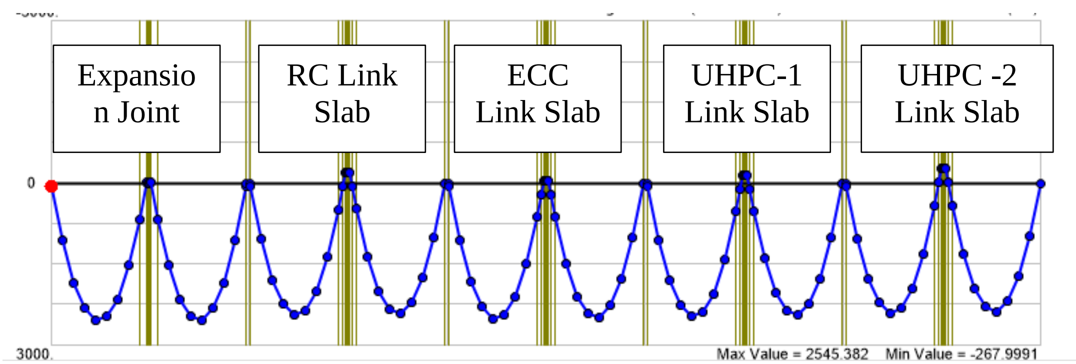

Figure 5-6 Bridges' moment about the horizontal axis under dead load (Span length 20 ft)

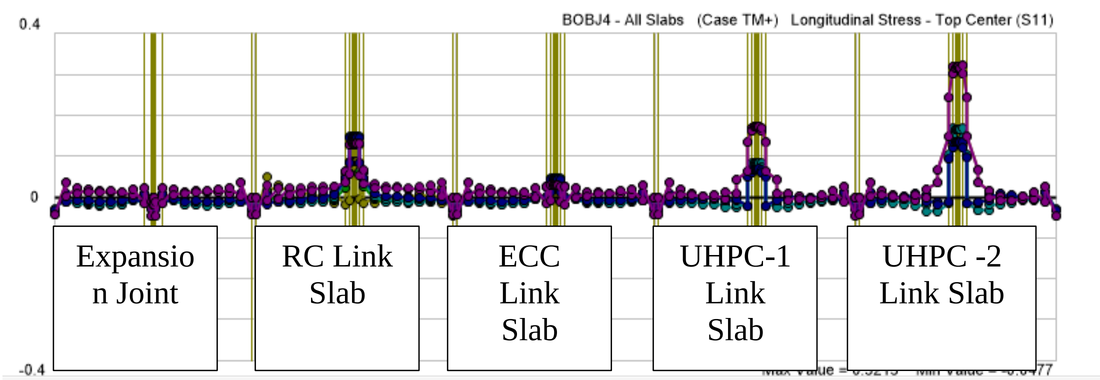

Figure 5-7 Longitudinal stress distribution under the temperature increasing uniformly of 55°F (20 ft)

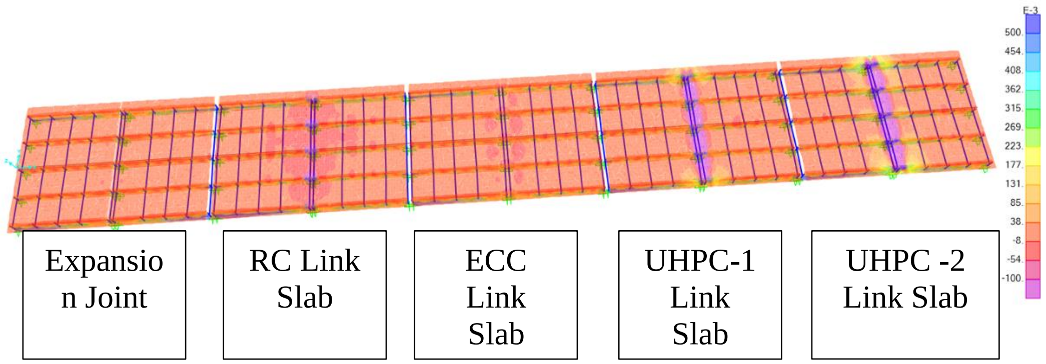

Figure 5-8 Stress distribution of the bridge under temperature gradient. (AASHTO Zone 2)

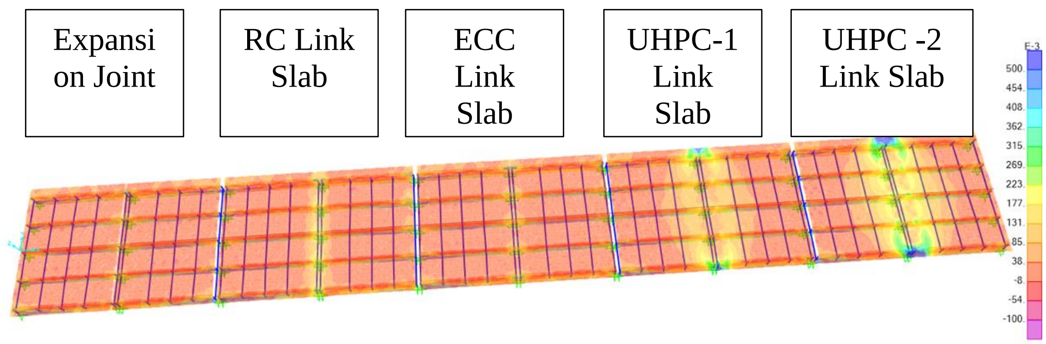

Figure 5-9 Stress distribution of the bridge under thermal expansions. (Increasing 55°F)

From the plot of stress contour due to temperature changes in the bridge, which is typically divided to the thermal expansion/ contraction, and the temperature gradient, it can be seen that the stress distribution is not uniformly distributed within the bridge decks and link slabs. Generally, the stress will significantly increase while it approaches the edge of the UHPC or RC link slab system. Notably, the outer edge has more considerable stress compared with the mid-parts. The (average) smallest stress will always be found compared with other link slab systems. This phenomenon was basically due to the ECC's higher ductility and lowest Young’s modulus. For regular concrete link slabs, stresses are relatively in a small range. However, they would cause potential cracks since this brittle material has the lowest ductility under tensile strength or bending moment. When using UHPCs as the construction material of link slabs, the stress within the link slab system and the stress in the adjacent decks near the bonding area increased significantly. As many previously investigated before, cracks might be allowed to show in the link slab system, and it shows a "strain control" strategy when applying the ductile fiber reinforce concrete as the construction material. Thus, the highest stress in the UHPC link slab would sometimes not be the most significant issue, but the large stress concentrated on the edge of adjacent bridge decks.

Figure 5-10 compares the stress distribution of the bridge decks among the difference in span lengths (40 ft, 60 ft, and 80 ft per span, respectively) and material properties. As per the prediction, the displacement along the longitudinal direction increases linearly as its span lengths increase. However, the stresses that accumulate in the link slabs are not increased linearly. With the lowest stress concentration observed in the ECC link slab for each set of bridge models, 'RC link slab' itself or 'UHPC-type 2 adjacent deck' makes them in the most severe condition since the material (regular concrete) is designed not to resist tension without the reinforcement inside.

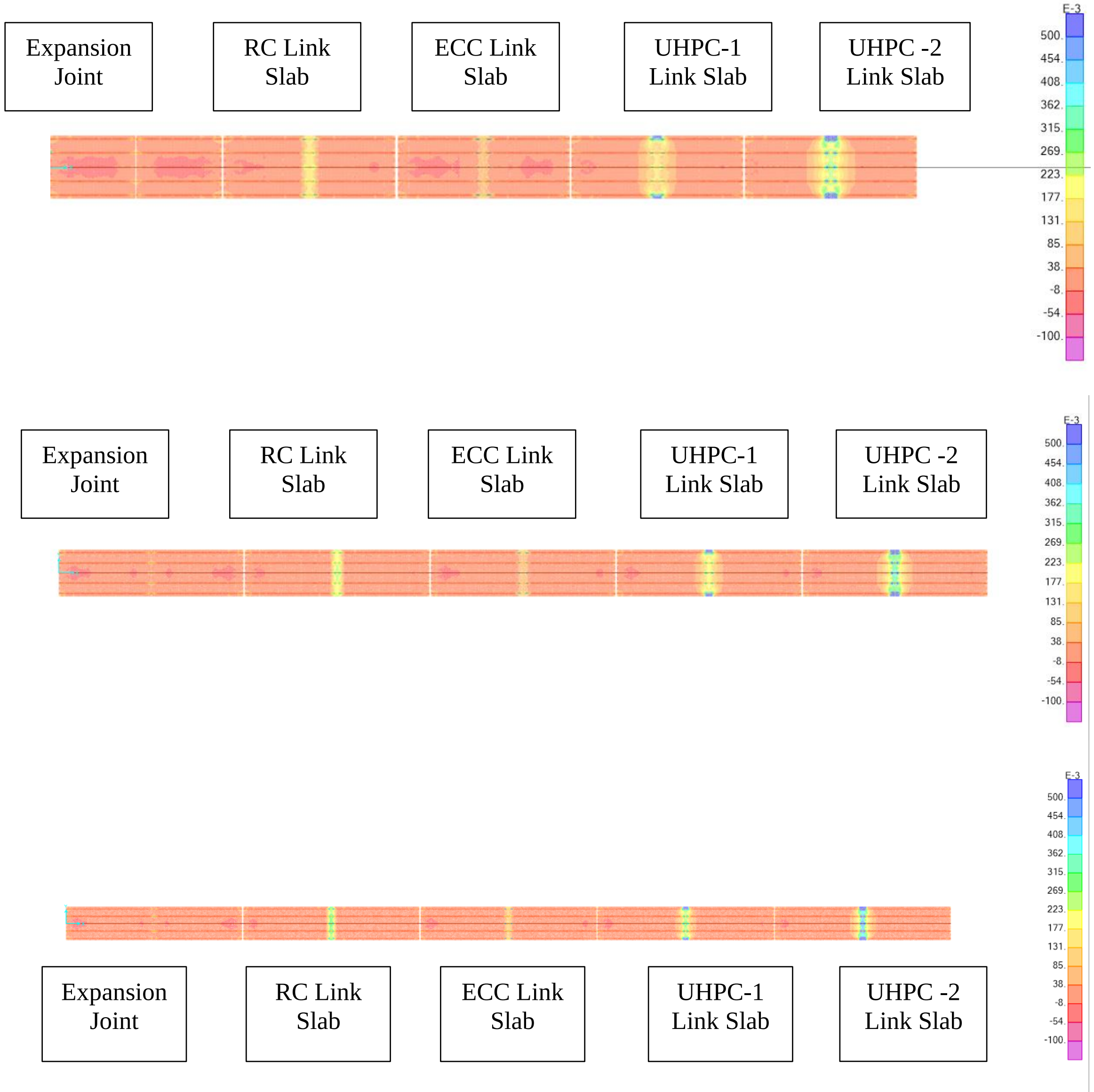

Figure 5-10 Stress distribution of the bridge with span lengths 40 ft, 60 ft, and 80 ft under thermal expansions. (Increasing 55°F)

Similarly, the parameters with skew angles of 0°, 5°, 15°, 30°, and 45° have been analyzed under the 50 ft span length bridge's configuration (Figure 5-11). In particular, the original simply supported bridge was re-modeled as continuous with the skew angle of 30°. In this model, the deck compressed above the pier primary due to the thermal expansion coefficients of the steel girders being slightly larger than the concrete decks. Besides, the maximum stress and longitudinal displacement did not increase significantly, but the average stress in the slab slightly increased when the skew angle became larger.

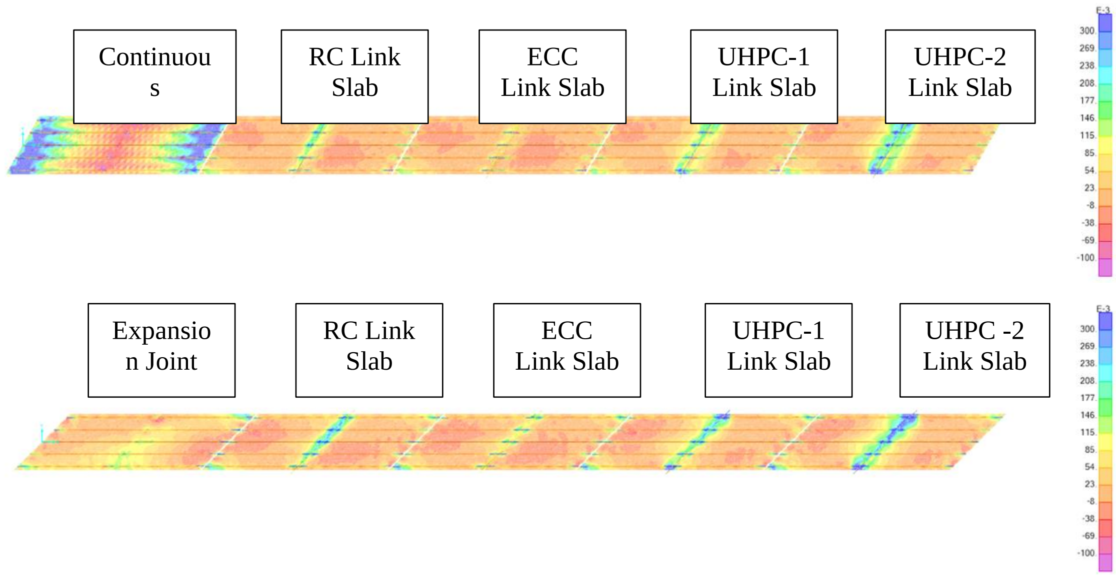

Figure 5-11 Stress distribution of the bridge with span length 50ft, 30°, or 45° skew angle under thermal expansions. (Increasing 55°F)

Additionally, the maximum stress will increase by the comparison of the observation when the length of the link slabs and their debond zone. However, for UHPC link slabs, the maximum stress due to temperature changes will concentrate at the location of the edge of the debond zone instead of the middle of the slab (Figure 5-12). In contrast, the stress in the RC seems approximately uniformly distributed.

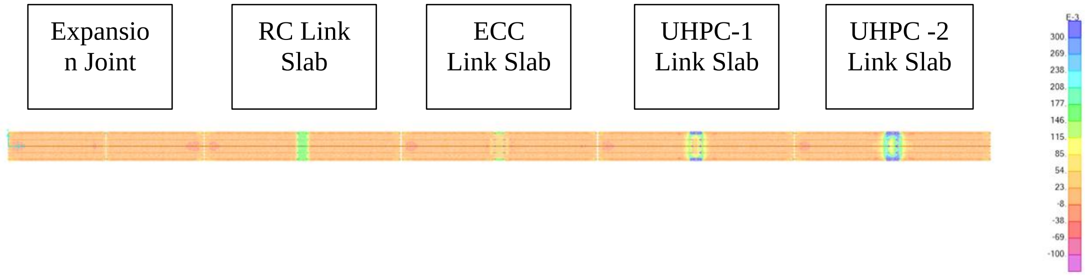

Figure 5-12 Stress distribution of the bridge with span length 100ft, 10 ft wide link slab with 5 ft debond zone

Besides, if not considering the debond zone, stress due to the thermal load will mainly be concentrated in the center of the link slabs (Figure 5-13).

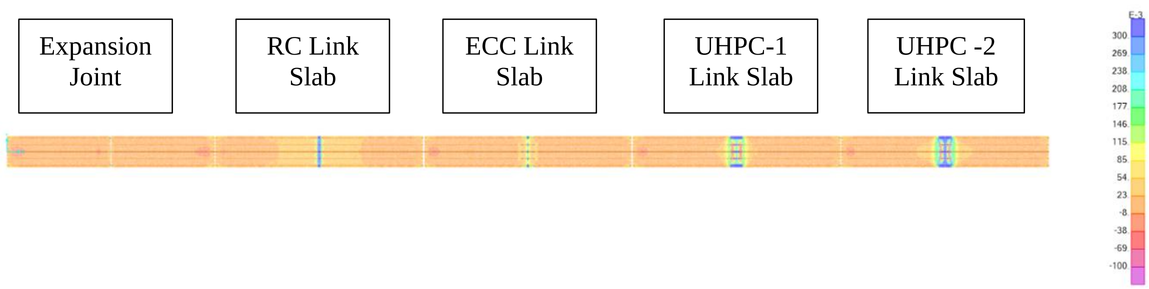

Figure 5-13 Stress distribution of the bridge with span length 100ft, 10 ft wide link slab without debond zone

Although link slabs are always treated as the non-structural component in previous design and analysis, all these results show from the FE models that analyzing the link slab system provides a general idea: when evaluating the general performance of the bridge with newly constructed link slabs, both the behavior of the link slab itself and the adjacent bridge deck should be carefully examined.

5.5 Structural performance assessment models

After analyzing and recording the parameters of the FE models, the summary with 16 features and one (1) evaluation is generated based on the input and output of the model. Then use the traditional machine learning process with various methods to train the classification model. In these models, 90 bridges with 16 features are used as the input, and the evaluation with one of the conditions from “Preferred”, “Good”, “Acceptable”, and “N/A” are used by randomly dividing these data into the training set and the test set. Then, to establish the prediction model using the training set and verify using the test set. Also, a 5-fold cross-validation was introduced in this training progress to prevent overfitting. These assessment model functions coded and trained using Matlab have been compared in this section. And then select the best machine learning model based on the comparative study.

In the proposal period, 75 bridges with 17 features sampled from the initial database were selected in the training set, and 15 were used in the test set. Then using the machine learning model to classify these training sets and got 77.3% accuracy by using the decision tree model, 70.7% in SVM, 72% in the random forest, 73.3% in Boosted trees, and 74.7% in the Kernel Logistic Regression. The accuracy become to 85.7%, 71.4%, 78.6%, 78.6%, and 71.4% respectively. Since the model is still training and more dataset will be added later, only several sets of results, as examples shown in Figure 5-14.

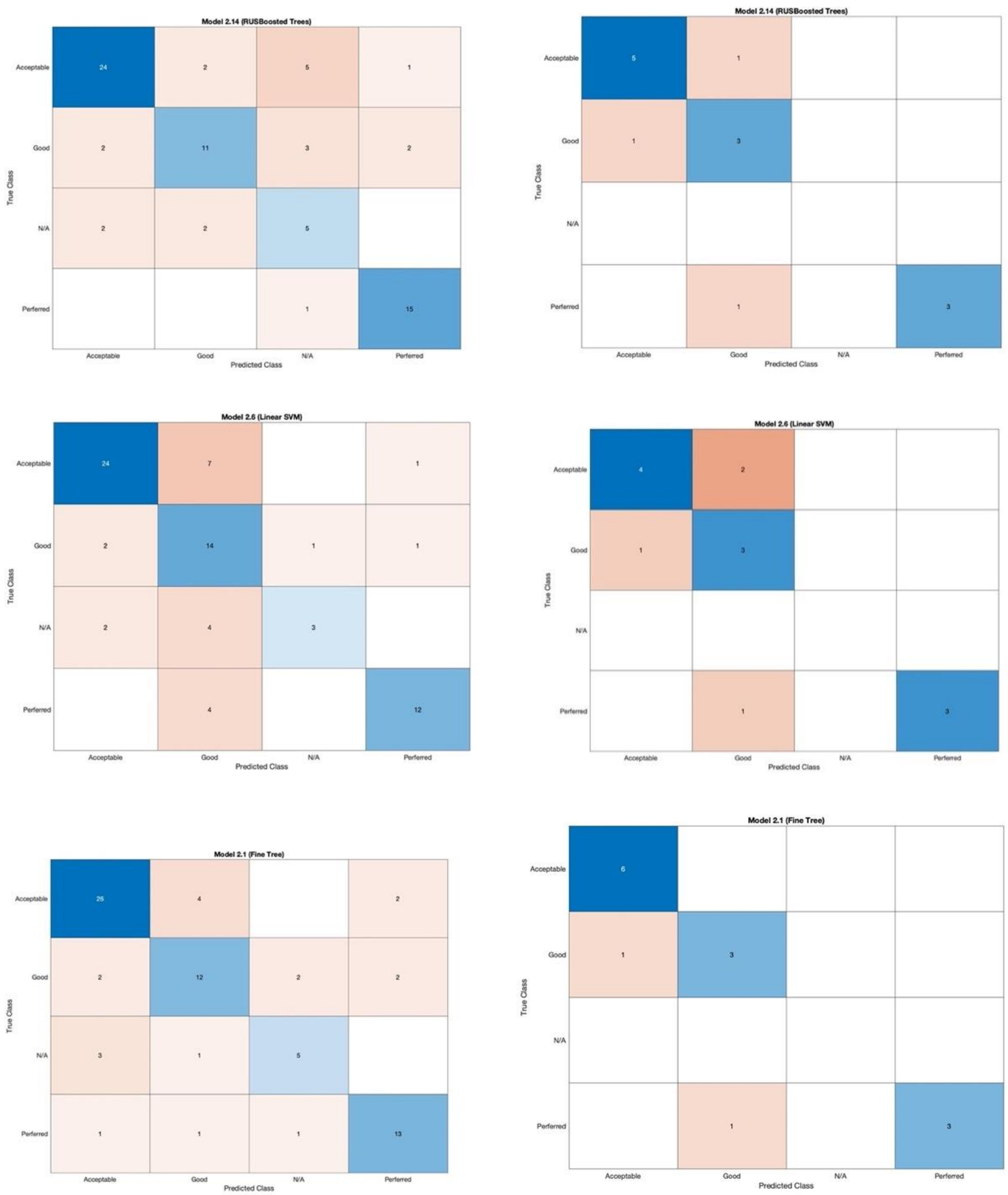

Figure 5-14 Examples of training model with the accuracy of validation (left) and training (right)

When using all the data for the training set, the accuracy with validation (Figure 5-15) are 67.78% (decision tree), 68.89% (Logistic regression), 70% (Neural Networks and SVM), 50% (Kernel Naïve Bayes), 77.78% (Random Forest), and 78.875% (RUSBoosted trees). A comparison of the accuracy shown in Table 5-2.

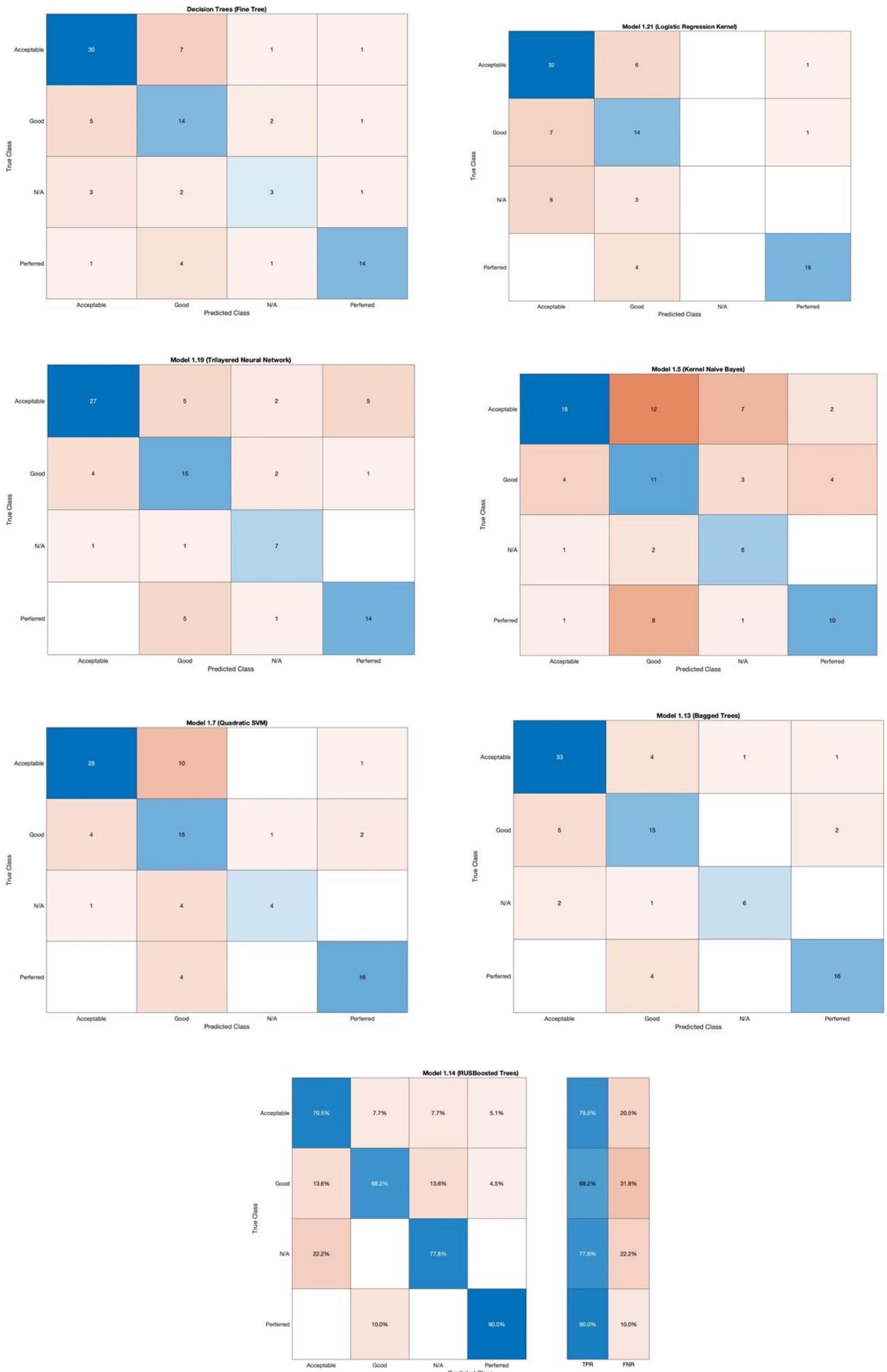

Figure 5-15 Example of training the model using all datasets.

Table 5-2 Comparisons of the accuracy of the trained models

Machine Learning model	Accuracy	
	Validation	Test
Decision Tree	77.3%	85.7%
Linear SVM	70.7%	71.4%
RUSBoosted trees	72%	78.6%
Boosted trees	73.3%	78.6%
Kernel Logistic Regression	74.7%	71.4%

Chapter 6: Case Study: MDTA Pilot Bridge with Link Slabs

In this chapter, another scenario of bridge condition assessment is proposed using the combination of structural health monitoring data and machine learning to predict the data for the next short period and then evaluate the structure's performance.

6.1 Introduction and essential design criteria for this project

One overpass bridge across the I-95 highway in the state of Maryland was selected as the pilot bridge to be rehabilitated with a newly constructed link slab system. Maryland Transportation Authority (MDTA) plans to upgrade those overpass bridges with connections using link slabs (Figure 6-1) since joint failure is one of the primary concerns in bridge maintenance. This project was the pilot case introduced in the state of Maryland that applied HPFRC link slabs to the existing multi-simple span bridges. Therefore, this case was proposed with nondestructive testing (NDT) and structural health monitoring to keep track of the condition of the pilot bridge and collect data for research purposes. Since the bridge is still under its service life, all the testing and monitoring work should not affect any function of the bridge, and sensors were not visible at the top of bridge decks. During the testing and monitoring period, vibrations of the bridge, longitudinal movement of the girder to the abutment, and strain in the link slabs were monitored and used to determine the serviceability of the bridge. In addition, two construction materials, Engineered Cementitious Composite (ECC) and Ultra-High-Performance Concrete (UHPC), were selected as the candidate materials for link slabs based on their high performance of compressive strength, tensile strength,

* Portions of this chapter previously appeared as: Fu, Chung C., A Pilot Application of Link Slab with Selected Material for MDTA Steel Bridges, Final report, Maryland Transportation Authority, April 2020

and ductility. Additionally, a finite element analysis was performed as part of the project for design and verification purposes.

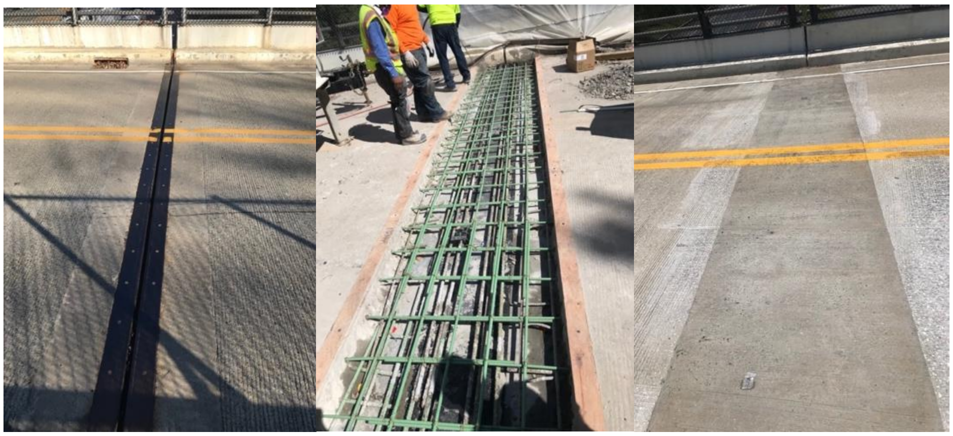

Figure 6-1 link slab in this project (before, during, and after constructions)

The project is located in Cecil County, Maryland, with five steel girders made compositely with concrete decks. The general bridge information is shown in Table 6-1. Pilot bridge information. The most recent bridge inspection report shows this bridge is in overall satisfactory condition before construction. The construction started with the removal of the original 2-inch compressive joint sealants between bridge decks. Then replace the expansion joints with the four-foot-wide, six-inch-deep link slab system, and widen the expansion joints at both abutments to release additional longitudinal deflection. In addition, bearings at both abutments were modified from fixed to expansion conditions by removing anchor bolts from the fixed plate and replaced with steel guides to limit the sliding of the bearing plates.

Table 6-1. Pilot bridge information

Items	Description
Structural Type	Steel girder- RC slab
Total Number of Spans	4
Span Lengths (215 feet and 6 inches or 65.68m in total)	Span 1: 34 feet (10.36m)
	Span 2: 76 feet and 3 inches (23.24m)
	Span 3: 76 feet and 3 inches (23.24m)
	Span 4: 29 feet (8.84m)
Skew	83°9’45″
Bearing Conditions	Multi-simply supported (F-E-F-E-F)
Structure/Roadway width	31 feet and 2 inches (9.5m)/ 26 feet (7.92m)
Deck depth	7 inches + 2 inches (177.8mm+50.8mm) overlay
Link slab dimensions	4-foot (1.22-m) wide each
	2 feet (0.61m) in debonded zone 4-inch (101.6-mm) slab 2-inch (50.8-mm) overlay

6.2 Finite element analysis and bridge condition assessments

Since there were no national codes or standards for the design of link slabs, the finite element (FE) model was built, and structural analyses were conducted using the commercial software CSiBridge®. In this case, only the superstructure with boundary conditions was modeled since the bridge behavior would not significantly affect the substructures. All bearing conditions, including fixed and expansion bearings, were idealized as pin or roller supports. All girders, decks, and link slabs were modeled using shell elements with a 36 in. (915 mm) mesh on the non-focused area and one in. (25.4

mm) to 2 in. (50.8 mm) mesh on the critical researched part (on the link slab and adjacent area). Additionally, in this case study, the pilot bridge analyses under multiple load cases, including AASHTO specified structural dead load, modal analysis, HL-93 live load, moving vehicle loads, and thermal movement, including long-term temperature changes and thermal gradient, were conducted.

The finite element model of the original bridge (Figure 6-2) was built based on the early design files, and the newly constructed link slab system was based on the retrofit design file where the material properties were chosen from lab-tested specimens collected from the construction site. For the ECC, 6,000 psi (41.4 MPa) in the compressive strength and 1,000 ksi (6.9 GPa) in Young's modulus were used, while for the UHPC 20,000 psi (137.9 MPa) in the compressive strength and 3,800 ksi (26.2 GPa) in Young's modulus were used in the pilot bridge numerical model.

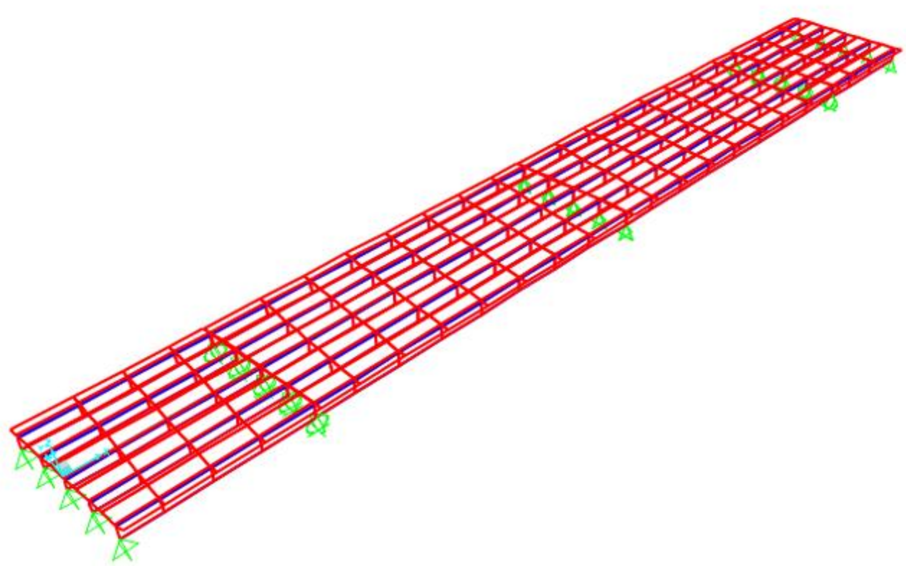

Figure 6-2 Finite element model (shown in frame) for the pilot bridge

In the modal analysis, the natural frequency of the original bridge was computed as 4.68 Hz, while the retrofitted case had a first mode natural frequency of 4.96 Hz (Figure 6-3), which showed that the link slab system would not significantly affect the structural behavior of the entire structure. The bridge could still be treated as multi-simply supported spans in hand calculations.

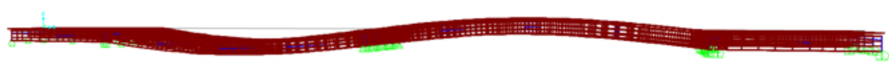

Figure 6-3 First mode shape of the bridge

Additionally, this FE bridge model was also employed to simulate the situation of a dump truck driving through the bridge. This case, refers to the diagnostic load test (Fu, 2020), which was conducted by applying the moving vehicle load on the bridge and recording the step-by-step time response. Figure 6-4 shows an example output for this analysis. Figure 6-4 (a) shows the maximum value (envelop) of the response stress distribution at the top of the bridge deck under one load case. And Figure 6-4 (b) demonstrates at one random moment that the truck on the bridge, and the response strain distribution counter were shown on the model accordingly. Meanwhile, the real diagnostic load tests were conducted, and the stresses at the locations that installed strain sensors were measured and recorded. Hence, the FE model was updated, calibrated, and validated using the measured data for further assessment.

(a) Stress distribution (maximum envelope) at the top of the bridge deck (with a speed of 20 mph)

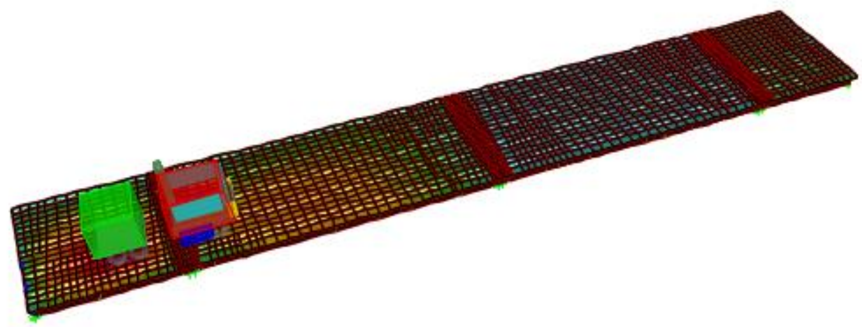

(b) Finite element simulation of the dump truck drive through the bridge

Figure 6-4 Stress distribution example for the bridge under the dump truck

In addition, the structure generated deformation and deflection due to thermal loads, including thermal expansion and/or contraction, and temperature gradient due to sunlight radiation and delayed effect in heat transfer. Since all fixed bearings on both abutments had been modified to expansion bearings along the longitudinal direction, most of the stress caused by thermal loads would be released with the longitudinal deformation.

In this project, the thermal expansion coefficients for the original superstructure of the bridge were assumed to be the general value of concrete ($5.5 \times 10^{-6} in/(in$ °F)) and steel ($6.5 \times 10^{-6} in/(in$ °F)).

Meanwhile, although the field-testing data showed a noticeable difference in the ability of heat transference between UHPC and ECC, the thermal expansion coefficients of these two materials were still assumed to be the same as regular concrete due to a lack of experimental and lab test results. Under this assumption, the initial estimations of girder movement using AASHTO LRFD Bridge Design Specifications (2017, Equation 12) along the longitudinal direction were between 0.748 in. (19mm) to 0.945 in. (24mm) in a 110°F (43.3℃) range when only considering the atmosphere of uniform temperature changes.

$$\Delta_T = \alpha\ L\ (T_{max} - T_{min}) \qquad \text{Equation 17}$$

Where:

L: the span length of the bridge

α: coefficient of thermal expansion

T_{max}, T_{min}: The maximum and minimum design temperatures are based on climate, construction materials, and location.

For the finite element analysis, the longitudinal deformation caused by uniform temperature changes was computed as 0.953 in. (24.2 mm) within the 110°F (43.3℃) range. Adding up the 0.039 in. (1 mm) to 0.157 in. (4 mm) changes in the longitudinal direction caused by the thermal gradient (AASHTO zone 2), the total displacement between the superstructure and the abutment was about 0.992 in. (25.2 mm) to 1.11 in. (28.2 mm). Then the structural behavior of the link slab in the simulation process was updated again using this set and long-term monitoring data for verification. The ideal long-term performance under uniform temperature changes shows in Figure *6-5*.

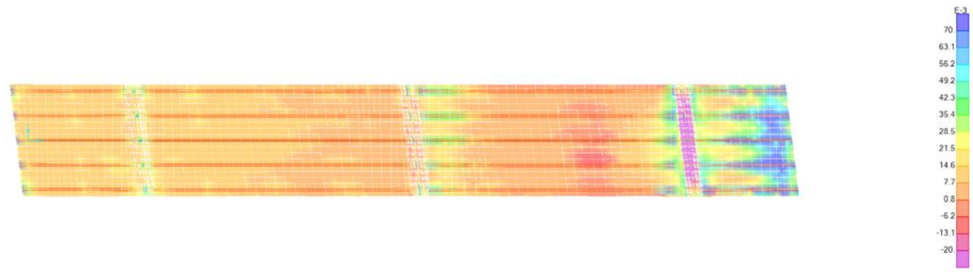

Figure 6-5 Stress simulated for the pilot bridge under the uniform temperature changes

<u>6.3 Load test and long-term monitoring data analysis</u>

Theoretical or analytical models, which are usually referred to as the numerical calculation or finite element analysis models of the structure, may not be precisely modeled due to the complexity of the real cases. For example, the boundary conditions are usually simplified as fixed or expansion; the material properties are simulated as linear or bi-linear, even for the composite material; and the long-term effects like creep and deterioration are usually not considered or simplified when analyzing the entire structure. The adopted diagnostic load test is a relatively short-term test that is promoted to reduce the uncertainties associated with the as-built condition of the structure (Frangopol et al., 2019).

The general procedure starts from the critical considerations of structural behavior. Then, define the objectives and analytical approach. Suppose the analytical approach cannot meet the goal. In that case, the general plan of the testing, including the sensor layout, loading vehicle access, traffic control, and expected results, is designed and arranged before execution. The execution and validation need to conduct a load test until obtaining valid field data. In addition, the analytical model should be refined and back validated by these data. And finally, generate the load rating model for the bridge assessment.

Diagnostic load tests are used to determine specific bridge response characteristics or to validate quantitative analytical assumptions. The bridge engineer's understanding of the bridge's behavior improves, and uncertainties related to material properties, boundary conditions, cross-section contributions, load distribution, and other aspects controlling structural performance and safety are reduced. As a result, it can be utilized to alter an existing bridge analytical assessment. Loads should be put at various points on the bridge during the test to determine the response of all important bridge members. The AASHTO LRFR Guide Manual included details to modify the analytical load rating following a diagnostic load test.

The diagnostic load test, in this case, is to test, monitor, and analyze the behavior of the link slab under service load. Under this situation, strains are recorded only in the link slab system area, while the long-term longitudinal displacement and vibrations are recorded for the entire bridge.

To conduct diagnostic load testing (live load test) and long-term structural health monitoring of the bridge, multiple sets of sensors were installed in the bridge before and during the construction of the link slab systems.

In this testing and monitoring case, 16 strain sensors were embedded in the link slab system during its construction period. Two accelerometers were installed on steel girders at span 3, and two displacement sensors were installed at both abutments to monitor the movement due to thermal expansion and contraction of the structure. The general sensor arrangement is shown in Figure 6-6.

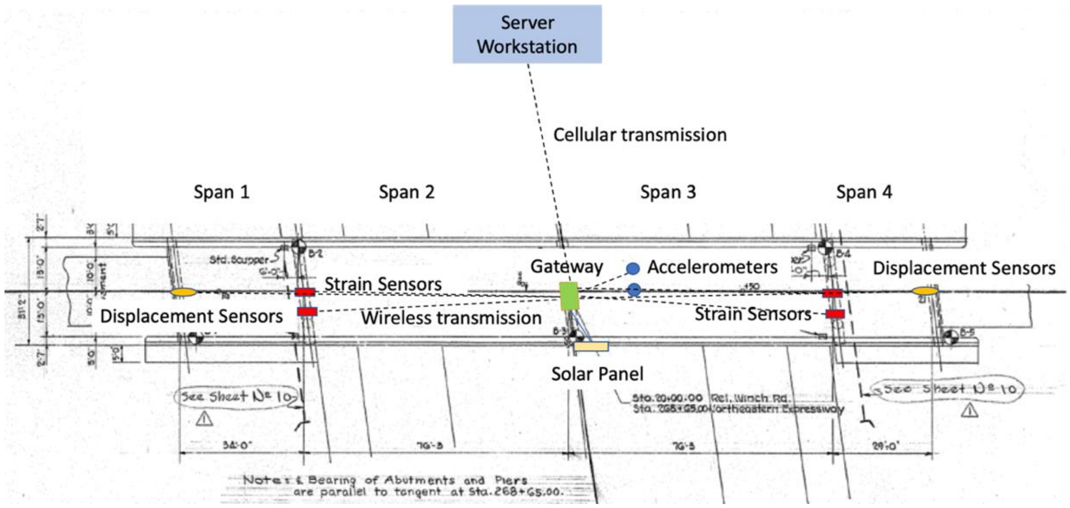

Figure 6-6 Sensor arrangement for the bridge CEX95200

The primary function of the link slab is to provide continuity of the deck slab yet offer negligible resistance against the girder end rotation. In order to measure the bending deformation of the link slab, the strain gauges are designated to locate at both the top and bottom sides of the link slab. However, it is hard to fix strain gauge tapes on specific locations and level them during concrete pouring. Therefore, an alternative method of strain gauge installation is developed to set and fix at specific locations before concrete pouring. It is proposed that strain gauges could be pre-installed on a thin aluminum plate and connected four strain gauges with plates at a customized 3D printing plastic frame as a set of sensors (Figure 6-7). After concrete pouring, the strain gauges are built into the link slabs. All sensors' installation pictures are shown in Figure 6-7, Figure 6-8, and Figure 6-9.

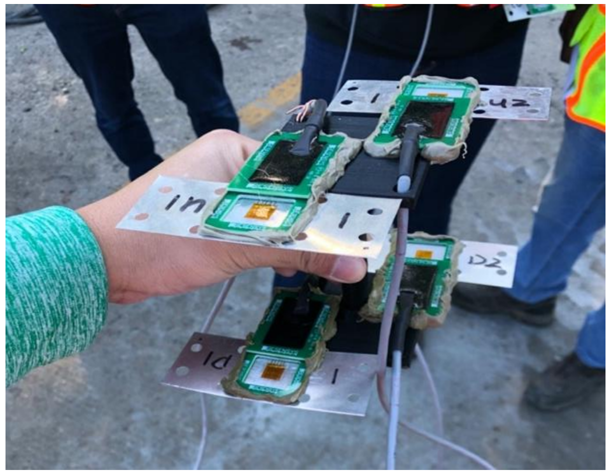

Figure 6-7 Customized sets of strain sensors

(a) Strain sensors' installation

(b) Displacement sensor

(c) Accelerometers

Figure 6-8 Sensor installation

Figure 6-9 Gateway/ Sensor adjustment

The live load test was performed on 11/27/2019. There were two trucks involved, and they were labeled based on the last two digits on their license plates, hence, trucks 03 and 08, respectively. Dimensions and load on each axle are presented in Figure 6-10 as a demonstration. The truck was weighed on-site by the MDTA police.

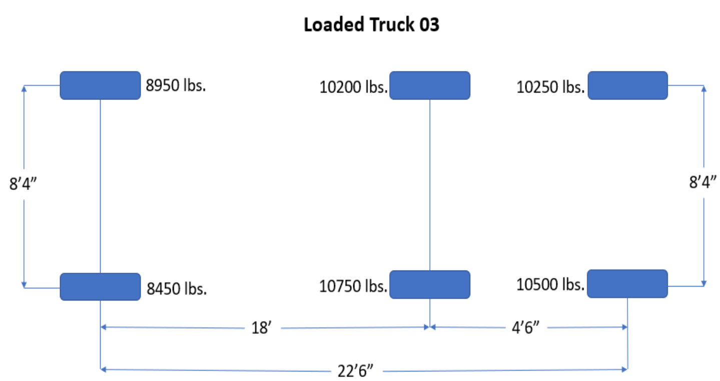

Figure 6-10 Dimensions and weight for the loaded truck 03

A stationary live load test was performed first, during which the two trucks were at rest, facing each other when each axle was weighed. This test was performed twice at two different locations. Then, 20 live load tests with a moving vehicle were conducted at four different speeds: 5, 20, 30, and 40 mph, respectively. During each run, the vehicle passed through the bridge at the designated speed and resumed back to its original position by backing. During backing, the vehicle passed through the bridge again. Thus, in each run, the truck passed through the bridge twice. The entire live load test is recorded for further investigation. Figure 6-11 was taken during the live load test.

Figure 6-11 Empty, stationary vehicles

After sensors were installed in the link slab and on the bridge, the real-time monitoring system started working instantly. The strain sensors captured both strains and temperatures in the material after the signal was adjusted successfully. Furthermore, the two figures below demonstrate strain and temperature changes after pouring the link slab. In these figures, red lines indicate the temperature detected in the link slab (left vertical axis), and blue lines are the strains detected from pouring to hardening. The patterns of the red line vary along with the material and environmental temperature. For the UHPC, it is obvious that the material is under the shrinkage stage and releases heat on the second day at midnight (Figure 6-12). For the ECC, it expands at the beginning and stays stable after half-day (Figure 6-13).

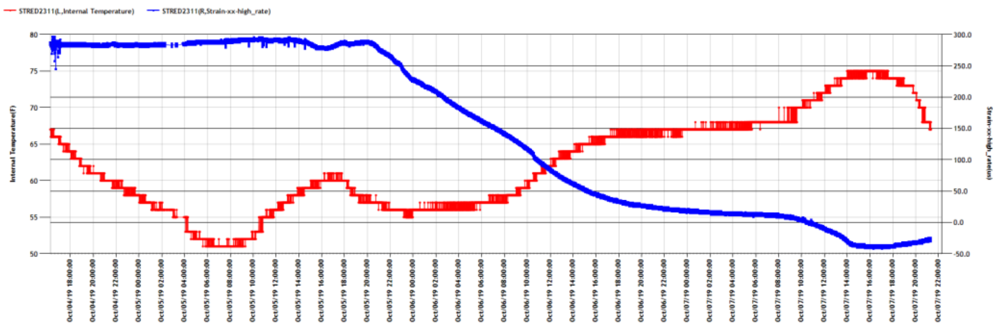

Figure 6-12 UHPC temperature and strain after pouring

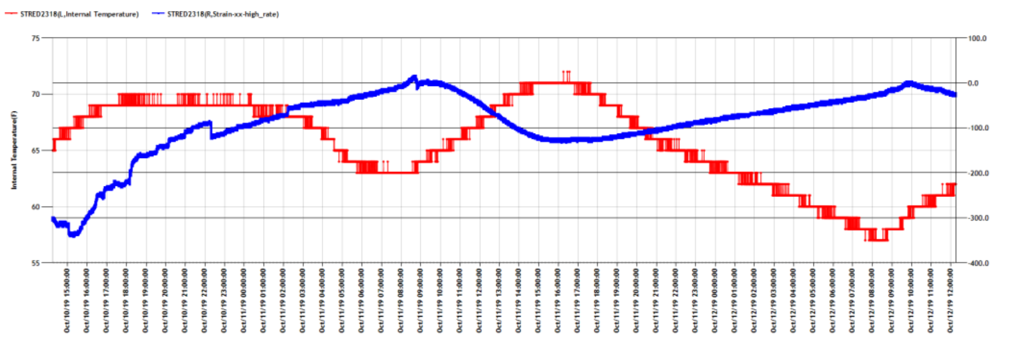

Figure 6-13 ECC temperature and strain after pouring

All the data from strain sensors and accelerometers were captured during the diagnostic load test. Figure 6-14 shows calibrated data from strain sensors showing the dump trucks driving through the retrofitted bridge at the speed of 20 mph, the calculated maximum stresses at the sensors' locations from numerical analyses were 23 psi (0.16 MPa) for the ECC link slab and 33.3 psi (0.23 MPa) for UHPC link slab, and the corresponding strains can be calculated as 23.3 and 8.77 micro-strains, respectively, which are relatively close to the field-tested results approximately 24 and 9 micro-strains, respectively. It means we may use simulated results for further studies and evaluation.

(a) Testing data for ECC

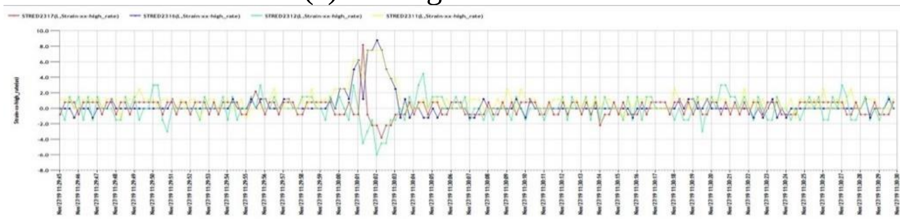

(b) Testing data for UHPC

Figure 6-14 Calibrated data of strains in link slab

The primary goal of this project was to design and construct a functional link slab system that worked compatibly with the original bridge without any large cracks or leakage. After completing the field testing and data collection, the post-processing procedures were conducted to validate the finite element model and the preliminary calculation, and finally, to simulate all the potential cases that could assess the bridge condition and predict the structural behavior of the entire structure. The strain measured from the sensors in the first-year monitoring period indicated that the link slabs in this project (Fu, 2020) were in good condition without any large cracks and were later verified by inspection. Then, to verify the bearing modification's effectiveness and predict the bridge's further movement, the bridge, the natural frequency of the bridge before, during, and after the entire construction works was measured and validated with the FE model. After this verification, the FE model was updated to match these measured data and used to predict the condition of the bridge. Moreover, the girder end displacement on both abutments was also monitored to verify the effectiveness of the bearing modifications.

Vibration data was collected and analyzed to validate the natural frequency of the structure using the Fast Fourier transform (FFT). The accelerometer captured the vibration data before and after the reconstruction with a sampling frequency of 50 Hz. The result showed that before reconstruction, the bridge's natural frequency was approximately 4.70 Hz, which was close to the finite element result of 4.68 Hz. In addition, vibration data was captured after a heavy truck drove over the bridge, and a short period of free vibration was recorded, and a natural frequency of 5.42 Hz was captured (Figure 11).

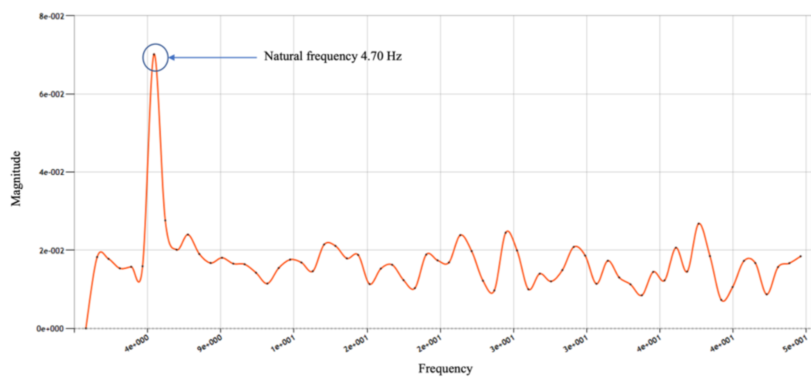

(a) Frequencies (cps) of the bridge before construction

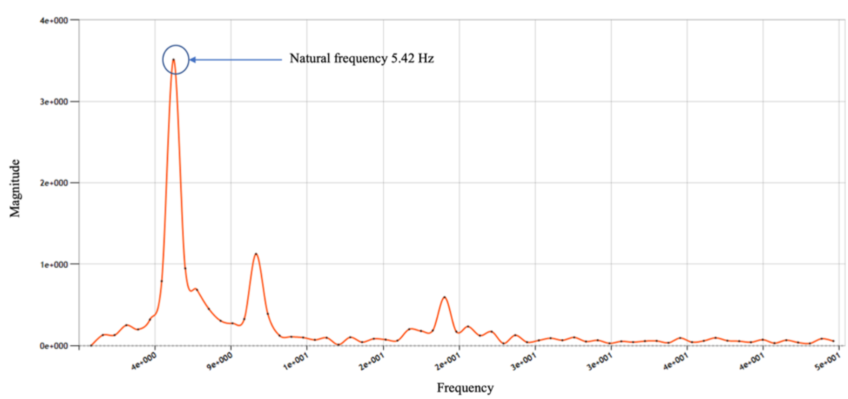

(b) Frequencies (cps) of the bridge after construction

Figure 6-15 Post-processing of vibration data

As the modal analysis of the finite element model showed frequencies within the acceptable range, this refined model was determined to correctly describe the whole bridge's structural performance. Further, this model was used to predict the displacement of the beam ends at each abutment.

During the one-year monitoring period, the maximum average temperature change in the course of this year (2020) was 74°F (23.3℃), with the movement of 0.394 in. (10mm) on the west abutment and 0.787 in. (20 mm) on the east abutment.

The primary difference between these two displacements was the bearing restraint plate on the west abutment partially limited the bearing movement along the longitudinal direction. The movement prediction was about 0.669 in. (17 mm) under the same temperature duration, which was close to the monitored data from the east abutment.

However, this evidence showed that the bearing modification design successfully released the movement along the longitudinal direction. Figure 6-16 shows an example of girder end movement in two different periods. As shown in Figure 6-16 (a), the typical girder end movement was assumed and measured when bearing plates could slide without restraints along the longitudinal direction. However, when the restraint plates were contacted and acted on the sliding plate, the movement would be limited (Figure 6-16 (b), east abutment) until the internal force from the superstructure was large enough to push the restraint plate back and self-adjusted to the right direction. Meanwhile, the strain sensor data showed irregular strain distribution on the west side, while the east side strain data showed a noticeable expansion or contraction relationship with temperature. When comparing the displacement between the east (red line) and the west abutment (blue line), it can be seen that the restraint plates have a significant influence on the bearings and would limit the stress release in the superstructure.

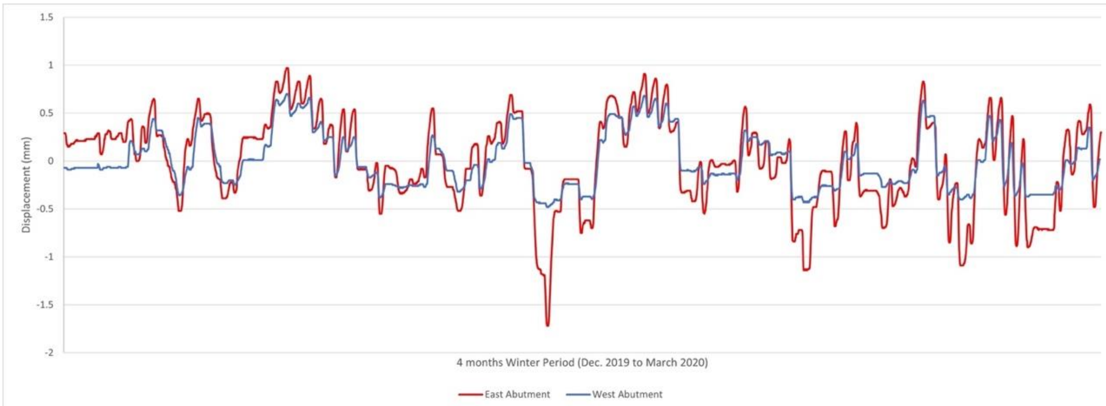

(a) Typical beam end movement data (mm)

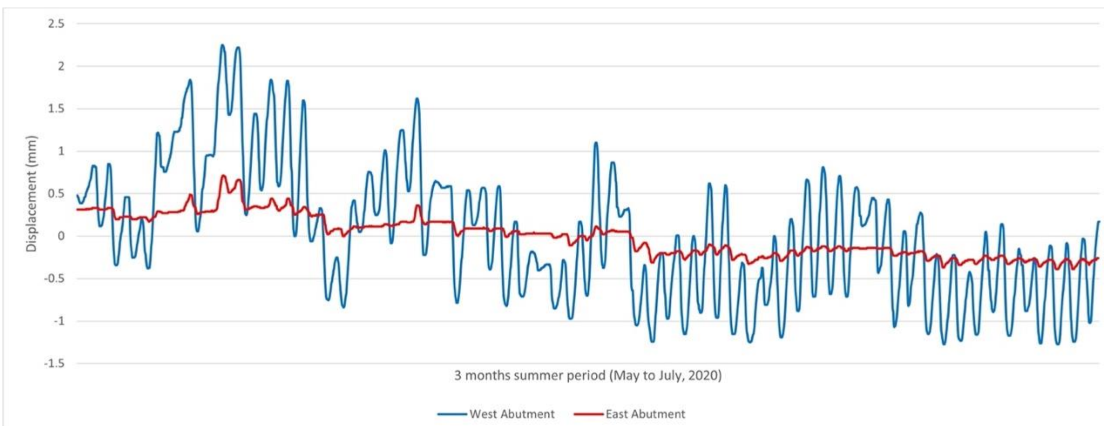

(b) Bearing plate on the west abutment was limited for movement by the restraint plates (mm)

Figure 6-16 Beam end displacement at abutment monitoring data

6.4 Strategy for performance assessment and improvement

6.4.1 Methodology

In this case, the LSTM network system is selected to finish the regression task. An input $X_i = \{x_1, x_2 \dots x_T\}$ are a sequence of continuous time series (T days in our experiment) and $x_t \in \mathbb{R}^d$ where d is feature space. The outputs $y \in \mathbb{R}^{m \times k}$ indicates m prediction indexes in the next k days. The whole process includes:

(1) Embedding input data to a certain feature space with W_x, where $W_x \in \mathbb{R}^{d \times n}$.

(2) Predicting the output of the current time step h_t according to the last hidden state h_{t-1} and input embedding. Where:

$$Sigmoid(x) = \frac{1}{1+e^{-x}} \quad \text{Equation 18}$$

$$tanh(x) = \frac{1-e^{-x}}{1+e^{-x}} \quad \text{Equation 19}$$

6.4.2 Data splitting and data processing

In this section, the whole monitoring data was downloaded from the server for analysis and forecasting using LSTM. In this analysis, a piece of data within a certain period was first selected. During the data processing, the Adam (Kingma et al. 2014) optimizer was used with a learning rate of 0.005. For every 100 epochs, the learning rate will decay by a factor of 0.2. The model is trained with a maximum of 1000 epochs.

This process is still undergoing, and a sample is provided here as:

Choose a set of data measured from the displacement sensor at the west abutment, selecting to export one data every 30 minutes. Then take the first 1200 data points for analysis by taking 88% of the data as a training set and 12% as a testing set. The actual measured data are plotted in Figure 6-17, with the prediction trained from the model and plotted in Figure 6-18 and Figure 6-19. Then the model is updated using the test set and shown in Figure 6-20.

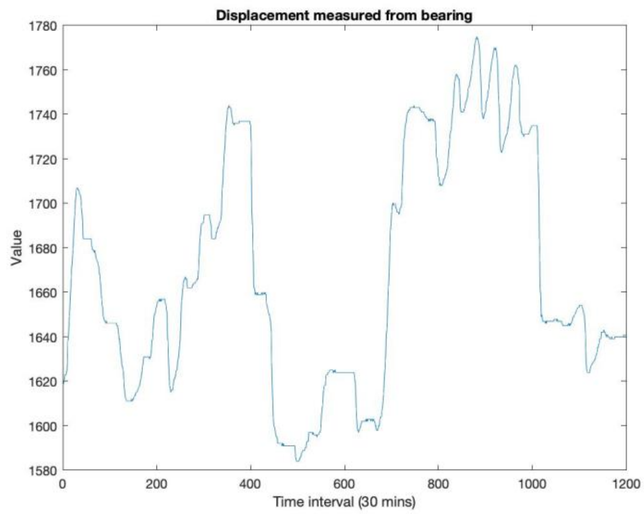

Figure 6-17 Actual data measured from the LVDT

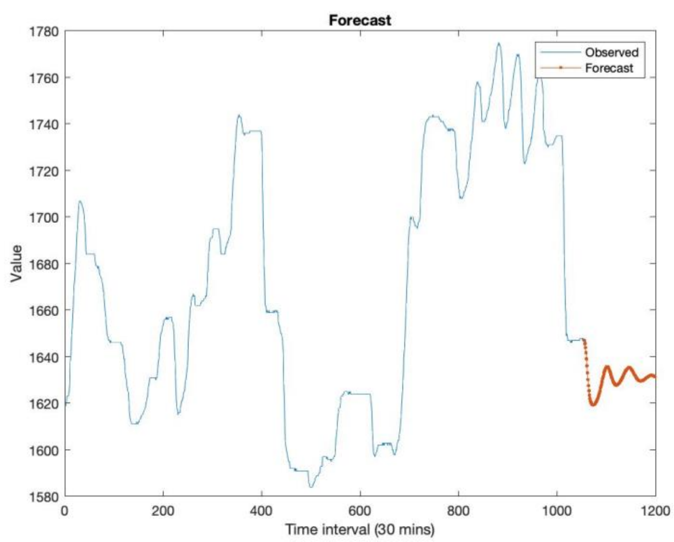

Figure 6-18 Actual data with last 12% forecasting using LSTM

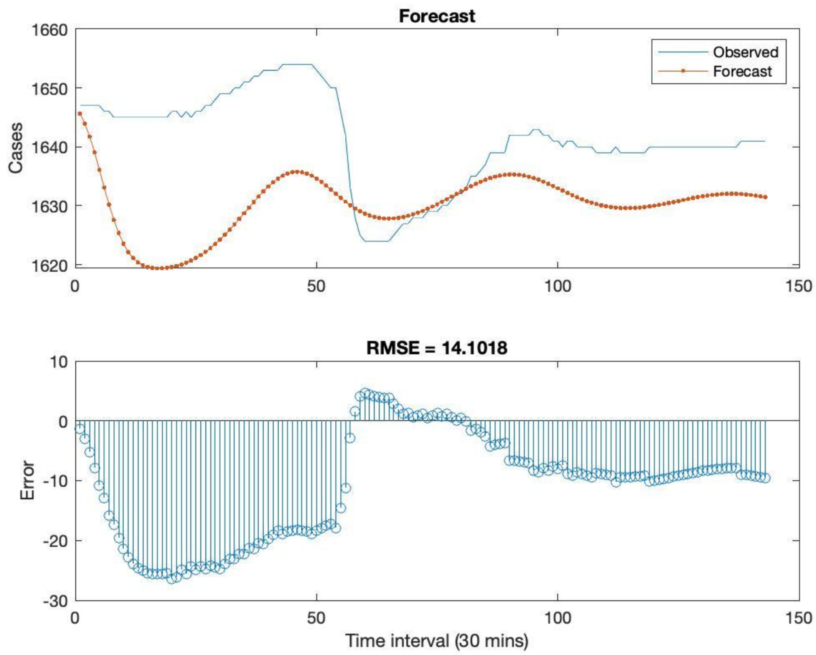

Figure 6-19 Compare the forecasted values with the test data.

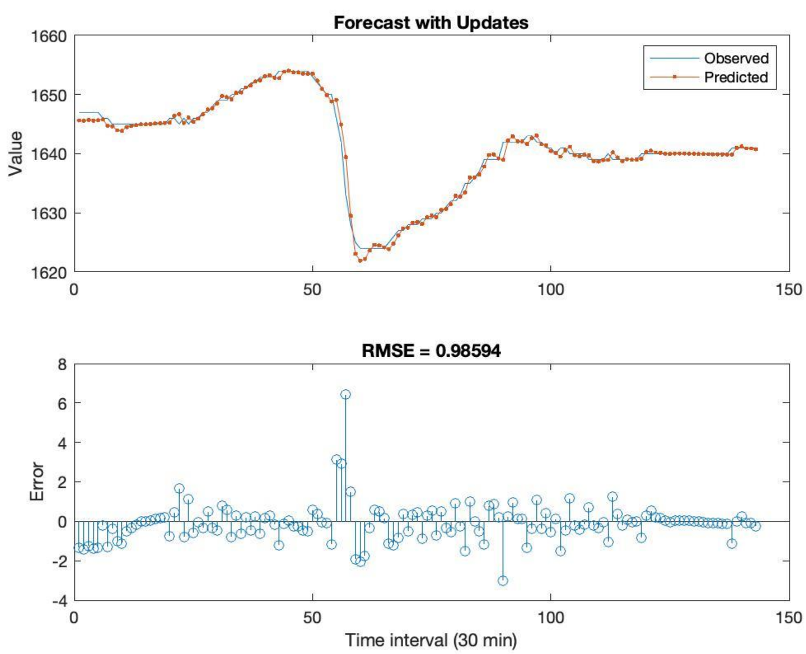

Figure 6-20 Update network state with observed values

Another example of training models for prediction was selecting the strain from the strain gauge embedded in the UHPC link slab. This set of strain data has a length of 750 hours, which is approximately a month. In this dataset, every datapoint is the average value captured within the length of 30 minutes. Then plot the measured data in Figure 6-21. By selecting the first 80% as the training data and keeping the 20% for testing. The best performance of the trained model is shown in Figure 6-22, with the comparison plotted in Figure 6-23, and the updated model plotted in Figure 6-24.

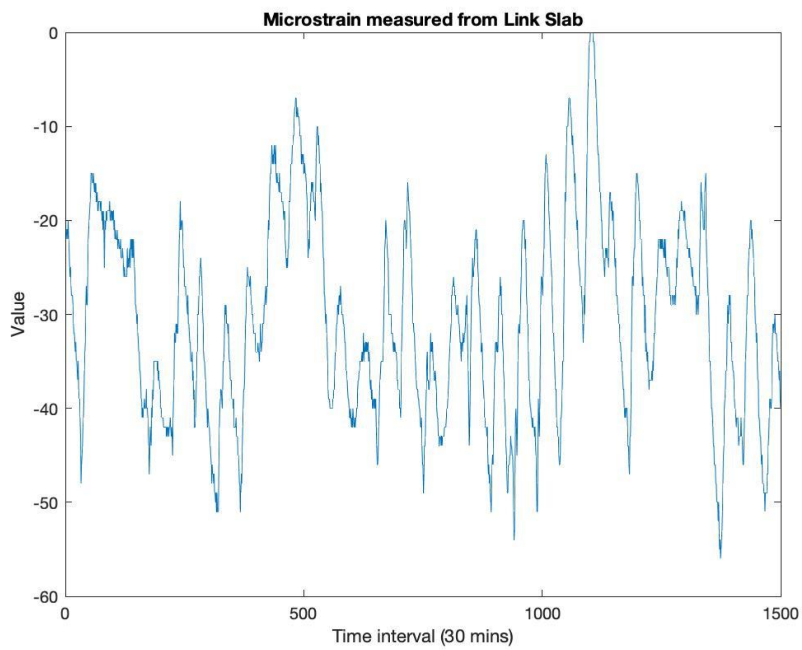

Figure 6-21 Actual data measured from the strain gauge

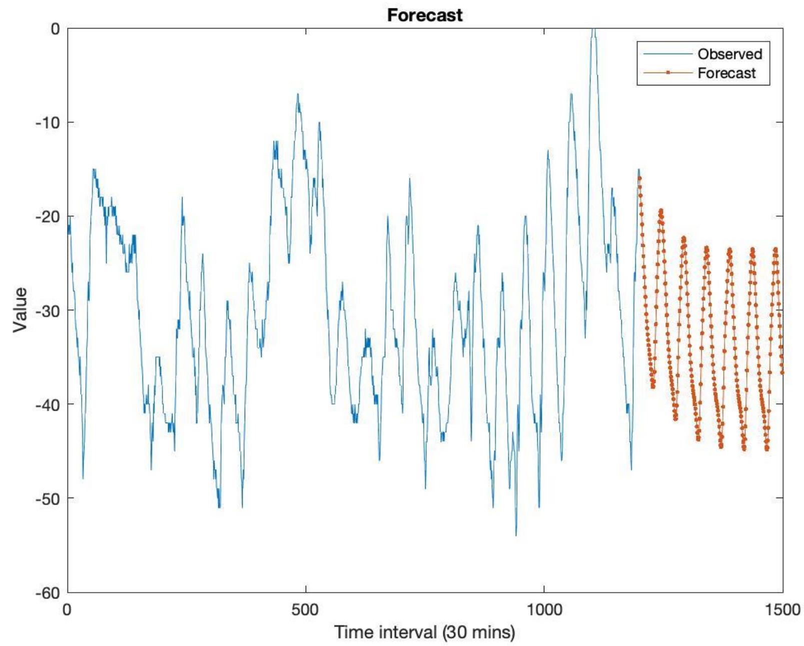

Figure 6-22 Actual data with last 20% forecasting using LSTM

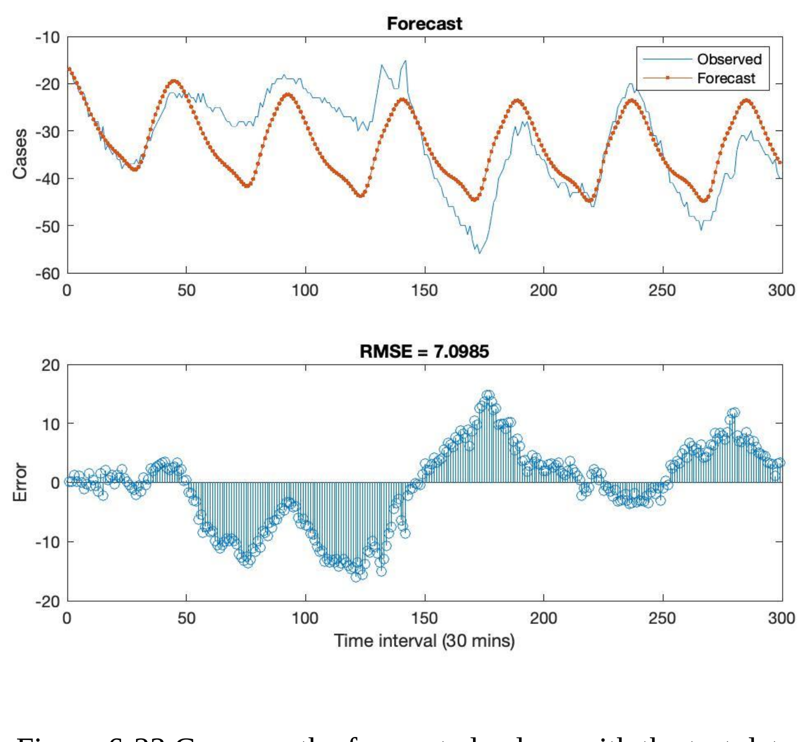

Figure 6-23 Compare the forecasted values with the test data.

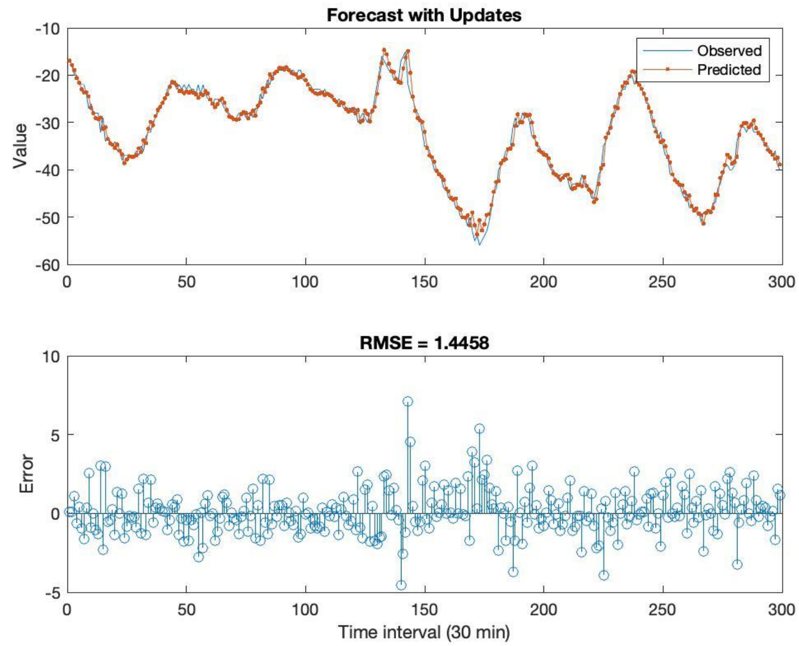

Figure 6-24 Update network state with observed values

However, this time series prediction is not always performed well since the current network only predicts one step further using the current value. Thus, another LSTM model was trained using data from the same sensor, selecting the displacement (Channel 1 or Column 1 in figures) and internal temperature (Channel 2 or Column 2 in figures) data from January 1st, 2020, to July 31st, 2021.

In this trial, splitting the data into paralleling 235 datasets. In each dataset, a set of 168 $(datapoints) \times 2$ (input features) cell is defined, where the input values are the average hourly displacement readings and the corresponding internal temperature. Then prepare 90% of the datasets as a training set, and 10% are the testing set. Using a sequence input layer with an input size of 2. The LSTM layer was defined with 128 hidden units and a fully connected layer with an output size of 2. The maximum epoch was defined to be 250 and shuffling the data every epoch.

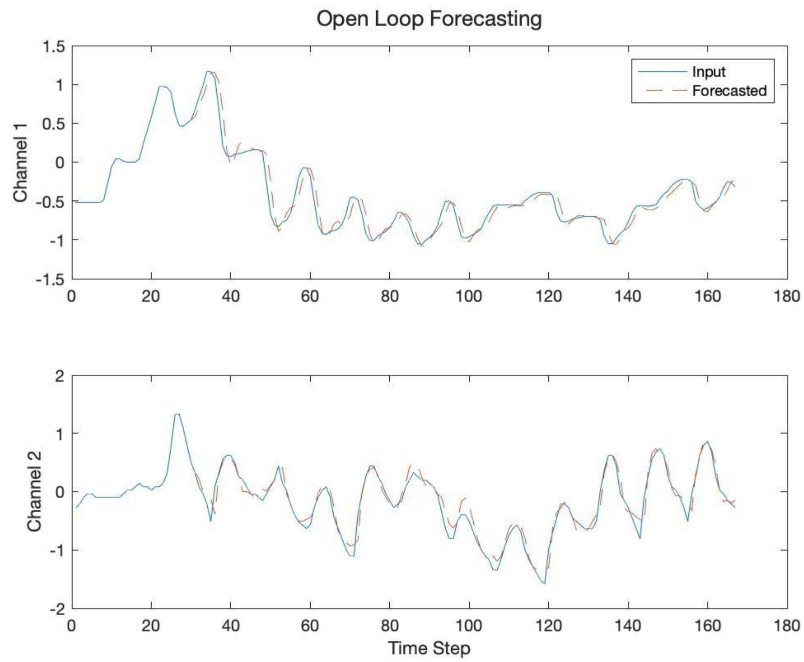

Figure 6-25 Open-loop forecasting

To forecast the displacement and temperature in this example, open-loop (Figure 6-25) and closed-loop forecasting (Figure 6-22) methods are selected to demonstrate their performance. The difference between these two methods is that open-loop forecasting relies on the actual input value to predict the next step, while closed-loop forecasting predicts subsequent time steps using the previous predicted value.

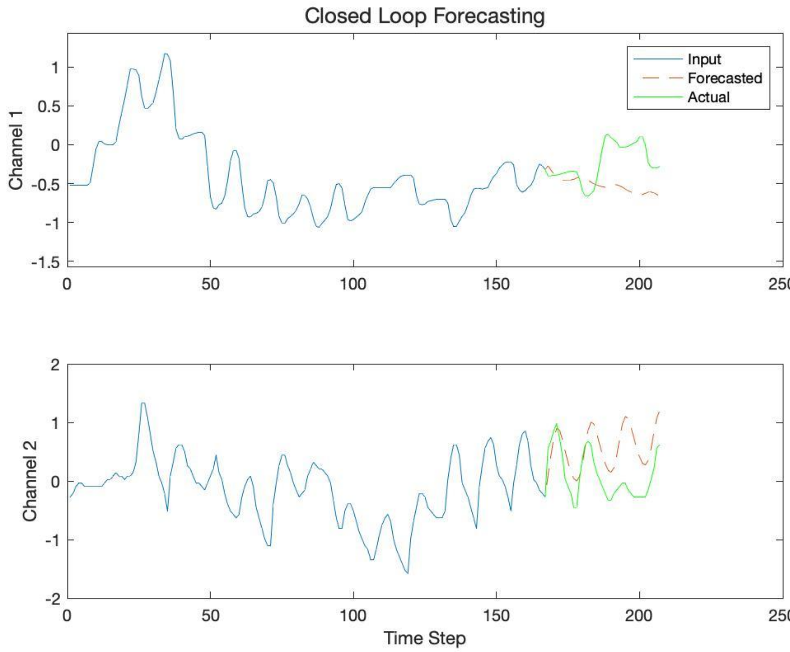

Figure 6-26 Closed-loop forecasting

Then a model updating process is developed by changing the data splitting into 100 datapoints × 790 datasets (examples of input data plots shown in Figure 6-27), with the time step of 0.5 hours, 600 epochs, and the hidden units of 150.

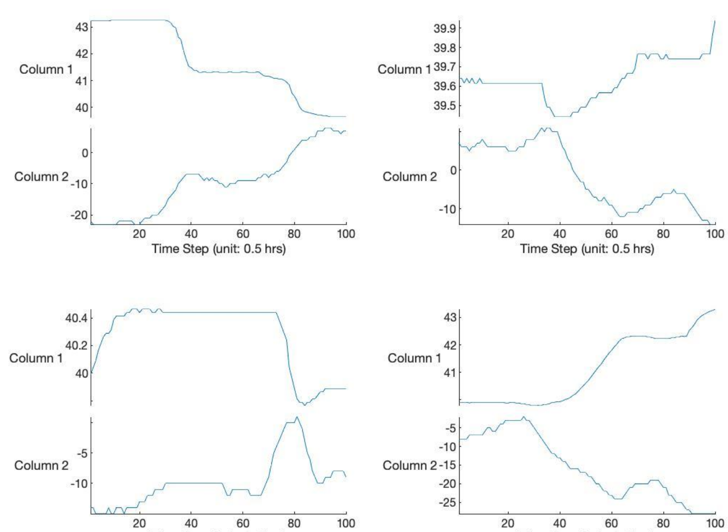

Figure 6-27 Example input data plots

After the network was trained, the root means squared error (RMSE) was calculated to evaluate the accuracy between the prediction and observed values. The visualized histogram is shown in Figure 6-28 with an average value of 0.035.

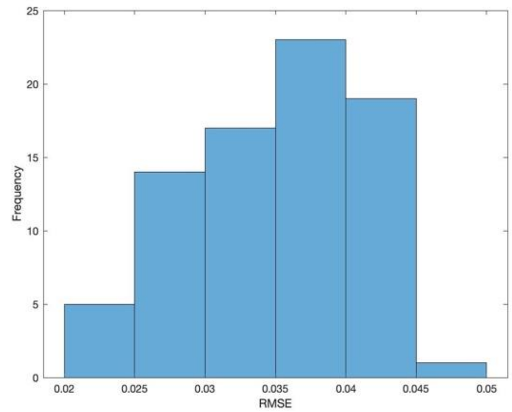

Figure 6-28 Histogram of RMSE

An example of open-loop forecasting and closed-loop forecasting are shown in Figure 6-29 and Figure 6-30:

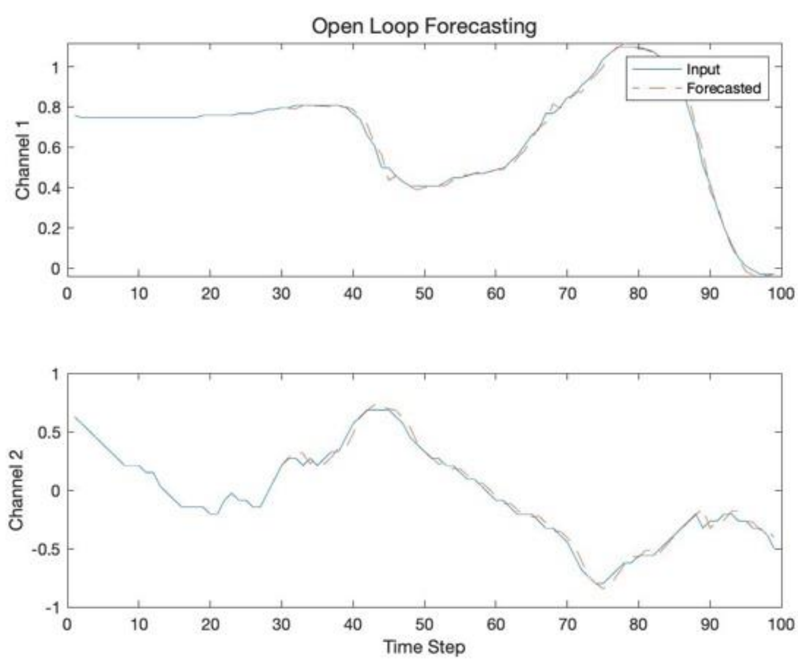

Figure 6-29 Open-loop forecasting

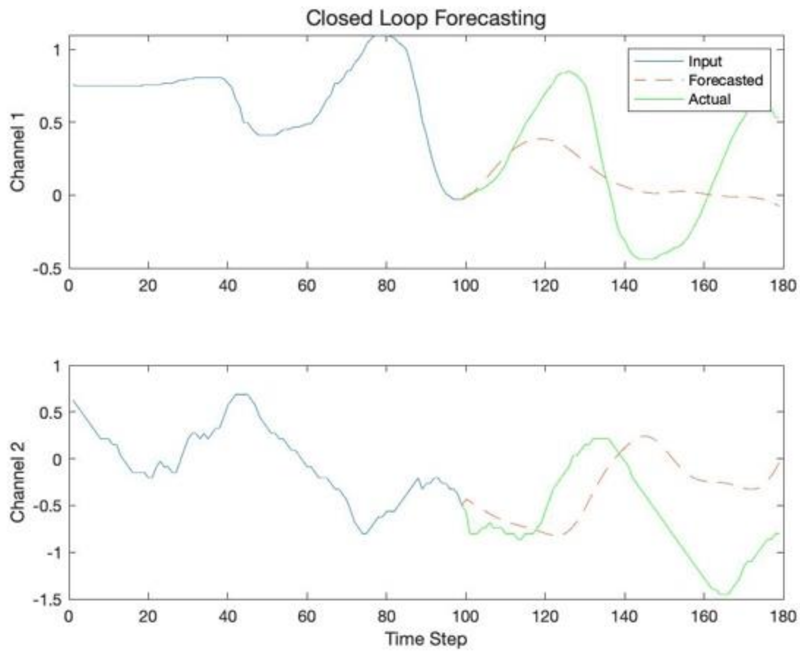

Figure 6-30 Closed-loop forecasting

Then, changing the data splitting methods into 80 datapoints $\times$ 950 datasets (example of input data plots shown in Figure 6-31), with the time step of 0.5 hours, 600 epochs, and the hidden units of 150, a more accurate prediction model has been trained.

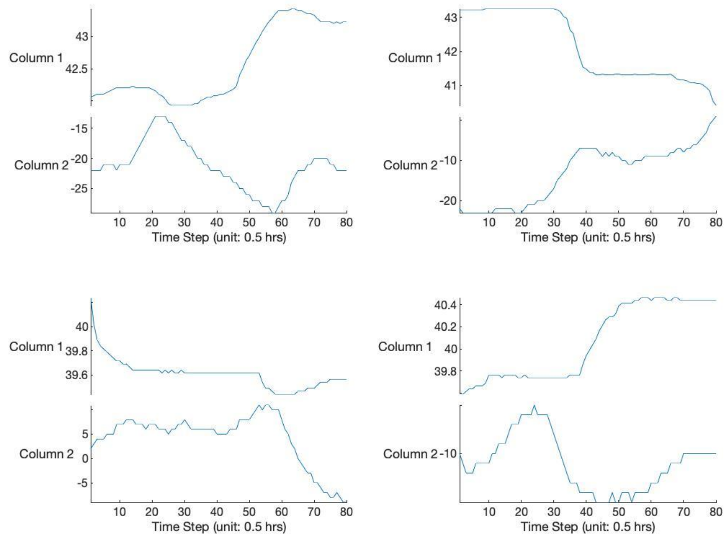

Figure 6-31 Example input data plots

After the network was trained, the root means squared error (RMSE) was calculated to evaluate the accuracy between the prediction and observed values. The visualized histogram is shown in Figure 6-32, with an average value of 0.035.

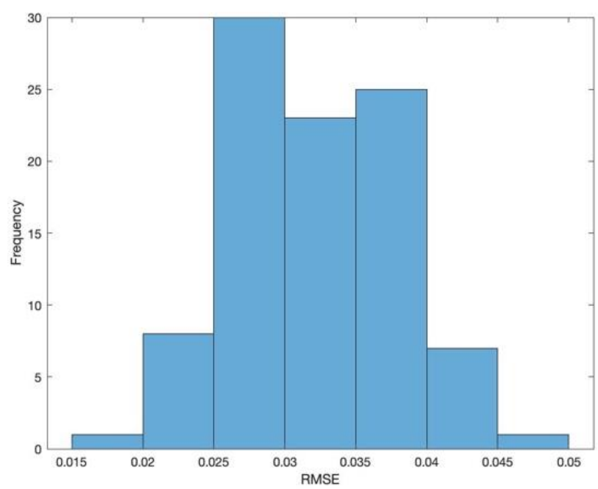

Figure 6-32 Histogram of RMSE

An example of open-loop forecasting and closed-loop forecasting are shown in Figure 6-33 and Figure 6-34:

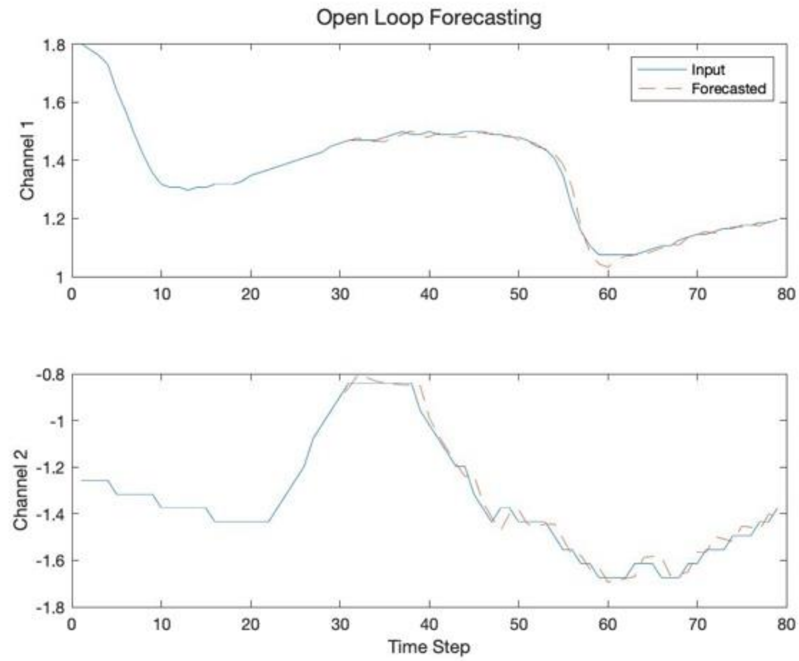

Figure 6-33 Open-loop forecasting

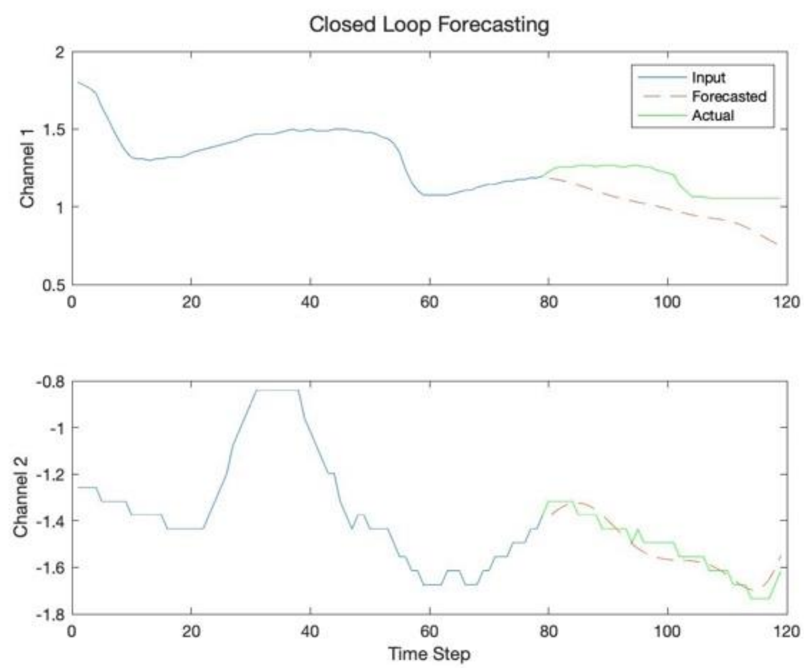

Figure 6-34 Closed loop forecasting

Chapter 7: Structural performance assessment criteria of rehabilitated steel bridges

7.1 Problem formulation

This chapter describes the first scenario of bridge performance assessment after a steel bridge rehabilitation. To develop the rapid performance assessment model, the configuration of the bridge in the evaluation database is generated from the sampling of the initial bridge database. Then a large batch of finite element models is built to simulate bridge deterioration by local defects and material aging. After the structure's performance has been studied, the fuzzy logic system is generated and updated, then the evaluation database for the model training is expanded using machine learning techniques. And finally, to find the best candidate for the bridge repair recommendations.

7.2 Methodologies

To get a further understanding of structure before and after preventive maintenance or structural rehabilitation, finite element models are needed as the database lacks the feature of structure behavior under service life. Then the evaluation of the repairing assessment is made using the Fuzzy Logic condition assessment method. In the first scenario, a large database for the model training is preferred to avoid overfitting. Thus, the assessment database will be created based on the result of the Finite Element analysis and evaluated by the Fuzzy Logic method while cross-checking by experts. After the fuzzy logic system is established, the input of the database will be expanded using arbitrary values within the range under the categorized input features. Then re-evaluate the expanded database using the fuzzy logic system to generate the training set and testing set for the machine learning classification model.

Membership functions that are constructed and applied in this research are:

- Generalized bell-shaped membership function

$$f(x; a, b, c) = \frac{1}{1+\left|\frac{x-c}{a}\right|^{2b}} \qquad \text{Equation 20}$$

- Trapezoidal membership function

$$f(x; a, b, c, d) = \max\left(\min\left(\frac{x-a}{b-a}, 1, \frac{d-x}{d-c}\right), 0\right) \qquad \text{Equation 21}$$

- Gaussian membership function

$$f(x; \sigma, c) = e^{\frac{-(x-c)^2}{2\sigma^2}} \qquad \text{Equation 22}$$

- Sigmoidal membership function

$$f(x; ak, ck) = \frac{1}{1+e^{-ak(x-ck)}} \qquad \text{Equation 23}$$

7.3 Parametric study on the repaired bridge model

In this chapter, a total of 1280 finite element models have been generated using Latin hypercube sampling from the original database. All these models use 3D shell elements (Figure 7-1) with the bearing condition of 'Fixed-Expansion-Expansion.' An unexpected extreme case might be generated when sampling the databased by span length and deck width individually. Thus, a more effective way for the bridge sampling for its configuration is to use the distribution of span length/ deck width ratio. This parametric study fixed the deck width to 374 inches. Then the span length could be calculated using the ratio from the sampling respectively. These batch of models are different in span lengths (16 different parameters from 21ft to 181ft.), aging of material (4 parameters with a modulus of elasticity decreasing from 0% to 20%), defect type (concrete deterioration, steel section loss, and bearing freezing), and defect locations (5 major locations which are both abutments, mid spans, top of the center pier.).

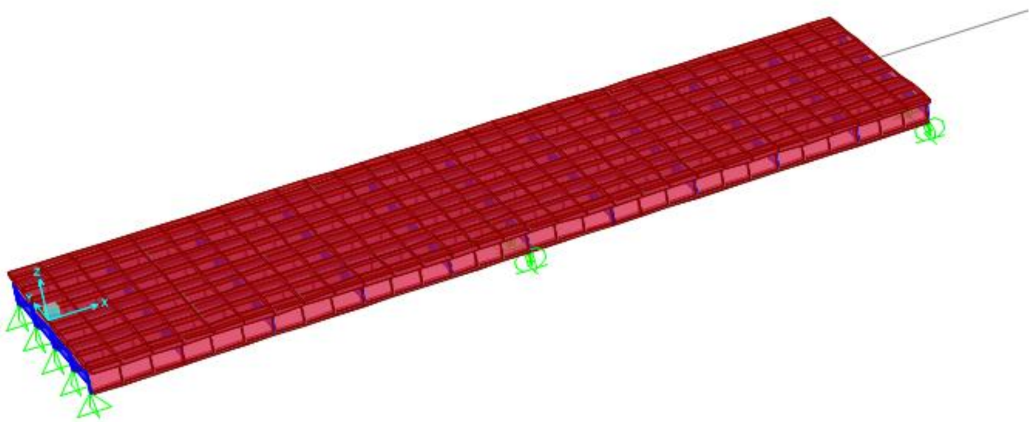

Figure 7-1 Finite element model for the parametric study

<u>*7.4 Data analysis*</u>

The FE modeling and simulation process in this chapter is similar to Chapter 5. After building, updating, and analyzing those models, the output needed in this research is the reactions, moment, shear, and stress distribution for the bridges under vertical load (DL and LL), and thermal load (including thermal gradient and thermal expansion/ contraction). All the results from (1) the original bridge; (2) the deteriorated (aging) bridge model without local defects; (3) the deteriorated (aging) bridge model with local defects; and (4) the deteriorated (aging) bridge model with local defects repaired with the material without deterioration have been parallel compared with each other. Then, the maximum moment, shear, and stress changes between (1) and (2) were used to study the aging effect of the structure. The comparison between (2) and (3) shows the severity of the defect location. The comparison between (3) and (4) demonstrates the effectiveness of the repaired work, and the comparison among (1), (2), and (4) provides a signal for behavior improvement.

Figure 7-2 shows the relationship between the material aging rate and the difference in structural response compared with (3) and (4). it can be clearly figured that the difference in structure response due to material aging reduction has no significant relation with the span length.

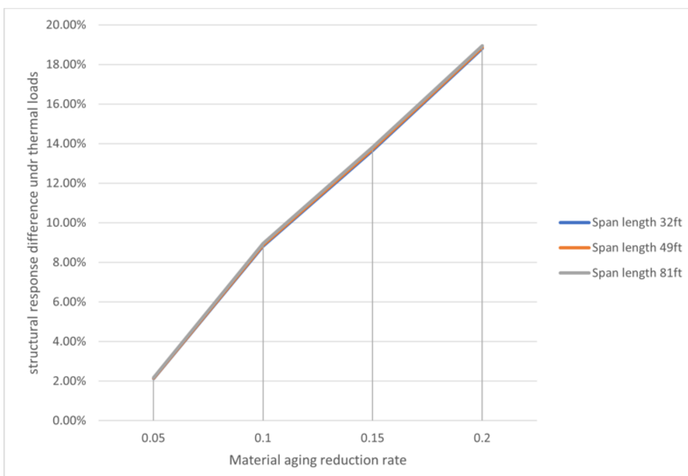

Figure 7-2 Comparison of the structural response difference under several span lengths due to material aging

The outputs of the bridge models are summarized, and the comparison between (3) and (4) has input in the repairing recommendation database. This database consists of 10 input features, which include (1) bridge age, (2) length/ width ratio, (3) previous inspection condition of the bridge, (4) percentage of local steel section loss, (5) percentage of local concrete section loss, (6) bearing conditions, (7) defect locations, (8) the budget of the repairing work, and (9 & 10) the maximum stress difference between the defected bridge and the repaired bridge under dead load or thermal load. Once this database was developed (with 544 datasets), it could be assigned to the fuzzy logic system for the repair recommendation.

7.5 Structural condition evolution using Fuzzy logic

7.5.1 Fuzzy logic properties

This research uses the Fuzzy Logic Designer in Matlab to generate the fuzzy logic system. As the input of the database showed ten features (listed above) and requested one (1) output (recommendation), the properties of the fuzzy logic is to construct ten sets of membership function as input and one (1) set of membership function as output. All the data has been converted into numbers so that the value of the output can be calculated. In this fuzzy logic system design process, the Type 1 Mamdani system (Figure 7-3) was first introduced because the output membership function could be easily defined and understood. After the system has been developed and updated, a Type 1 Sugeno (Figure 7-4) system has been converted from the previous system for future use (data clustering using Neuro-Fuzzy techniques).

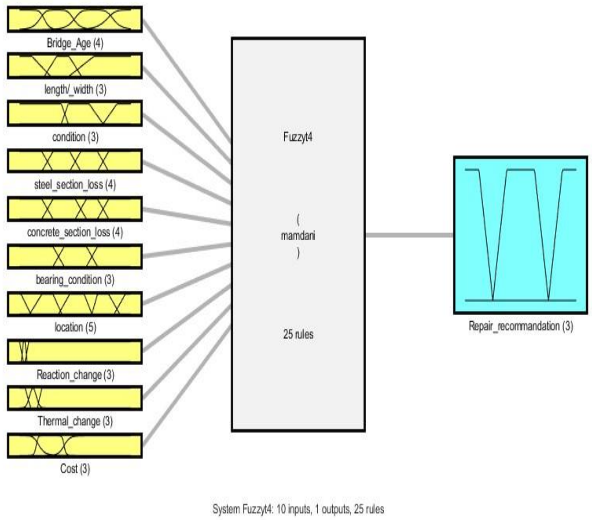

Figure 7-3 Type 1 Mamdani system properties

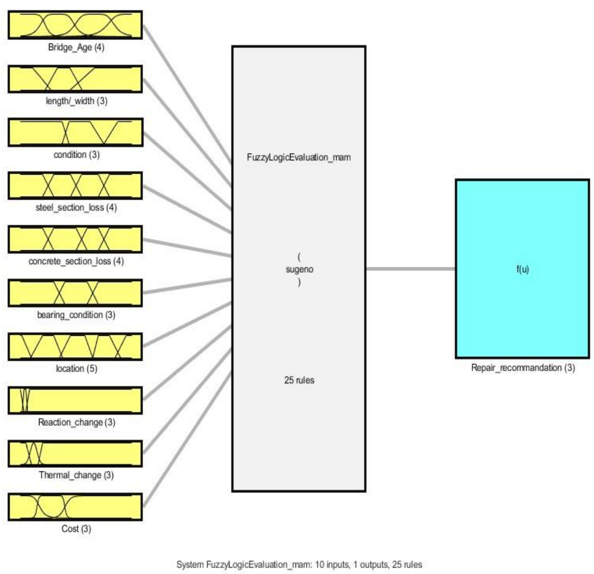

Figure 7-4 Type 1 Sugeno system properties

7.5.2 membership function

The membership constructed in the fuzzy logic system is listed in Figure 7-5 and shown in Table 7-1.

Table 7-1. Membership functions of the input features in the fuzzy logic system

Input Variables	Range	Membership function		
		Name	Type	Parameters
Bridge Age MF1	[0 120]	Young	Generalized bell-shaped membership function	[27.14 4.92 5.328e-16]
		Young-Mid	Generalized bell-shaped membership function	[18.889 2.5 40]
		Mid-Old	Generalized bell-shaped membership function	[21.746 2.5 80]
		Old	Generalized bell-shaped membership function	[26.8254 2.5 120]
Span length MF2	[0 180]	Short span	Trapezoidal membership function	[-81 -9 20 50]
		Mid span	Trapezoidal membership function	[40 60 80 100]
		Long span	Trapezoidal membership function	[80 120 180 261]
Previous condition MF3	[1 9]	Poor	Trapezoidal membership function	[-1.15 -1 4 4.5]
		Fair	Trapezoidal membership function	[4 4.5 6 7]
		Good	Trapezoidal membership function	[7 8 10 12]
Steel section loss MF4	[0 20]	Light	Trapezoidal membership function	[-9.3 -3.1 4 6]
		Medium	Trapezoidal membership function	[4 6 9 11]
		Very severe	Trapezoidal membership function	[14 16 23 25]
		Severe	Trapezoidal membership function	[9 11 14 16]
Concrete section loss MF5	[0 20]	Light	Trapezoidal membership function	[-6 -0.6666 4 6]
		Medium	Trapezoidal membership function	[4 6 10 12]
		Severe	Trapezoidal membership function	[10 12 14 16]
		Very severe	Trapezoidal membership function	[14 16 20 26]
Bearing condition MF6	[0 10]	Poor	Trapezoidal membership function	[-3.753 -0.417 3 4]
		Mid	Trapezoidal membership function	[3 4 6 7]
		Good	Trapezoidal membership function	[6 7 12 15]

Input Variables	Range	Membership function		
		Name	Type	Parameters
Location MF7	[0 10]	SideA	Trapezoidal membership function	[-2.25 -0.25 0.1321 1]
		mid1	Trapezoidal membership function	[0.916 2 3 3.8]
		mid2	Trapezoidal membership function	[3.5 4.5 5.8 6.5]
		mid3	Trapezoidal membership function	[6.5 7 8 9]
		sideB	Trapezoidal membership function	[8.5 9.5 10 12.25]
Reaction Change MF8	[0 300]	Bad	Trapezoidal membership function	[-101.7 -48.33 0 10]
		Notice	Trapezoidal membership function	[5 10 15 20]
		Good	Trapezoidal membership function	[15 25 326.2 353.8]
Thermal Change MF9	[0 500]	Acceptable	Trapezoidal membership function	[-169.5 -80.55 25 50]
		Notice	Gaussian membership function	[15 60]
		Good	Trapezoidal membership function	[80 100 900 1200]
Cost (Budget) MF10	[0 20000]	low	Generalized bell-shaped membership function	[3500 3.23 -1.14e-13]
		mid	Generalized bell-shaped membership function	[2500 7.29 5500]
		high	Sigmoidal membership function	[0.001886 8000]

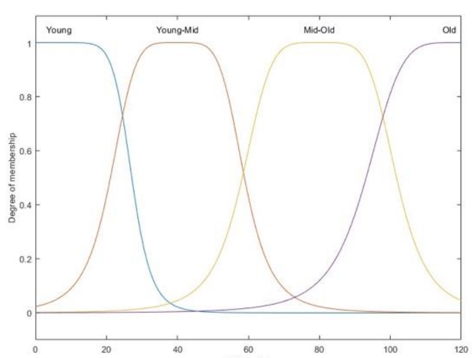

(a). MF1

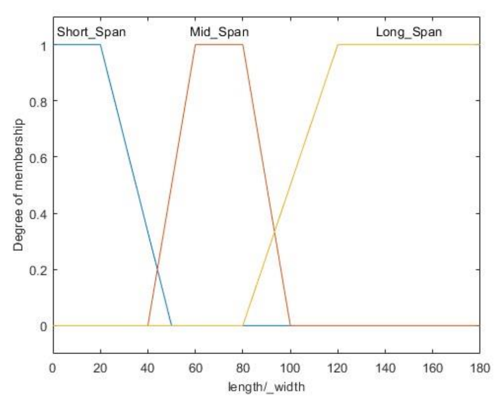

(b) MF2

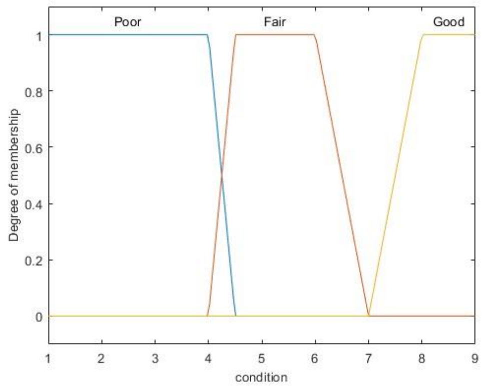

(c). MF3

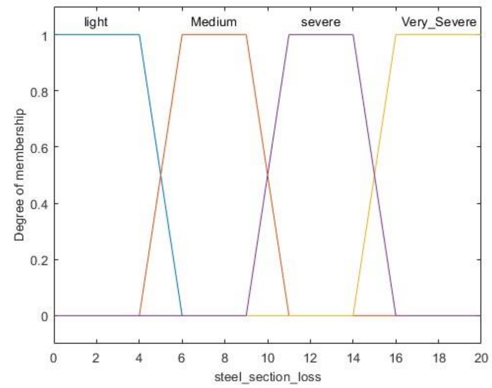

(d) MF4

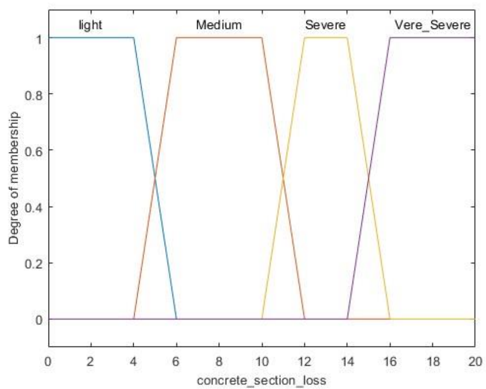

(e). MF5

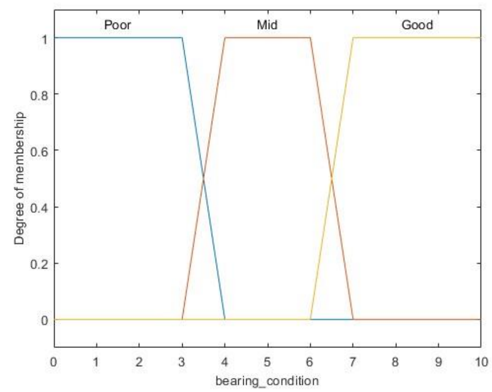

(f) MF6

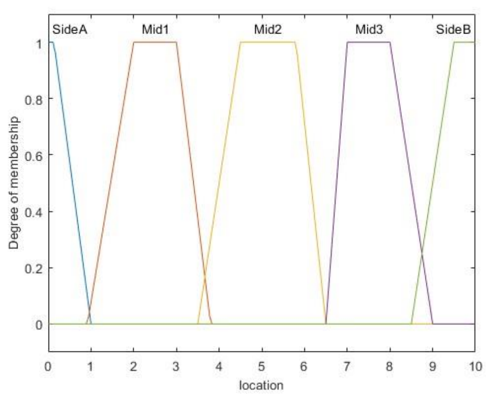

(g). MF7

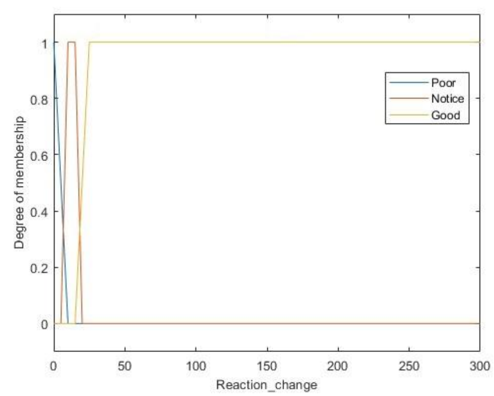

(h) MF8

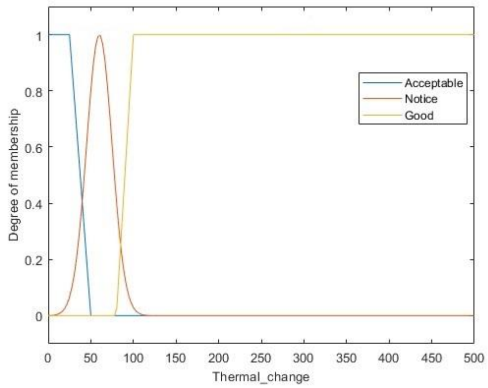

(i). MF9

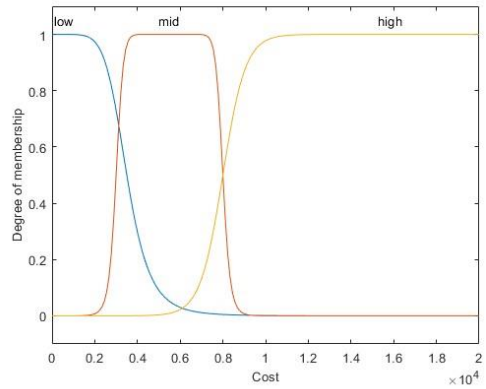

(j) MF10

Figure 7-5 Membership function of Type 1 Mamdani and Type 1 Sugeno system

Considering the uncertainty of those membership functions, a Type 2 Sugeno system has also been introduced for later verification of the recommendations. Those membership functions have been plotted in Figure 7-6.

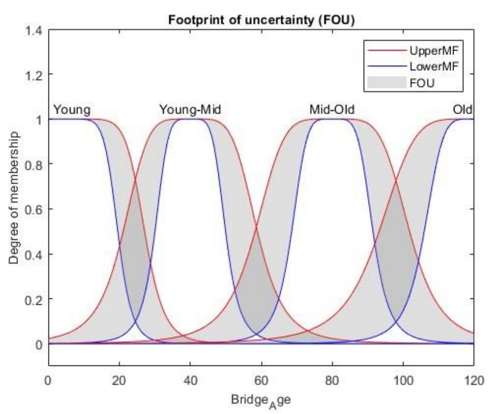

(a). MF1

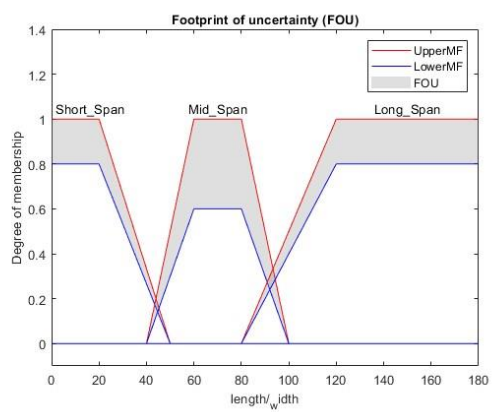

(b) MF2

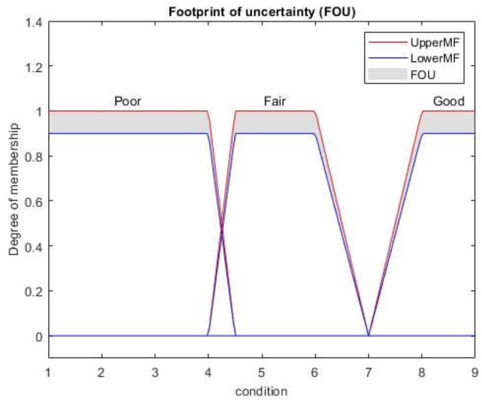

(c). MF3

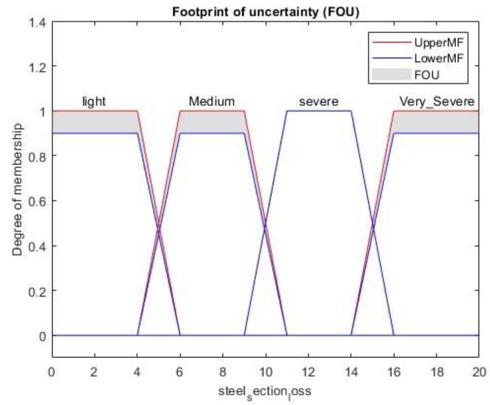

(d) MF4

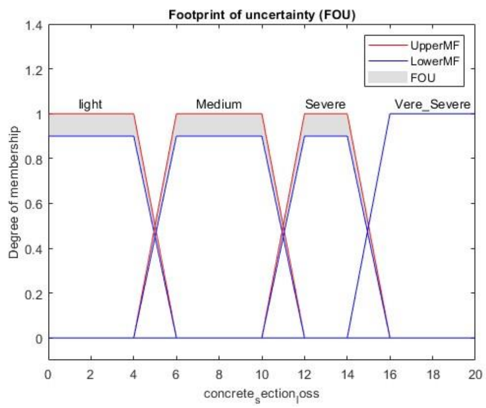

(e). MF5

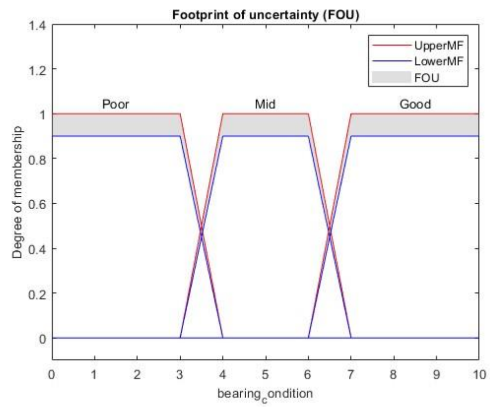

(f) MF6

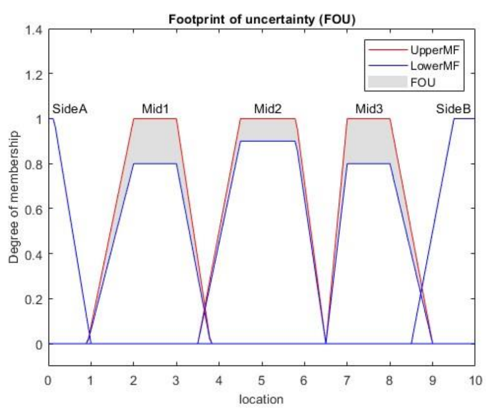

(g). MF7

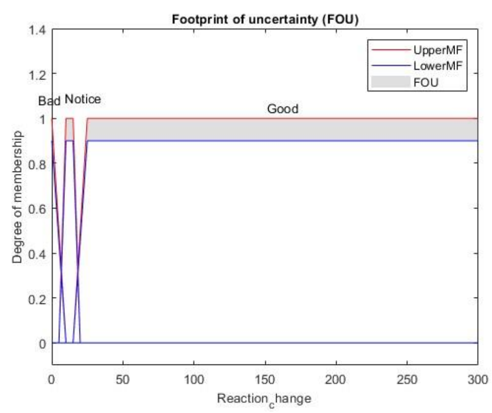

(h) MF8

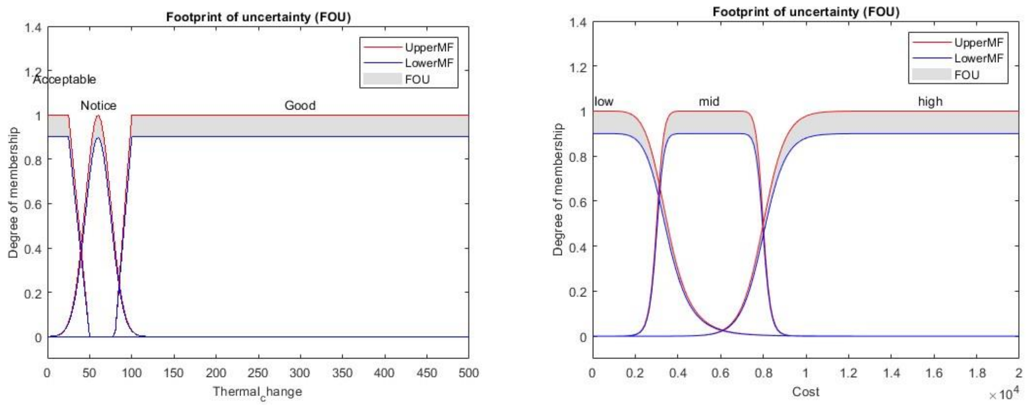

(i). MF9 (j) MF10

Figure 7-6 Type 2 Sugeno membership functions

The membership function for the Type 1 Mamdani system is plotted in Figure 7-7. Combining the rules of the logic system (listed in Table 7-2), the bridge repair recommendation would be given. In this process, all rules are evaluated and selected based on the recommendations from experts and engineers.

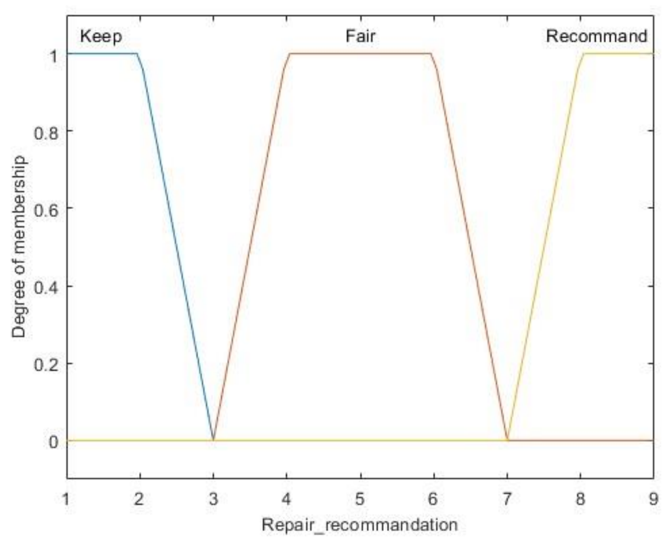

Figure 7-7 Type 1 Mamdani output membership function

Table 7-2. Rules for the fuzzy logic system

No.	Rules	
	If	Then (Repair recommendation)
1	If (Bridge_Age is not Old) and (condition is Good) and (steel_section_loss is light) and (concrete_section_loss is light) and (bearing_condition is Good) and (Cost is not high)	Keep
2	If (Bridge_Age is Old) and (condition is Poor) and (steel_section_loss is severe) and (location is Mid2) and (Cost is not high)	Fair
3	If (steel_section_loss is Very_Severe) or (concrete_section_loss is Vere_Severe) or (bearing_condition is Poor)	Recommend
4	If (Bridge_Age is Old) and (length/_width is not Short_Span) and (condition is Poor) and (Cost is low)	Recommend
5	If (Bridge_Age is not Old) and (condition is Good) and (steel_section_loss is light) and (concrete_section_loss is light) and (bearing_condition is Good	Keep
6	If (condition is Poor) and (Reaction_change is Good) and (Cost is not high)	Recommend
7	If (condition is Poor) and (Thermal_change is Good)	Recommend
8	If (Bridge_Age is not Old) and (steel_section_loss is not Very_Severe) and (concrete_section_loss is not Vere_Severe) and (bearing_condition is not Poor) and (Cost is high)	Fair
9	If (length/_width is not Long_Span) and (condition is not Poor) and (Thermal_change is not Good) and (Cost is high)	Keep
10	If (Reaction_change is Good) or (Thermal_change is Good)	Recommend
11	If (steel_section_loss is Very_Severe) and (location is Mid2) and (Reaction_change is Good) and (Cost is not high)	Recommend
12	If (concrete_section_loss is Vere_Severe) and (location is SideB) and (Reaction_change is Good) and (Cost is not high)	Recommend
13	If (concrete_section_loss is Vere_Severe) and (location is Mid2) and (Reaction_change is Good) and (Cost is not high)	Recommend
14	If (steel_section_loss is Very_Severe) or (concrete_section_loss is Vere_Severe) or (bearing_condition is Poor)	Recommend
15	If (bearing_condition is Poor) and (location is Mid2) and (Thermal_change is not Acceptable)	Recommend
16	If (steel_section_loss is severe) and (bearing_condition is not Good)	Recommend
17	If (concrete_section_loss is Vere_Severe) and (bearing_condition is not Good)	Recommend
18	If (steel_section_loss is Very_Severe) and (bearing_condition is not Good)	Recommend
19	If (condition is not Good) and (steel_section_loss is Very_Severe) and (bearing_condition is not Good)	Recommend
20	If (condition is Poor) and (bearing_condition is Poor)	Recommend
21	If (condition is Poor) and (steel_section_loss is Very_Severe) and (location is Mid1)	Recommend

No.	Rules	
	If	Then (Repair recommendation)
22	If (condition is Poor) and (concrete_section_loss is Vere_Severe) and (location is Mid2)	Recommend
23	If (condition is Poor) and (concrete_section_loss is Vere_Severe) and (location is SideB	Recommend
24	If (condition is Poor) and (bearing_condition is not Good) and (location is SideB)	Recommend
25	If (condition is Poor) and (bearing_condition is not Good) and (location is Mid2) and (Reaction_change is not Bad)	Recommend

The structure of this fuzzy logic system shows in Figure 7-8. Following the process to assign each feature value to the inputs, then calculate the output value by applying the rules of the logic. The visualized rules and surfaces are shown in Figure 7-9 and Figure 7-10. After the system shows the result of recommendations, it converts this into a verbal format. Then manually check if the result is reasonable. When an unexpected recommendation occurs, the membership function and rules must be manually re-evaluated and updated.

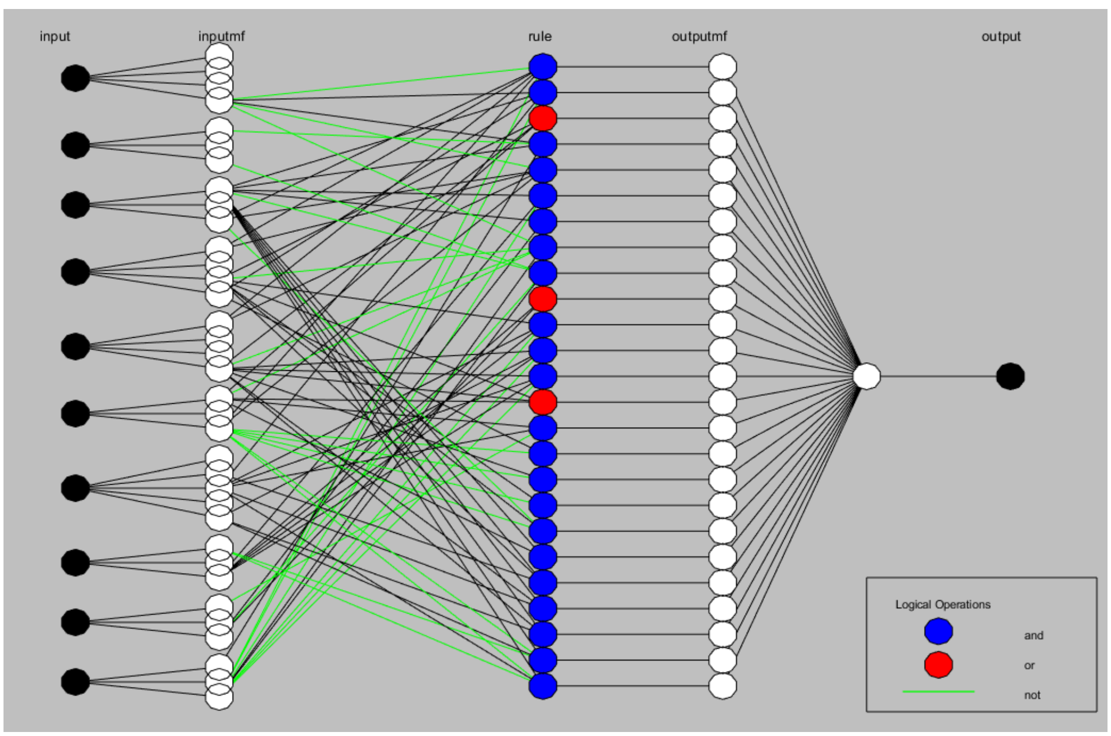

Figure 7-8 Structure of the fuzzy logic system

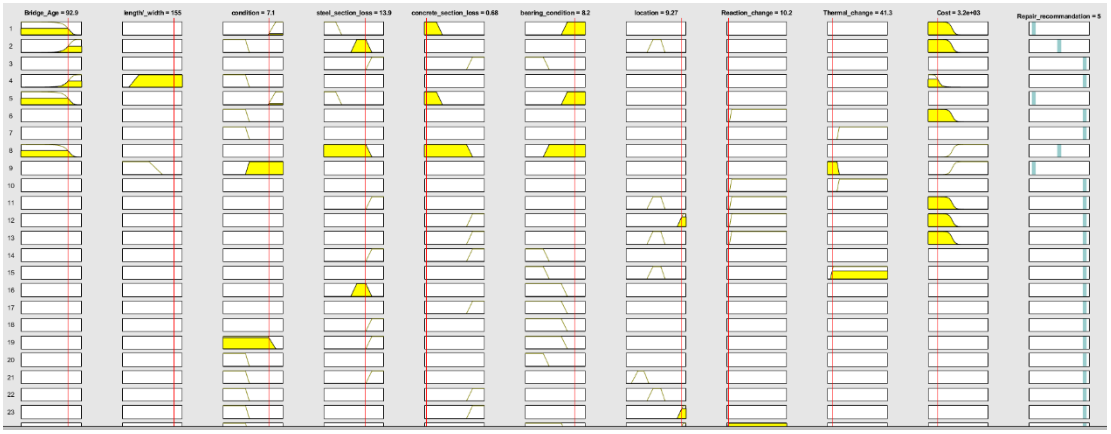

Figure 7-9 Visualised rule of the fuzzy logic system

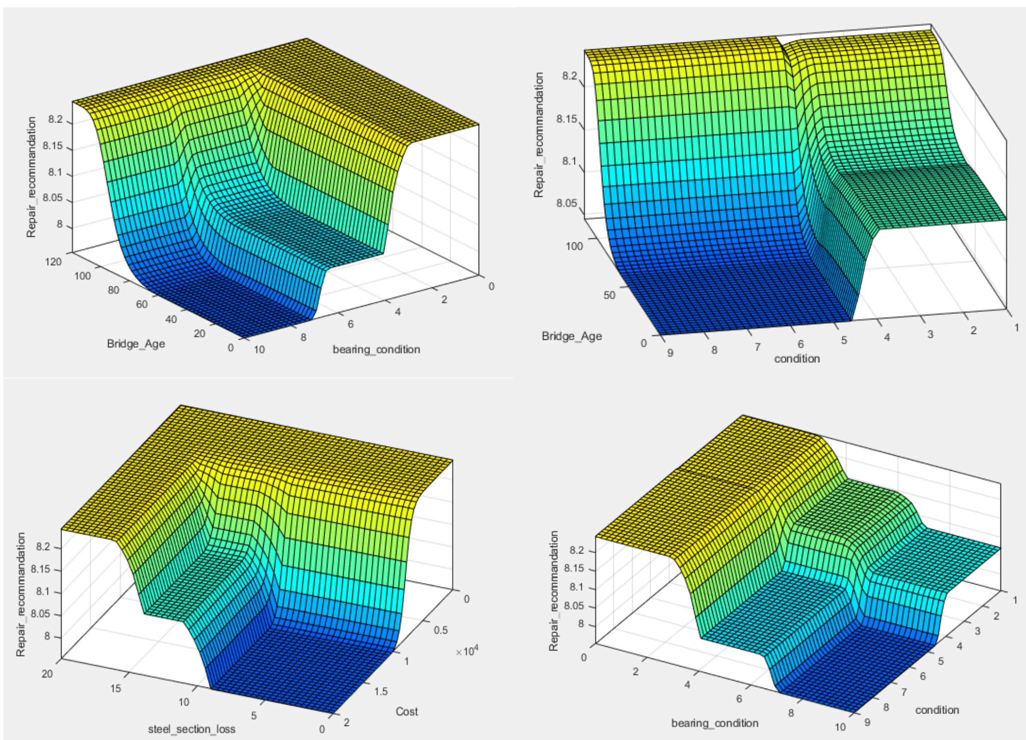

Figure 7-10 Visualized surface of the fuzzy logic system

After the initial bridge repair recommendation database has been generated and the effectiveness of the fuzzy logic system has been evaluated, more data with random features has been introduced to expand the database for further assessment. The final database has been expanded with a total of 4640 datasets. Then using the fuzzy logic system for the recommendations. Combined with the input and output features, a new database with 11 features has been developed. Then deleting two features that require FE analysis and only keeping the bridge basic information and defect information. Thus, the rapid bridge performance assessment training database has been fully developed.

7.6 Model prediction and structural performance assessment

This section focuses on the model training and selections. By importing the rapid bridge performance assessment training database, which has been described before, using the seven (7) bridge and defects information features as input and repair recommendations as output, the rapid structure performance assessment model is trained using machine learning techniques.

7.6.1 Rapid assessment of bridge repairing

The bridge performance assessment training database includes an output for repair recommendations, which has more than 50% of them showing as repair recommended (Figure 7-11). This shows a similar distribution as the 'bridge condition' feature (more than 50% of 'Fair') in the initial database.

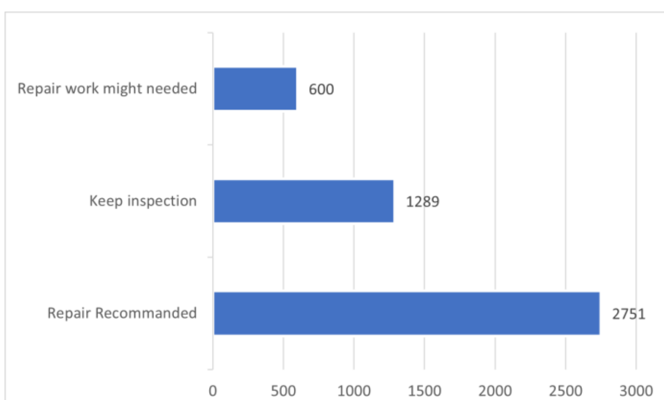

Figure 7-11 Repair recommendation distribution of the database

The model training process starts from the model selection. In this research, all potential machine learning classification methods have been used for model training.

To protect against overfitting, five-fold cross-validation is introduced and estimates the accuracy on each fold. The result of the training process is listed in Table 7-3. The validation confusion matrix, as well as the true positive rate (TPR) and false-negative rate (FNR), are plotted in Figure 7-12.

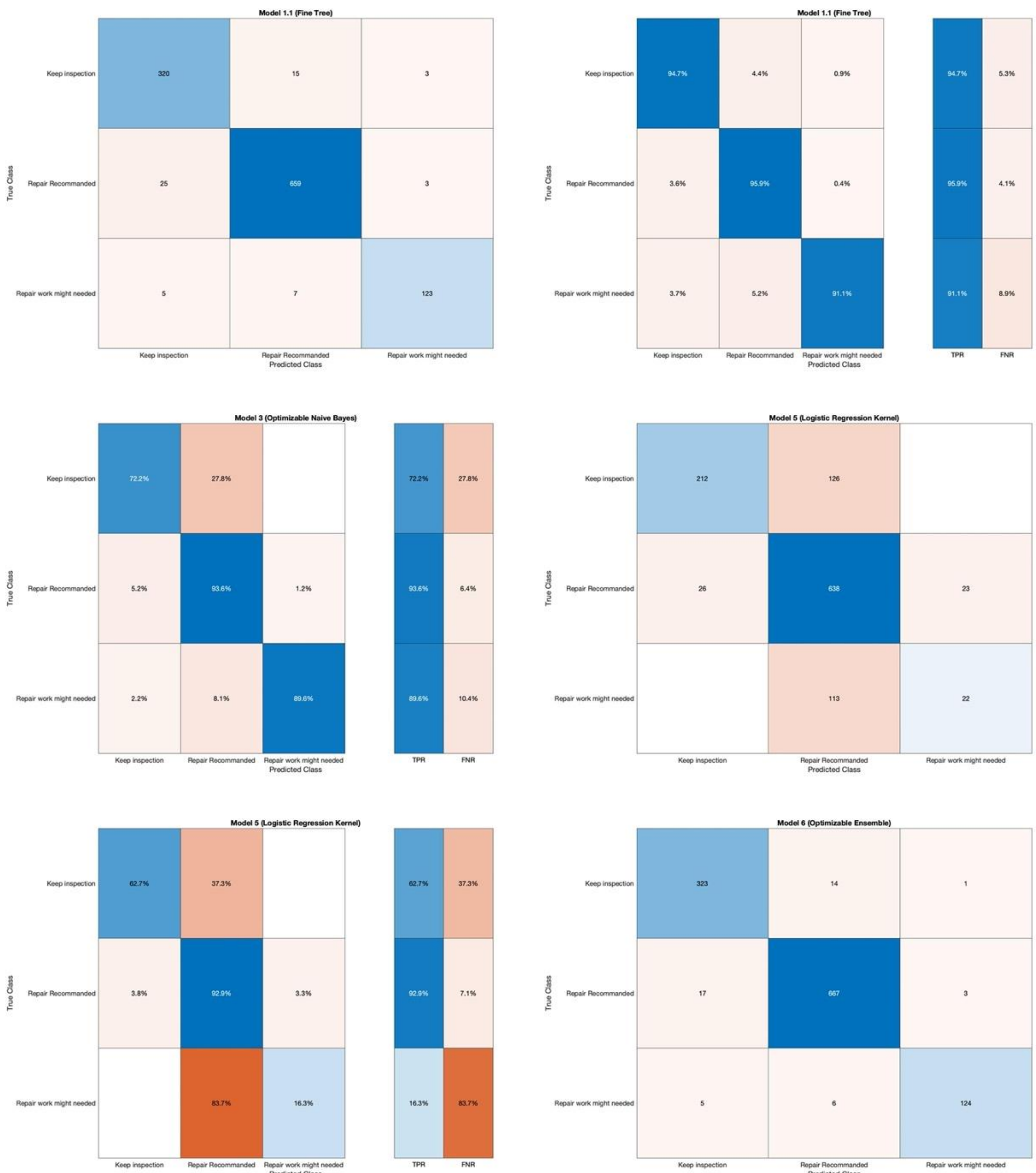

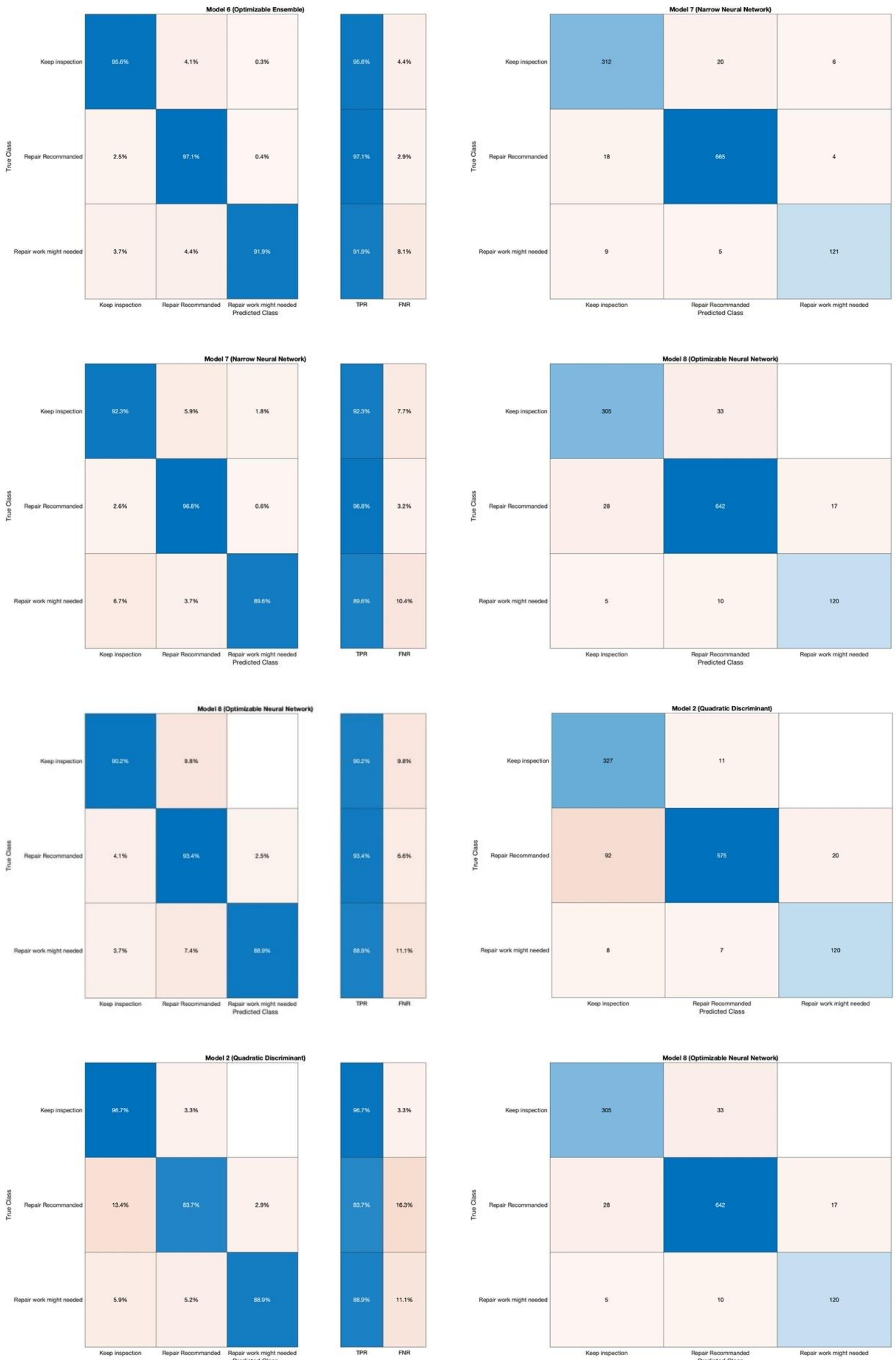

Figure 7-12 Validation confusion matrix of the model

Table 7-3. Summary of the validated accuracy of the model

Model Name	Accuracy
Fine tree	95.0%
Medium tree	92.1%
Coarse tree	88.4%
Fine KNN	92.2%
Medium KNN	93.4%
Coarse KNN	92.4%
Cosine KNN	93.7%
Weighted KNN	93.7%
Quadratic Discriminant	88.1%
Optimizable Naïve Bayes	86.9%
Optimizable SVM	95.2%
Logistic Regression Kernel	75.2%
Optimizable Ensemble	96.0%
Narrow Neural Network	94.7%
Optimizable Neural Network	92.0%

7.6.2 Assessment model updating

As previse model shows excellent performance on the assessment, more variants would be added to the output features, where including details of the bridge repair recommendations. i.e., new variants subjected to bearing replacement, deck replacement, and fatigue crack checking on steel girders have been introduced with some noise that was randomly added (Figure 7-13). Then using, the same scenario of model training, which includes both training and cross-validation of the model, to generate machine learning models for comparison and selecting the best model for the rapid performance assessment model of this research. Table 7-4 shows a summary of the feature importance score that was applied to the model. The result of the training process is listed in Table 7-5, and the validation confusion matrix, as well as the true positive rate (TPR) and false-negative rate (FNR), are plotted in Figure 7-14. Figure 7-15 and Figure 7-16 show example plots during the training process.

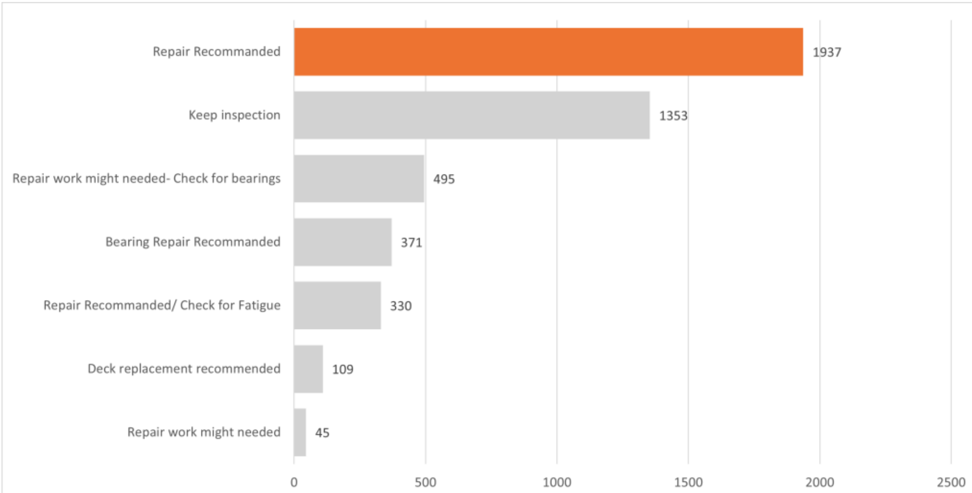

Figure 7-13 Updated repair recommendation distribution of the database

Table 7-4. Summary of the Feature importance score of the model

Algorithm	Features	Importance score	Figure
RelieIF	Bearing condition	0.2475	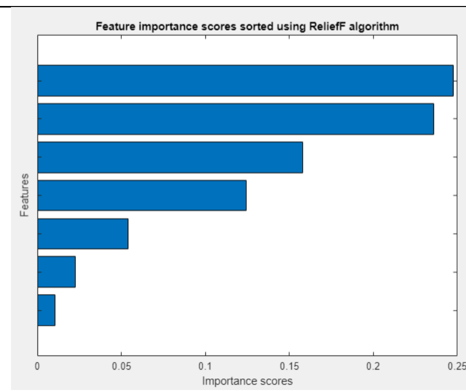
	Repair cost	0.2357	
	Steel section loss	0.1581	
	Concrete section loss	0.1242	
	Bridge Age	0.0541	
	Previous condition	0.0228	
	Span length	0.0103	
MRMR	Repair cost	0.4211	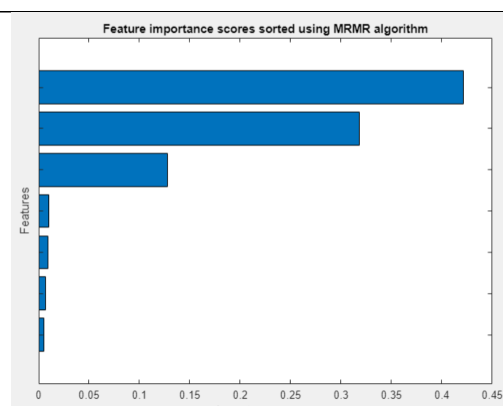
	Previous condition	0.3179	
	Bridge Age	0.1280	
	Steel section loss	0.0098	
	Bearing condition	0.0092	
	Concrete section loss	0.0067	
	Span length	0.0054	

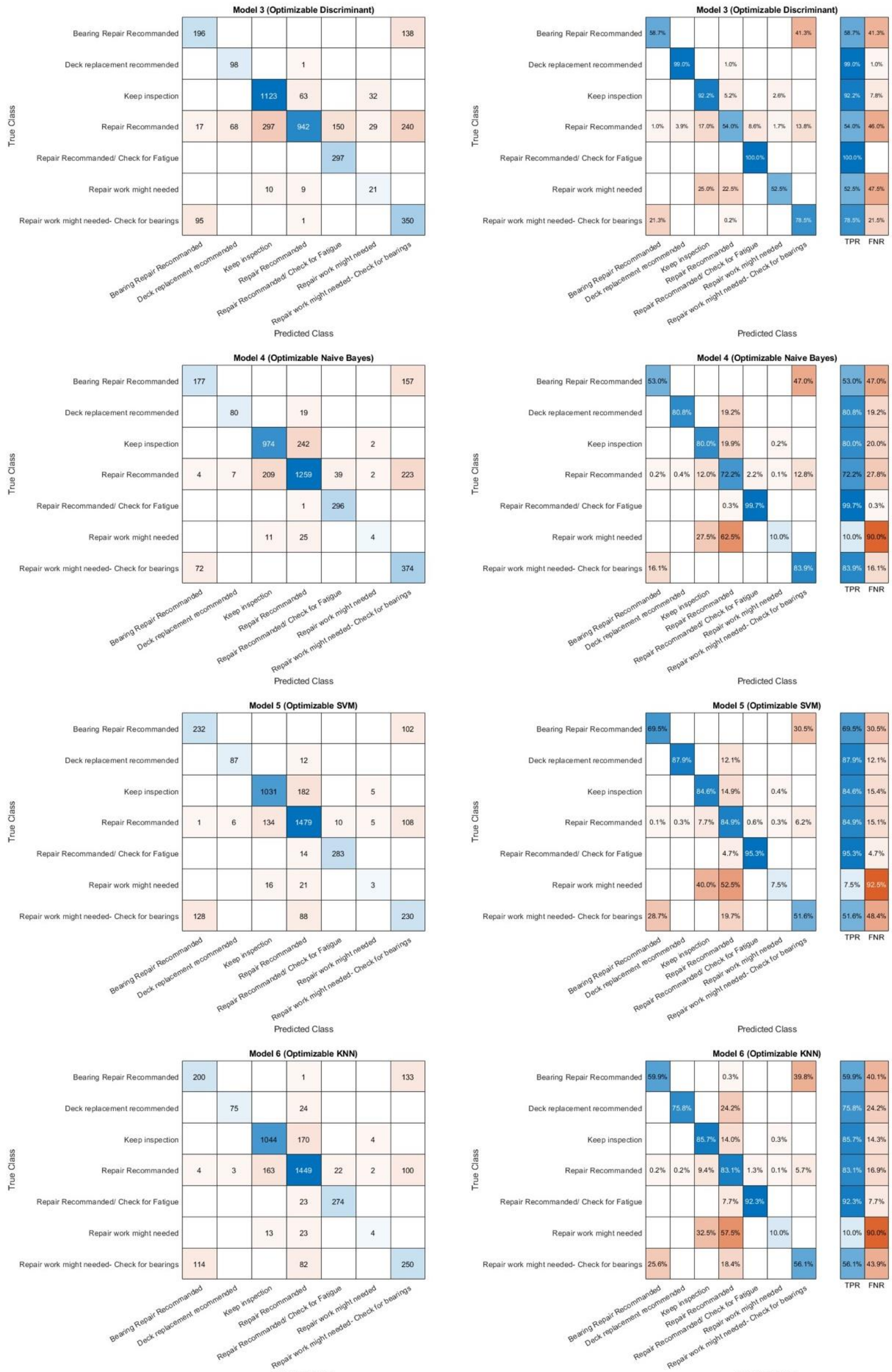
Model 3 (Optimizable Discriminant)
Model 4 (Optimizable Naive Bayes)
Model 5 (Optimizable SVM)
Model 6 (Optimizable KNN)
True Class
Predicted Class
Bearing Repair Recommanded
Deck replacement recommended
Keep inspection
Repair Recommanded
Repair Recommanded/ Check for Fatigue
Repair work might needed
Repair work might needed- Check for bearings
TPR
FNR

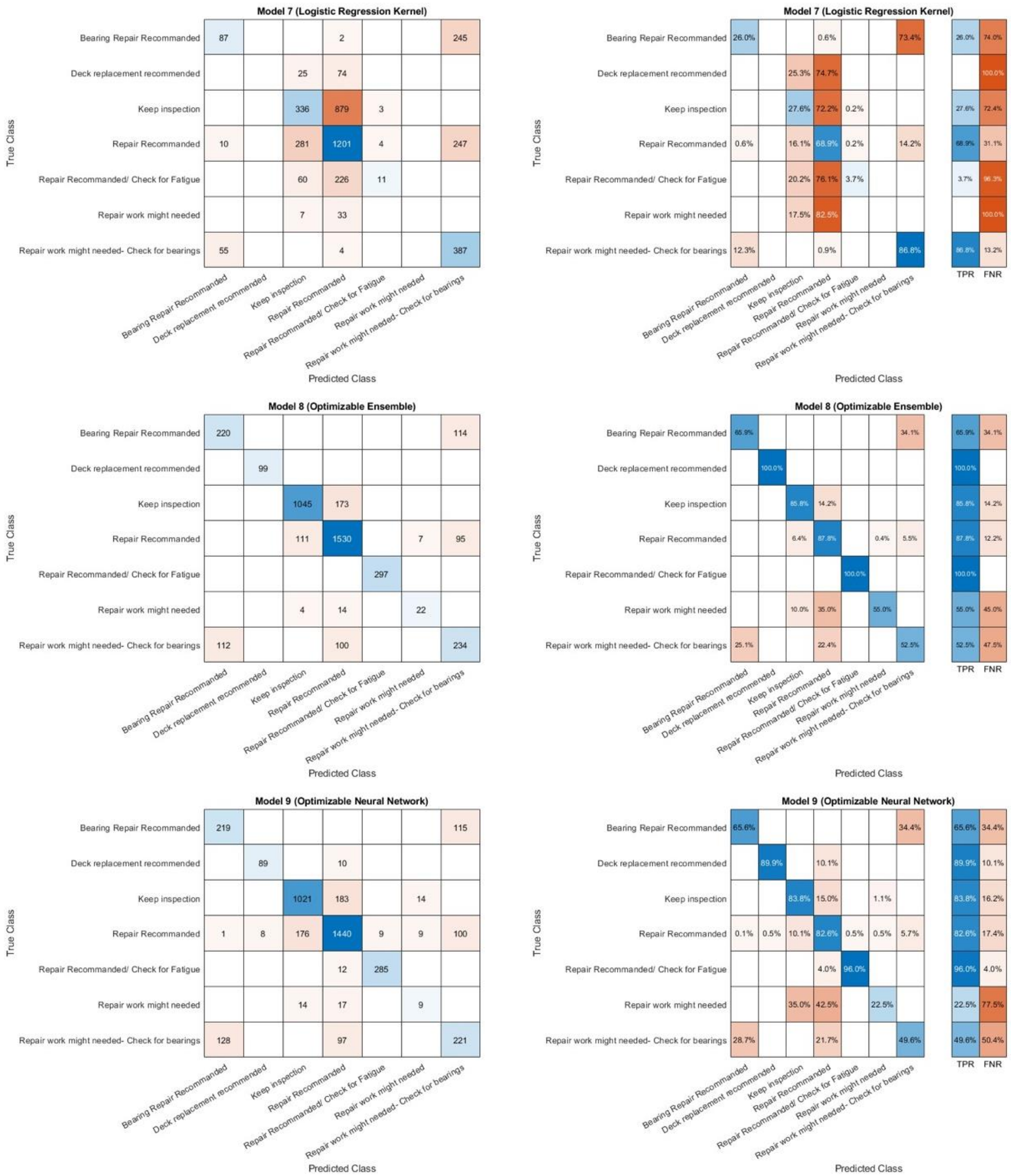

Figure 7-14 Validation confusion matrix of the model

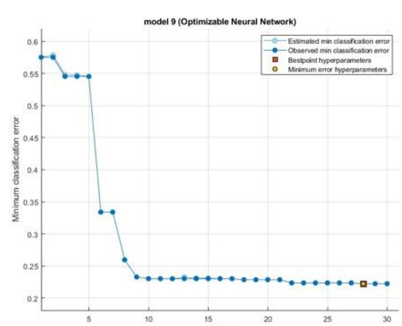

Figure 7-15 Example of the minimum classification error plot during model training

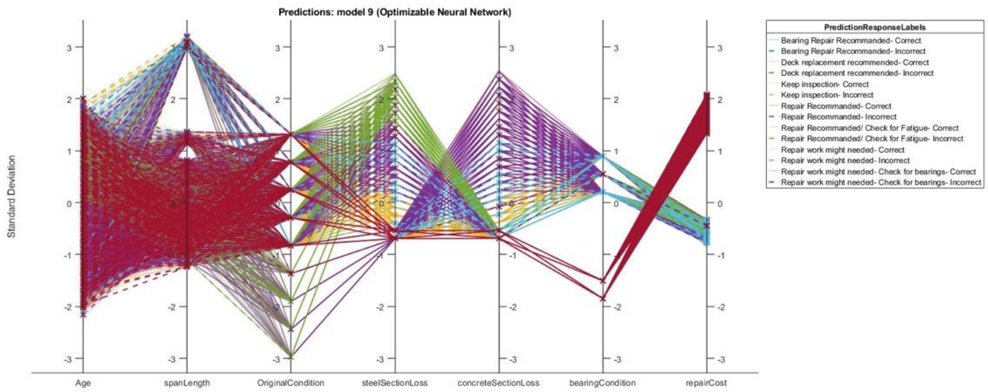

Figure 7-16 Parallel coordinate plot from the trained model

Table 7-5. Summary of the validated accuracy of the model

Model Name	**Accuracy**
Fine tree	80.8%
Medium tree	80.8%
Coarse tree	70.2%
Fine KNN	74.6%
Medium KNN	78.0%
Coarse KNN	75.2%
Cosine KNN	76.5%
Weighted KNN	78.2%
Quadratic Discriminant	72.5%
Optimizable Naïve Bayes	75.5%
Optimizable SVM	80.1%
Logistic Regression Kernel	48.4%
Optimizable Ensemble	82.5%
Neural Network	78.6%
Optimizable Neural Network	92.0%
Cubic KNN	78.8%

Chapter 8: Case Study: Structural Rehabilitation and Monitoring Data Analysis of a Steel Bridge crossing Patapsco River

In this chapter, the second case study is described. In this case, data analysis and structural performance forecasting are conducted. Procedures used in this chapter include data collecting using structural health monitoring techniques, cross-validation by finite element analysis, and data forecasting and assessment using the LSTM deep learning algorithm. This case highlights that the structure has undergone a long-term monitoring (more than five years) process with several design and rehabilitation works done during the monitoring period. Moreover, these structures had been inspected with the defect of steel stringers section loss, bearing freezes, severe concrete deck deterioration, etc. Thus, this project is selected as a case to study the behavior of strain changes in girders and bearing movement.

Figure 8-1 Picture of the proposed bridge

8.1 Introduction and repairing plans

The dual steel bridges carrying I-70 eastbound and westbound over Patapsco River and CSX Trans in Baltimore County are selected for analysis and discussion. Both bridges consist of three units: a seven-girder two-span-continuous unit (Span 1 and Span 2), a two-girder three-span-continuous unit (Span 3 to Span 5), and a seven-girder simple span (Span 6), from west to east, respectively. Both bridges were constructed in 1965, with pier repair and bearing replacement in 2002 and deck replacement in 2019.

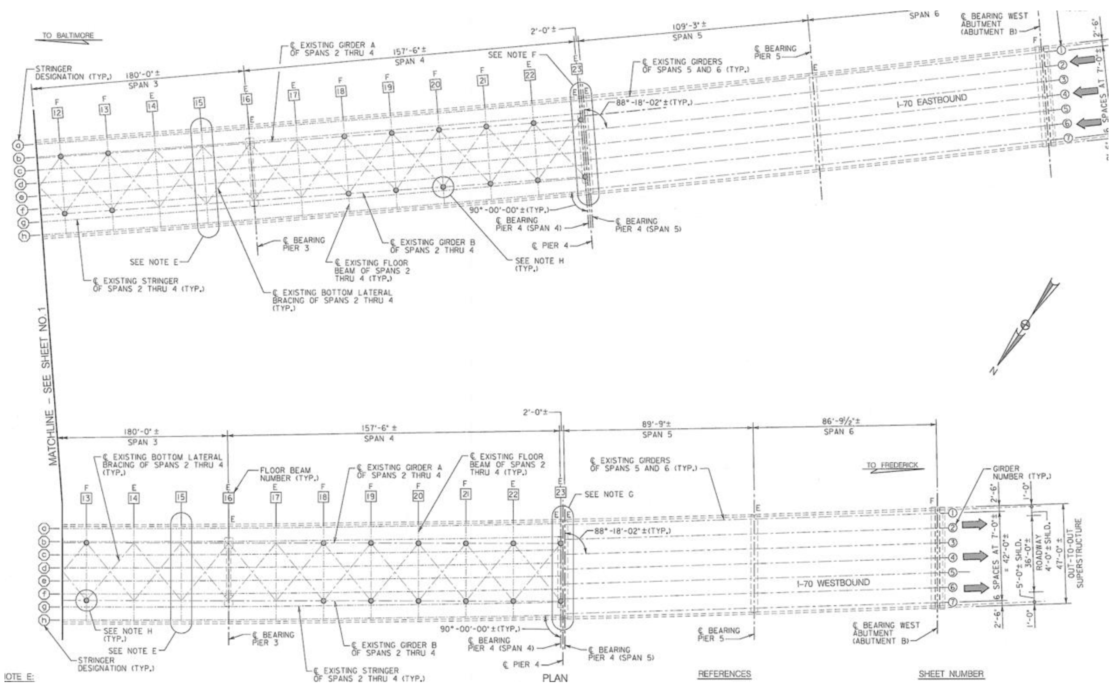

Figure 8-2 General plan of the proposed bridge

This research focused on the rocker bearing freezing and unfreezing in unit 2. The bridge was installed with a "strong back support system" and partially replaced the end-span rocker bearings with bronzed expansion bearings. The problem occurs at the bearings located in Pier 4 on the Westbound, which were previously frozen unexpectedly and partially unfroze after the repair of the pier. Comparison has been made for bearings at Pier 3 on the eastbound, which keeps partially frozen for more than five years without bearing or pier repair or replacement.

Thus, this research has collaborated with and collected data from the Maryland Department of Transportation State Highway Administration (MDSHA) for the archived design plans, inspection report, worklist, and structural health monitoring data. Then a finite element model was built for bridge analysis under thermal loading. After the structural behavior is captured and the model has been cross-validated with monitoring data, the potential reasons that might cause the bearing to freeze and unfreeze have been raised. Finally, the deep learning model to forecast the structural health monitoring data has been introduced and updated.

8.2 Model selection and establishment

8.2.1 Model establishment

The proposed bridge selects the steel floor system, consisting of stringers and floor beams, to support the entire superstructure. And the finite element model has been built based on the configuration of the superstructure. All the girders and decks use 3D shell elements. The material properties of steel are A709 Grade 50 steel, and the compressive strength of concrete is 4000 psi with the modulus of elasticity of 3600ksi. The model is built using the finite element analysis software CsiBridge and the visualized configuration shown in Figure 8-3.

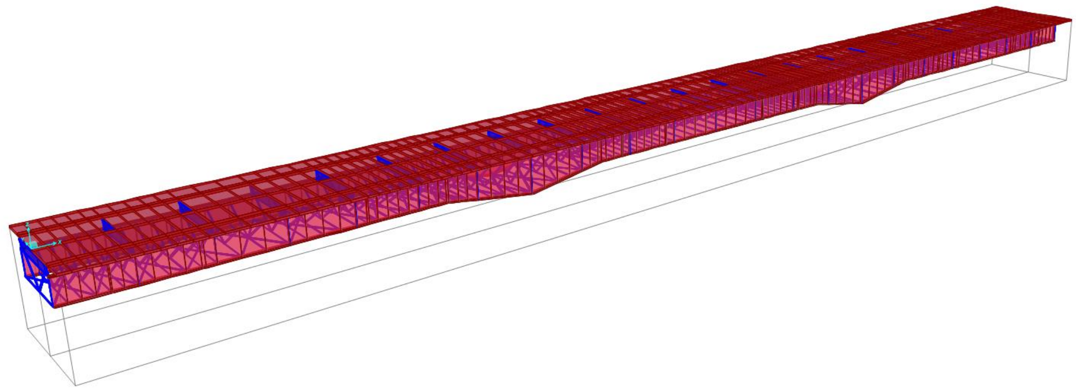

Figure 8-3 Finite Element model of the proposed bridge

8.2.2 Assessments criteria

In this study, simplified roller or hinge supports were assigned to the FE model to simulate the condition of bearing frozen or movement. Then change the bearing condition by restraining the boundary condition in the longitudinal, horizontal, and vertical directions to find the behavior change of the structure. The bridge model is considered workable when the computed value matches or is close enough to the structural health monitoring data.

8.3 Structural behavior analysis

In this research, as the bearings are mainly moving by temperature changes, the analysis case that only applies the thermal load to the structure, including both temperature gradient or thermal expansion or contraction, is used for the analysis.

Both steel and concrete's general thermal expansion coefficients have been applied when simulating the structure behavior under thermal load. Then simulating the bridge without bearing freezing, a longitudinal displacement on bearing at pier four could reach 1.9364 inches per 55 °F changes. Then applying, the longitudinal displacement value to calculate the bearing movement. The height of replaced bearing from the bridge design file could be estimated between 10.5 inches to 15 inches. Then it could be found that the bearing tilt will follow the trend with the upper limit of 0.192 $deg/$°F and a lower limit of 0.134 $deg/$°F.

Moreover, this value has been cross-checked with the structural health monitoring data. After the data processing, a general of 0.14 $deg/$°F tilt was measured from bearings under normal working conditions. Thus, the model has been validated with reliable performance under thermal loading.

8.4 Structural health monitoring data analysis

The LSTM forecasting model training and updating for performance forecasting are described in this section. The data processing and predicting will focus on data filtering, splitting, and adjusting the training options in the LSTM networks.

In this project, two types of bearing were selected, frozen bearings and free bearings. A general expansion bearing (free bearing) shows a strong relationship with temperature change, with the measurement of 0.14 $deg/$°F tilt. In contrast, a frozen bearing shows a weak relationship between movement and temperature changes. An estimated frozen bearing is monitored to be 0.013 $deg/$°F. The one-month period monitoring data example of free bearing data compared with temperature changes is plotted in Figure 8-4, and frozen bearing monitoring data shows in Figure 8-5.

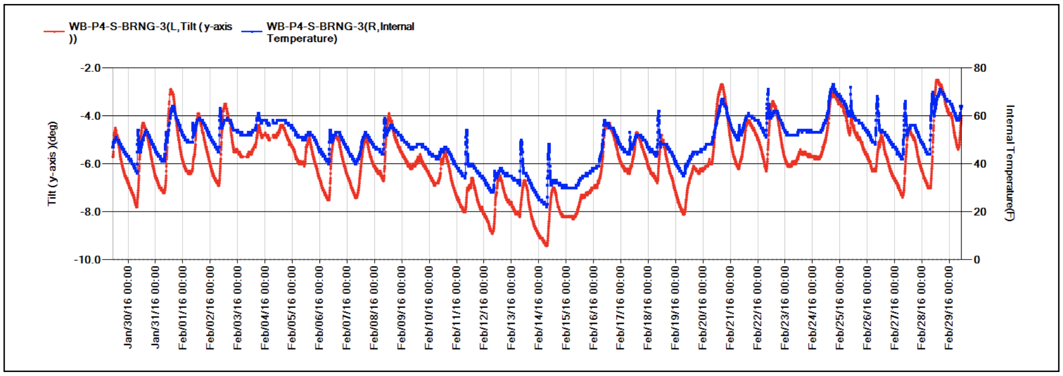

Figure 8-4 Example of rocker bearing tilt behavior with temperature changes

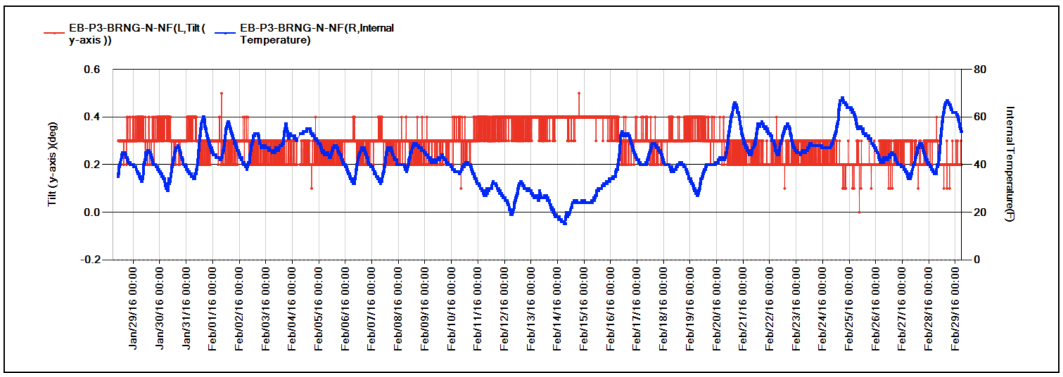

Figure 8-5 Example of freeze rocker bearing tilt behavior with temperature changes

The behavior of the bearing at Pier 3 was not completely frozen since it still showed the features with periodic movement from the five-year data analysis (Figure 8-6). However, compared with the bearing tilt in Pier 4 (Figure 8-7), the movement was still relatively low, and the bearing was still considered frozen.

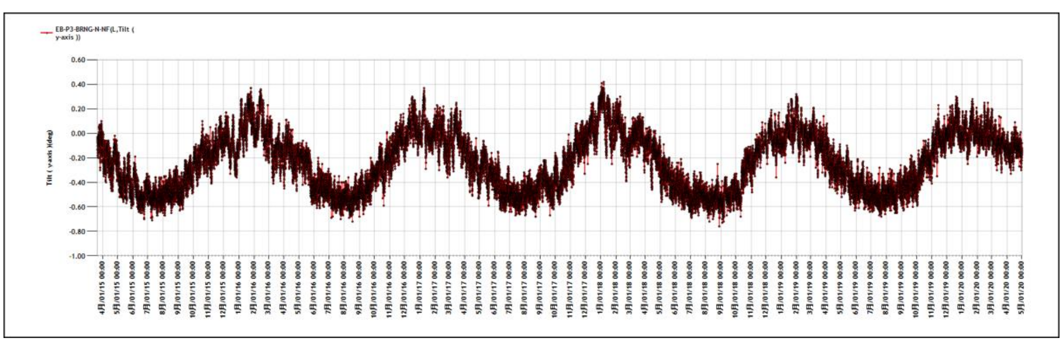
Figure 8-6 A five-year frozen bearing tilt with temperature changes

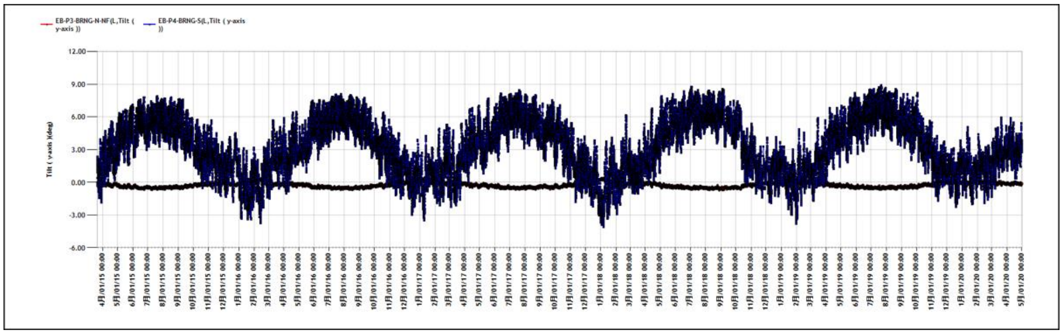

Figure 8-7 A five-year bearing tilt changes comparison

Then use a set of data from the long-term frozen bearing to train the model. The first trial is to choose the initial learning rate of 0.0002, learning rate drop period of 30, and learning rate drop factor of 0.3, with 700 hidden units in the networks. The data point is selecting the daily average value of the tile over five years. Then set the validation in every five epochs. The forecasting model with and without testing shows in Figure 8-8, Figure 8-9, and Figure 8-10. Moreover, the final updated trained model shows in Figure 8-11.

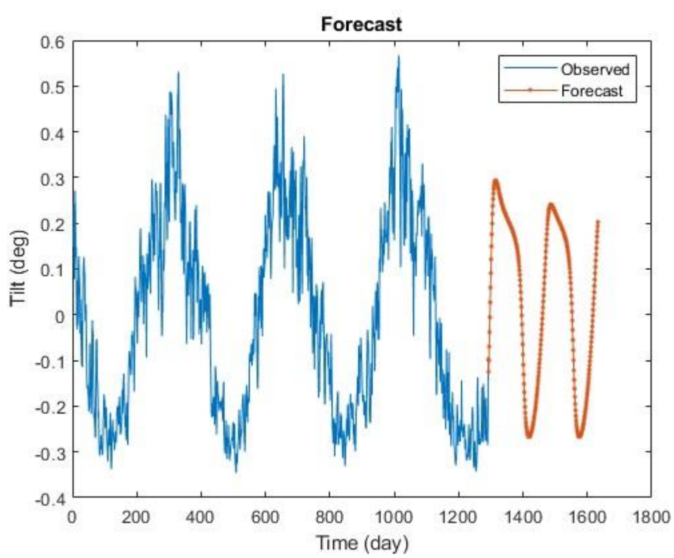

Figure 8-8 Results of data forecasting

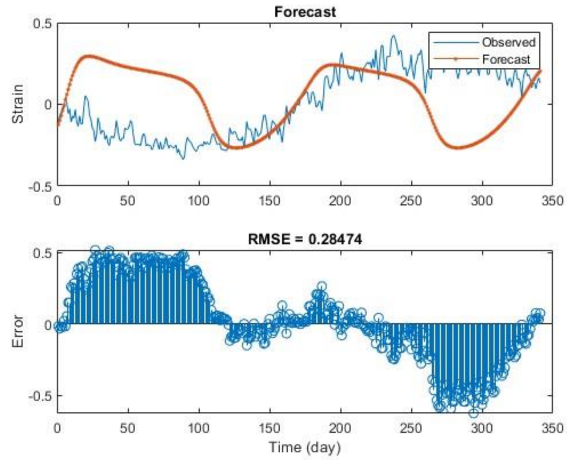

Figure 8-9 Comparison of observed data and the forecasting model

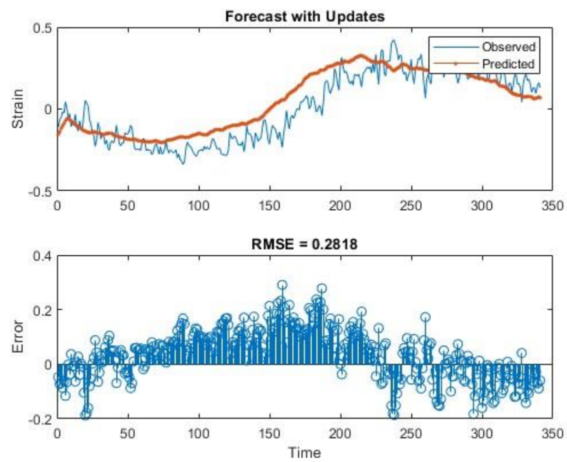

Figure 8-10 Initial models updated with observed data

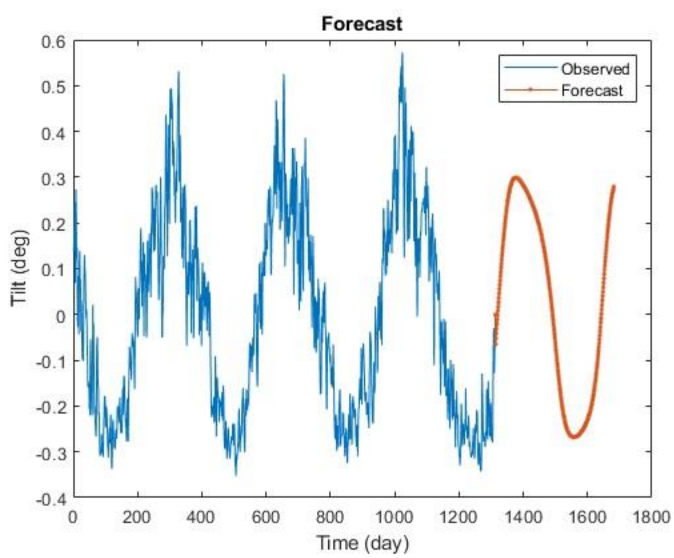

Figure 8-11 The final training model by adjusting data splitting and training options

However, this time series prediction is not always performed well since the current network only predicts one step further using the current value. Thus, another LSTM model was trained using data from the same sensor, selecting the displacement and internal temperature data from Oct 29th, 2014, to Sept 30th, 2016. Then splitting the data into a paralleling 600 datasets. In each dataset, a set of 60 $(datapoints) \times 2$ (input features) cell is defined (Figure 8-12), where the input values are the average of 0.5-hour tilt angle readings and the corresponding internal temperature. Then prepare 90% of the datasets as a training set, and 10% are the testing set. Using a sequence input layer with an input size of 2. The LSTM layer was defined with 180 hidden units and a fully connected layer with an output size of 2. The maximum epoch was defined to be 600 and shuffling the data every epoch.

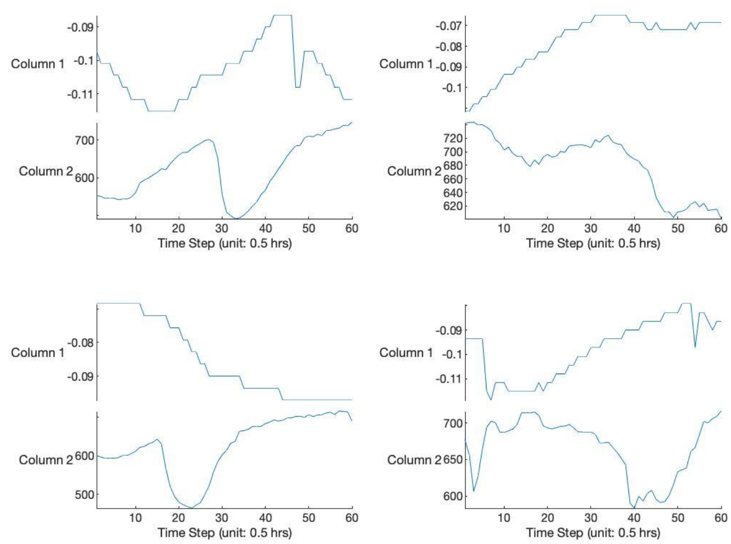

Figure 8-12 Example input data plots

After the network was trained, the root means squared error (RMSE) was calculated to evaluate the accuracy between the prediction value and the observed value. The visualized histogram is shown in Figure 8-13 with an average value of 0.05.

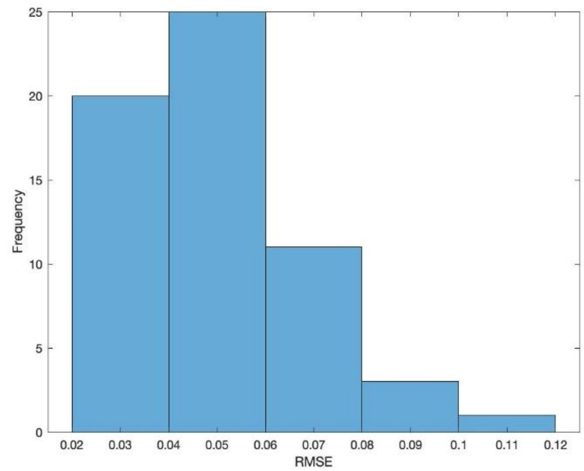

Figure 8-13 Histogram of RMSE

To forecast the displacement and temperature in this example, open-loop forecasting and closed-loop forecasting method are both selected to demonstrate their performance. Examples of performance forecasting are plotted in Figure 8-14 and Figure 8-15.

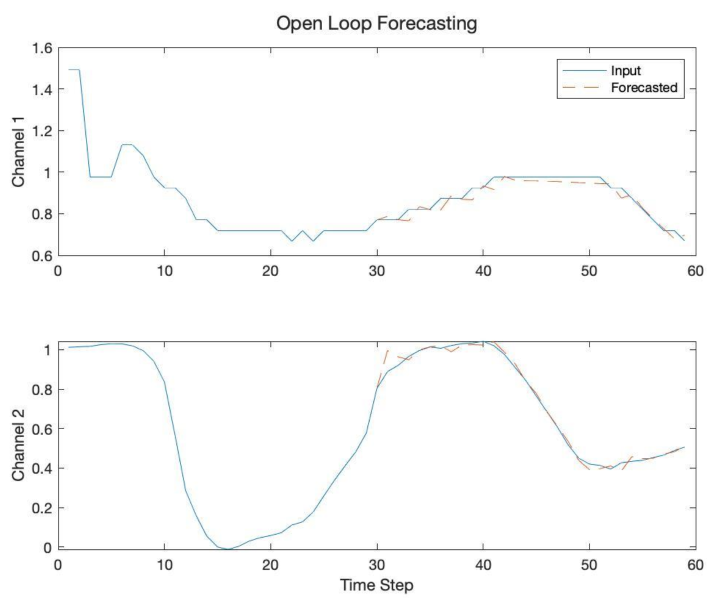

Figure 8-14 Open loop forecasting

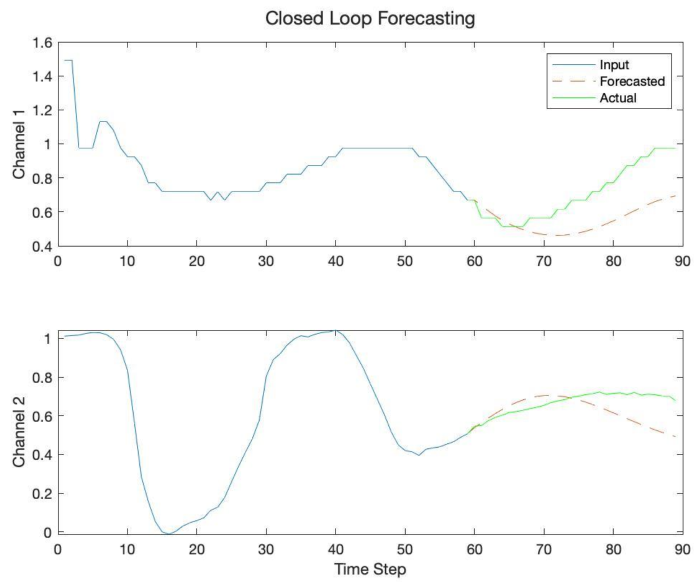

Figure 8-15 Closed loop forecasting

Chapter 9: Summary, Conclusions, and Recommendations

9.1 Summary

This research focused on the bridge structural performance assessment after the bridge preventive maintenance work of typical I girder steel bridges and the general assessment of steel bridges after rehabilitation. A rapid structural performance assessment method has been proposed in two scenarios,

(1) The rapid assessment to classify if the design is under an acceptable range using machine learning methods;

(2) Comparing structural health monitoring data with predictions to evaluate the structure's current condition.

This research generates three types of databases, which are

(1) The Initial Database, which covers bridge configuration and current condition rating;

(2) The Simulated Database, which randomly selects data from the initial database as input, adding its structural performance using finite element analysis and performance evaluation using the fuzzy logic system;

(3) The Rapid Assessment Database developed from both input and output from the previous two databases and filtered salient features and reaction values from FE models.

Moreover, a series of unique materials (high-performance fiber reinforced concrete, HPFRC) for preventive maintenance and structure rehabilitation has been designed, mixed, tested, and evaluated. Furthermore, by introducing structural health monitoring techniques, sensors were instrumented during testing, and the material and structural performance of the test was captured and analyzed.

Besides, two parametric studies for bridge preservation and maintenance are introduced and studied, the optimal design of the link slab system and the detailed performance investigation of deteriorated bridges after repair.

This study also introduced two case studies for structural performance assessment and time-series data forecasting.

1. The first case is preventive maintenance work with newly constructed link slabs on a multi-span simply supported overpass bridge.
2. The second bridge underwent several inspections, maintenance, and rehabilitation work while equipped with strain gauges and tilt meters for long-term monitoring.

9.2 Overview of the findings and conclusion

This study focuses on rapid structural performance assessment and real-time structural health monitoring data prediction. These two assessments rely on data analysis, structural analysis, and the application of fuzzy logic, machine learning, and deep learning techniques.

1. The simulated bridge database was generated using Latin Hypercube Sampling from the distribution of bridge attributes developed from the original database. This is more effective than the Monte Carlo simulation while representing enough features from the initial database with a smaller sample size.
2. This research conducted lab tests on multiple products to study the material behavior of high-performance fiber-reinforced concrete (HPFRC). It found that all

fiber-reinforced concrete specimens under compression or bending show better performance than regular concrete. In particular, ductile ECC has a low modulus of elasticity and high flexibility, while UHPC delivers a better performance under compression and a higher modulus of elasticity. To avoid segregation during the self-mixing ECC, a particular procedure for mixing is required based on different mixing equipment. Moreover, this chapter introduced a new type of "embedded sensor" that buries the strain gauges into the concrete by attaching the sensor to a metal plate and fixing the plate's position. The effectiveness of this type of sensor is then validated by lab and field tests.

3. As for the optimal design of the link slab system, the structural performance strongly relates to the new material. When using regular concrete for the link slab, the expected cracks occur due to tensile strength and bending moment transferred in the system. When using high-performance concrete, it should be noticed that the accumulated stress in the link slab and adjacent bridge decks will increase if the modulus of elasticity of the new material is too high. This parametric study uses a fixed deck width so that the change of span length could be sampled from 20 ft (minimum span length of bridge) to 120 ft. (approximate most significant span/deck ratio for a simply supported span bridge). Also, the configuration of the link slab, including the width, depth, and length of the deboned zone, is critical in the design, where it could be tested using a machine learning model with a decision tree or random forest. Moreover, skew angles are another factor that might cause stress concentration around the link slab system. And the adjacent location between the link slab and the original bridge deck shows a highly stress concentration if not

added to the deboned zone. Furthermore, changing the boundary condition for this multi simply supported span bridge to all expansion bearing with one center bearing fixed is essential to the design. The first case study demonstrates a bearing modification design that cross-checks with this argument and shows the importance of the change of boundary condition.

4. To study the performance of rehabilitated bridges, it could be found that material aging is an essential feature in the repair work. Meanwhile, it shows a low relationship with the geometry of the structure. When bridge bearing is frozen, or the expansion joint is filled, the thermal load will accumulate in the structure, creating a more than 600% reaction increase compared with the original model. Thus, the bearing condition is suggested to be more carefully investigated during periodic inspections.
5. The machine learning classification techniques provide a new way of decision-making and data classifying. The proposed rapid assessment model could help asset managers predict the repair structure's performance and provide recommendations considering the maintenance budget or cost. In particular, when doing the model training, RUSBoosted trees or random forests perform better than all other classification methods. The trained models are recommended for the rapid assessment of link slab design and repaired bridges' performance evaluation.
6. The LSTM network works well for data prediction if well trained. In particular, for short-term data like the experimental cyclic loading case, the network could predict its performance without further data processing. For the long-term case associated with temperature change or structure deterioration, data were split into seven days

to 1 month. The prediction for the short-term (1/2 of the splitting time) is still working, while the long-term (yearly) prediction needs re-filtering and training for another network. Besides, instrumentation with the SHM system is only available to essential bridges.

The primary contributions of this research are:

A rapid assessment model for bridges after preventive maintenance or rehabilitation was proposed. Combining the machine learning techniques, the model can be used without detailed computation or analysis. Furthermore, a time series forecasting model training from monitoring data is introduced and could help simulate structural performance in the near future. Using these two models would help analyze the structure behavior without computation or FE modeling, make predictions, and help in decision-making.

This research focuses on the structural performance of steel bridges after preventive maintenance or repair, especially the potential negative impact on the installation of link slab systems and the effectiveness of the repair plans.

A group of parametric studies of the link slab design was conducted in this research, which provides a general guideline to the link slab design, including its configuration and material. Another group of parametric studies of the bridge before and after repair shows the difference in the behavior of the structure under different ages, defect types, and locations.

9.3 Suggestions for Future Research

Some recommendations for future studies related to this work are described in this section.

- Database updating and expansion

Three databases generated in this research are recommended to be expanded with corresponding data. For example, the more detailed and accurate configuration of the structure, existing repairing plan and construction year, the rating for each element from the previous inspection report, load ratings, condition changes for the last two to five inspections, locations, and AADT is highly recommended to be included in the database and can be much more helpful to implement the current database. Moreover, the scenario to generate the database, validate its effectiveness, and then use it for decision-making and model training could be expanded in all maintaining, repairing, or renovating structures, including all types of bridges and buildings.

- Fuzzy logic system validation

When possible, the new features "structure repair recommendation by expert" is highly recommended to be included in the first database so it can be combined with all other databases and uses neuro-fuzzy logic to help improve and cross-validate the accuracy during the decision-making process.

- Model training and validation

In this study, two types of models are trained using either the rapid assessment database or the actual SHM data. The rapid assessment model could be continuously expanded with a more comprehensive database. Thus, the model can be more accurate in bridge condition assessment and show both the expected inspection result and repair recommendations. Besides, the forecasting model using the SHM data could be trained in a more general case that applies all the displacement or tilt data from a different location on the same bridge to the training set. Therefore, the training database could be expanded, and a model for the whole bridge might be trained instead of one model for each location.

- Structural performance evaluation

  More parameters could be implemented in the structural performance evaluation after repair. This study primarily investigates the length/ width ratio, defect type, defect location, and material aging effect. However, other parameters, such as location (correlated with temperature changes, snow, earthquake, corrosion, etc.), structure type, skew angles, initial imperfections (cracks and stress concentration locally), etc., are recommended to be investigated coupled with the performance model in this study.

Appendices

Table A-1 Steel bridges distribution by the states in the US

State Name	Number of Steel Bridges
Ohio	11269
Missouri	10803
New York	10340
Oklahoma	7802
North Carolina	7716
Kansas	7525
Iowa	7438
Nebraska	7237
Pennsylvania	7020
Illinois	7020
Texas	7014
Virginia	6706
Indiana	5101
Arkansas	4948
Michigan	4416
Georgia	3618
New Jersey	3612
West Virginia	3378
Maryland	3242
Wisconsin	3157
Massachusetts	3011
Colorado	2928
Alabama	2863
California	2805
Kentucky	2496
Tennessee	2406
Connecticut	2262
Minnesota	2077
Vermont	1720
Louisiana	1660
Mississippi	1458
South Dakota	1453
Wyoming	1451
Florida	1418
Maine	1410
New Hampshire	1388
Montana	1291

State Name	Number of Steel Bridges
South Carolina	1258
Oregon	1196
Washington	1141
North Dakota	1093
Idaho	896
Utah	864
Arizona	852
Alaska	829
New Mexico	578
Rhode Island	404
Delaware	372
Puerto Rico	351
Nevada	265
District of Columbia	164
Hawaii	113
Virgin Islands	2
Guam	2
Grand Total	**173839**

Bibliography

23 CFR 490.409 - Calculation of National Performance Management Measures for Assessing Bridge Condition

23 CFR Part 650 - National Bridge Inspections Standards Regulation (NBIS)

Agrawal, Anil K., Akira Kawaguchi, and Zheng Chen. "Deterioration rates of typical bridge elements in New York." Journal of Bridge Engineering 15, no. 4 (2010): 419-429.

Alampalli, S.; Yannotti, A.P. In-service performance of integral bridges and jointless decks. Transp. Res. Rec. J. Transp. Res. Board 1998, 1624, 1–7.

American Association of State Highway and Transportation Officials. AASHTO LRFD Bridge Design Specifications, eighth edition, Customary U.S. Units. Washington, DC: American Association of State Highway and Transportation Officials; 2017.

Au, A., Lam, C., Au, J., & Tharmabala, B. (2013). Eliminating Deck Joints Using Debonded Link Slabs: Research and Field Tests in Ontario. Journal of Bridge Engineer-ing,18(8), 768-778. doi:10.1061/(asce) be.1943-5592.0000417

Breiman L, Friedman JH, Olshen RA, Stone CJ. Classification and regression trees. Boca Raton, FL: Chapman & Hall/CRC; 1984.

Bridge Preservation Guide - Maintaining a Resilient Infrastructure to Preserve Mobility, U.S. Department of Transportation, Federal Highway Administration, Spring 2018, https://www.fhwa.dot.gov/bridge/preservation/guide/guide.pdf, (last access at Dec 1st, 2021)

Caner A, Zia P. Behavior and design of link slabs for jointless bridge decks. PCI journal. 1998 May 1;43(3):68-80.

Catbas Necati, Kijewski-Correa Tracy, Aktan Emin, 2013, Structural Identification of Constructed Systems. Approaches, methods and technologies for effective practice of ST-ID. American Society of Civil Engineering.

Cesare, Mark A., Carlos Santamarina, Carl Turkstra, and Erik H. Vanmarcke. "Modeling bridge deterioration with Markov chains." Journal of Transportation Engineering 118, no. 6 (1992): 820-833.

Chang, Minwoo, Marc Maguire, and Yan Sun. "Stochastic modeling of bridge deterioration using classification tree and logistic regression." Journal of Infrastructure Systems 25, no. 1 (2019): 04018041.

Chen, D., Zou, J., Zhao, L., Xu, S., Xiang, T., & Liu, C. (2020). Degradation of Dynamic Elastic Modulus of Concrete under Periodic Temperature-Humidity Action. Materials (Basel, Switzerland), 13(3), 611. https://doi.org/10.3390/ma13030611

Cover TM, Hart PE. Nearest neighbor pattern classification. IEEE Trans Inf Theory 1967;13(1):21–7.

Cristian-Claudiu Comisu, Nicolae Taranu, Gheorghita Boaca, Maria-Cristina Scutaru, Structural health monitoring system of bridges, Procedia Engineering, Volume 199, 2017, Pages 2054-2059, ISSN 1877-7058, https://doi.org/10.1016/j.proeng.2017.09.472.

CSiBridge, Computer and Structures, Inc. Berkeley (2017).

D. P. Kingma and J. Ba. Adam: A method for stochastic optimization. CoRR, abs/1412.6980, 2014.
Dai, Jian-Guo, Ke-Quan Yu, Zhou-Dao Lu, and Surendra P Shah. “Direct Tensile Properties and Stress–Strain Model of Uhp-Ecc.” Journal of Materials in Civil Engineering 32, no. 1 (2020). https://doi.org/10.1061/(ASCE)MT.1943-5533.0002975.
Dan M. Frangopol et al. Primer on Bridge Load Testing, Transportation Research Circular, November 2019.
Daniel S. Wilks, Chapter 15 - Discrimination and Classification, Editor(s): Daniel S. Wilks, Statistical Methods in the Atmospheric Sciences (Fourth Edition), Elsevier, 2019, Pages 695-719, ISBN 9780128158234
Dolen, Timothy P., Material Properties Model of Aging Concrete, Report DSO-05-05, Dam Safety Technology Development Program. Bureau of Reclamation, 2005
Dompere, K. K. Fuzziness and Approximate Reasoning : Epistemics on Uncertainty, Expectation and Risk in Rational Behavior. Studies in Fuzziness and Soft Computing, V. 237. INSERT-MISSING-SERVICE-NAME. Berlin: Springer, 2009. https://doi.org/10.1007/978-3-540-88087-5.
Dorffner, Georg. "Neural networks for time series processing." In Neural network world. 1996.
Dubois, Didier, and Henri M. Prade. Fuzzy Sets and Systems: Theory and Applications. Mathematics in Science and Engineering, v. 144. New York: Academic Press, 1980.
El-Safty, A. K. Analysis of Jointless Bridge Decks with Partially Debonded Simple Span Beams. PhD dissertation. North Carolina State University, Raleigh, 1994.
FHWA Report number PD-96-001 “Recording and Coding Guide for Structure Inventory and Appraisal of the Nation’s Bridges, December 1995.
Figueiredo, Eloi & Moldovan, Ionut & Marques, Manuel. (2013). Condition Assessment of Bridges: Past, Present and Future. A Complementary Approach.
Fiorillo G, Nassif H. Application of Machine Learning Techniques for the Analysis of National Bridge Inventory and Bridge Element Data. Transportation Research Record. 2019;2673(7):99-110. doi:10.1177/0361198119853568
Friedman, Jerome H. The elements of statistical learning: Data mining, inference, and prediction. springer open, 2017.
Fu, Chung C., A Pilot Application of Link Slab with Selected Material for MDTA Steel Bridges, Final report, Maryland Transportation Authority, April 2020
Fu, Chung C., Yifan Zhu and Kuangyuan Hou, Utilization of Dynamic and Static Sensors for Monitoring Infrastructures, Advanced Remote Sensing Technology for Coastal Environment, Disasters, and Infrastructure, IntechOpen, Jan. 2019
Gilani, A. , and Jansson, D. Link-Slabs for Simply Supported Bridges: Incorporating Engineered Cementitious Composites. Draft Report No. MDOT SPR-54181. Michigan Department of Transportation, Lansing, 2004.
Fu, Gongkang & Dinesh Devaraj; Final report to Michigan Department of Transportation, Methodology of homogeneous and non-homogeneous Markov Chains for modeling bridge element deterioration. (2008-08-01); https://rosap.ntl.bts.gov/view/dot/18196

Graybeal, Ben, Design and Construction of Field-Cast UHPC Connections, FHWA Publication No: FHWA-HRT-14-084, Oct 2014
Guo J, Wu J, Guo J, Jiang Z. A damage identification approach for offshore jacket platforms using partial modal results and artificial neural networks. Appl Sci 2018;8:2173.
Haykin (2008) Neural Networks and Learning Machines, 3rd edition
Hochreiter, S. and J. Schmidhuber. Long short-term memory. Neural computation, 9(8):1735–1780, 1997.
Hou, K.Y, Zhu, Y., Fu, C. C., Li, N., Validation of Fiber Reinforced Concrete Performance in Laboratory and Field for Bridge Rehabilitation, International Bridge Conference.
Hou, M.; Hu, K.; Yu, J.; Dong, S.; Xu, S. Experimental study on ultra-high ductility cementitious composites applied to link slabs for jointless bridge decks. Compos. Struct. 2018, 204, 167–177
Housner, G. W, L. A Bergman, T. K Caughey, A. G Chassiakos, R. O Claus, S. F Masri, R. E Skelton, T. T Soong, B. F Spencer, and J. T. P Yao. "Structural Control: Past, Present, and Future." Journal of Engineering Mechanics 123, no. 9 (1997): 897–971. https://doi.org/10.1061/(ASCE)0733-9399(1997)123:9(897).
Husain, I., and Bagnarol, D. Design and Performance of Jointless Bridges in Ontario: New Technical and Material Concepts. In Transportation Research Record: Journal of the Transportation Research Board, No. 1696, TRB, National Research Council, Washington, D.C., 2000, pp. 109–121.
INFORMATION: Guidance on Highway Preservation and Maintenance. MEMORANDUM, U.S. Department of Transportation, Federal Highway Administration, February 25, 2016; https://www.fhwa.dot.gov/preservation/memos/160225.cfm, (last access at Dec 1st, 2021)
Jiang, Y., and K. C. Sinha. Bridge Service Life Prediction Model using the Markov Chain. Transportation Research Record: Journal of the Transportation Research Board, 1989. 1223: 24–30.
Jin-Keun Kim, Sang Hun Han, Young Chul Song, Effect of temperature and aging on the mechanical properties of concrete: Part I. Experimental results, Cement and Concrete Research, Volume 32, Issue 7, 2002, Pages 1087-1094, ISSN 0008-8846
Karbhari M. Vistasp, Lee L. S-W, 2009, Vibration-based damage detection techniques for structural health monitoring of civil infrastructure system, in Structural health monitoring of civil infrastructure systems. Woodhead Publishing Limited, Cambridge, UK, ISBN 978-1-84569-392-3.
Kaufmann, A., and Madan M. Gupta. Introduction to Fuzzy Arithmetic: Theory and Applications. Van Nostrand Reinhold Electrical/Computer Science and Engineering Series. New York, N.Y: Van Nostrand Reinhold Co, 1985.
Larus Larusson, Joel C. Reyes, Bryan Lum, Gregor Fischer and Ian N. Robertson, Research Report UHM/CEE/13-04 (July 2013) Development of Flexible Link Slabs using Ductile Fiber Reinforced Concrete
Li, Biao, Lihua Xu, Yin Chi, Biao Huang, and Changning Li. "Experimental Investigation on the Stress-Strain Behavior of Steel Fiber Reinforced Concrete

Subjected to Uniaxial Cyclic Compression.” Construction & Building Materials 140 (2017): 109–18.
Li, V. C., M. D. Lepech, and M. Li, "Field Demonstration of Durable Link Slabs for Jointless Bridge Decks Based on Strain-Hardening Cementitious Composites," University of Michigan, Ann Arbor MI, 2005.
Li, V.C., 2007. Engineered cementitious composites (ECC) material, structural, and durability performance. Book Chapter in Concrete Construction Engineering Handbook, Ed. E. Nawy, to be published by CRC Press, 2007. Available from https://deepblue.lib.umich.edu/bitstream/handle/2027.42/84661/ECC_Book_Chapter.pdf?sequence=1
Lin, Zhibin, Hong Pan, Xingyu Wang, and Mingli Li. Improved Element-Level Bridge Inspection Criteria for Better Bridge Management and Preservation, MPC-19-403. North Dakota State University - Upper Great Plains Transportation Institute, Fargo: Mountain-Plains Consortium, 2019.
Liu, Heng & Zhang, Yunfeng. (2020). Bridge condition rating data modeling using deep learning algorithm. Structure and Infrastructure Engineering. 16. 1-14. 10.1080/15732479.2020.1712610.
Malekjafarian A, Golpayegani F, Moloney C, Clarke S. A Machine Learning Approach to Bridge-Damage Detection Using Responses Measured on a Passing Vehicle. Sensors (Basel). 2019;19(18):4035. Published 2019 Sep 19. doi:10.3390/s19184035
Mander, J. B, R Park, and M. J. N Priestley. “Theoretical Stress-Strain Model for Confined Concrete.” Journal of Structural Engineering 114, no. 8 (1988): 1804–26. https://doi.org/10.1061/(ASCE)0733-9445(1988)114:8(1804).
Mangalathu S, Jeon J-S. Classification of failure mode and prediction of shear strength for reinforced concrete beam-column joints using machine learning techniques. Eng Struct 2018;160:85–94.
Mangalathu S, Jeon J-S. Machine learning-based failure mode recognition of circular reinforced concrete bridge columns: a comparative study. J Struct Eng 2019;145(10):04019104.
McKenna FT. Object oriented finite element programming frameworks for analysis, algorithms and parallel computing. Ph.D thesis. University of California at Berkeley; 1997.
Morcous, G. “Performance Prediction of Bridge Deck Systems Using Markov Chains.” Journal of Performance of Constructed Facilities 20, no. 2 (2006): 146–55. https://doi.org/10.1061/(ASCE)0887-3828(2006)20:2(146).
N. Srivastava, G. E. Hinton, A. Krizhevsky, I. Sutskever, and R. Salakhutdinov. Dropout: a simple way to prevent neural networks from overfitting. Journal of Machine Learning Research, 15(1):1929–1958, 2014.
National Cooperative Highway Research Program, and AS. Nowak. 1999. Calibration of LRFD bridge design code. Washington, DC: TRB
Okeil, A. M. and A. El-Safty, "Partial continuity in Bridge Girders with Jointless Decks," Practice Periodical on Structural Design and Construction, vol. 10, no. 4, pp. 229-238, 2005.
Quinlan, J. R. (1986). "Induction of decision trees"(PDF). Machine Learning. 1: 81–106. doi:10.1007/BF00116251. S2CID 189902138.

Rafael A. Irizarry and Hector Corrada Bravo, Linear methods for classification, Feb 2010, Retrieved Apr., 2022 from https://www.biostat.jhsph.edu/~hcorrada/PracticalML/pdf/lectures/classification.pdf
Richardson, D. R. Simplified Design Procedures for the Removal of Expansion Joints from Bridges Using Partial Debonded Continuous Decks. MS thesis. North Carolina State University, Raleigh,1989.
Rosenblatt, F. (1958). "The Perceptron: A Probabilistic Model For Information Storage And Organization in the Brain". Psychological Review. 65 (6): 386–408. CiteSeerX 10.1.1.588.3775. doi:10.1037/h0042519. PMID 13602029.
Rosenblatt, Frank (1957). "The Perceptron—a perceiving and recognizing automaton". Report 85-460-1. Cornell Aeronautical Laboratory.
Sarker, Ruhul A, and Charles S Newton. Optimization Modelling : A Practical Approach. Boca Raton: CRC Press, 2008.
Sasmal, Saptarshi & K., Ramanjaneyulu & Iyer, Nagesh. (2012). Condition Ranking and Rating of Bridges Using Fuzzy Logic. 10.5772/37052.
Sasmal, Saptarshi, K Ramanjaneyulu, and S Gopalakrishnan. “Fuzzy Logic Based Condition Rating of Existing Reinforced Concrete Bridges.” Journal of Performance of Constructed Facilities 20, no. 3 (2006): 261–73. https://doi.org/10.1061/(ASCE)0887-3828(2006)20:3(261).
Sivanandam, S. N, S Sumathi, and S. N Deepa. Introduction to Fuzzy Logic Using Matlab. INSERT-MISSING-SERVICE-NAME. Berlin: Springer, 2007. https://doi.org/10.1007/978-3-540-35781-0.
Sousa, H., Félix, C., Bento, J., Figueiras, J. (2011) Design and implementation of a monitoring system applied to a long-span prestressed concrete bridge; Structural Concrete. 12(2):82-93.
Sousa, H., Cavadas, F., Henriques, A., Bento, J., Figueiras, J. (2013) Bridge deflection evaluation using strain and rotation measurements; Smart Structures & Systems 11(4): 365-386.
SPECIFICATION FOR THE NATIONAL BRIDGE INVENTORY BRIDGE ELEMENTS, Jan, 2014, https://www.fhwa.dot.gov/bridge/nbi/131216_a1.pdf
Stein M. Large sample properties of simulations using Latin hypercube sampling. Technometrics 1987;29(2):143–51.
Stuart J. Russell, Peter Norvig (2010) Artificial Intelligence: A Modern Approach, Third Edition, Prentice Hall ISBN 9780136042594.
Swartz R.A., Lynch J.P., 2009, Wireless sensors and networks for structural health monitoring of civil infrastructure systems, in Structural health monitoring of civil infrastructure systems. Woodhead Publishing Limited, Cambridge, UK, ISBN 978-1-84569-392-3.
T. Mikolov. Recurrent neural network based language model. In Interspeech, volume 2, page 3, 2010.
Tan, A. C., M. Kaphle and D. Thambiratnam, "Structural health monitoring of bridges using acoustic emission technology," 2009 8th International Conference on Reliability, Maintainability and Safety, 2009, pp. 839-843, doi: 10.1109/ICRMS.2009.5269952.

Tee, A. B., Bowman, M. D. & Sinha, K. C. (1988) A fuzzy mathematical approach for bridge condition evaluation, Civil Engineering Systems, 5:1, 17-24, DOI: 10.1080/02630258808970498
Tee, Ah Beng. "The Application of Fuzzy Mathematics to Bridge Condition Assessment." Order No. 8912002, Purdue University, 1988. https://www.proquest.com/dissertations-theses/application-fuzzy-mathematics-bridge-condition/docview/303586088/se-2?accountid=14696.
The Math Works, Inc., MATLAB, version 2022a (Natick, MA: The Math Works, Inc., 2022), accessed April 28, 2022, https://www.mathworks.com/.
Title 23 United States Code (current as of October 19, 2012, including public laws through P.L. 112-196), https://www.fhwa.dot.gov/map21/docs/title23usc.pdf
UHPC Link slab design, NYSDOT, Available from https://www.dot.ny.gov/divisions/engineering/structures/repository/events-news/NYSDOT_2017_UHPC_Workshop_Scarlata.pdf
Ulku, Evren, Upul Attanayake, and Haluk Aktan. "Jointless Bridge Deck with Link Slabs : Design for Durability." Transportation Research Record 2131, no. 1 (2009): 68–78. https://doi.org/10.3141/2131-07.
Vagnoli, M., R. Remenyte-Prescott, J. Andrews, "A machine learning classifier for condition monitoring and damage detection of bridge infrastructure", Civil Engineering Research in Ireland conference (CERI2018), Dublin, 29-30 August 2018.
Wang, Ling, Jian Chu, and Weijie Mao. "An optimum condition-based replacement and spare provisioning policy based on Markov chains." Journal of Quality in Maintenance Engineering (2008).
Wei Z.-L, Yu R, Cheng C.-Y, and 4th International Conference on Frontiers of Manufacturing Science and Measuring Technology, ICFMM 2014 Guilin, CHN 2014 06 19 - 2014 06 20. "Theoretical Study on Bridge Structure Condition Evaluation Based on Health Monitoring Data." Applied Mechanics and Materials 599-601 (2014): 751–54. https://doi.org/10.4028/www.scientific.net/AMM.599-601.751.
Werbos, P.J. (1975). Beyond Regression: New Tools for Prediction and Analysis in the Behavioral Sciences.
Wing, K. M. , and Kowalsky, M. J. Behavior, Analysis, and Design of an Instrumented Link Slab Bridge. Journal of Bridge Engineering, Vol. 10, No. 3, 2005, pp. 331–344.
Yang, Jidong, Manjriker Gunaratne, Jian John Lu, and Bruce Dietrich. "Use of recurrent Markov chains for modeling the crack performance of flexible pavements." Journal of Transportation Engineering 131, no. 11 (2005): 861-872.
Yin T, Zhu HP. Probabilistic Damage Detection of a Steel Truss Bridge Model by Optimally Designed Bayesian Neural Network. Sensors (Basel). 2018;18(10):3371. Published 2018 Oct 9. doi:10.3390/s18103371.
Zaremba, Wojciech, Ilya Sutskever, and Oriol Vinyals. "Recurrent neural network regularization." arXiv preprint arXiv:1409.2329 (2014).
Zhong, Junfei, Jiyang Shen, Wei Wang, Jun Shi, Xiaocong Yang, and Guangchun Zhou. 2019. "Working State of ECC Link Slabs Used in Continuous Bridge Decks" Applied Sciences 9, no. 21: 4667. https://doi.org/10.3390/app9214667
Zhu, Yifan, Kuangyuan Hou, Chung C. Fu, Naiyi Li, and Ruel E. Sabellano. "Finite Element Analysis and Long-Term Monitoring of a Highway Overpass Bridge with

Newly Constructed Link Slabs and Modified Bearings." Transportation Research Record, (December 2021).
Zia P, Caner A, El-Safte AK (1995) Jointless bridge decks. Research project 23241-94-4. Center for Transportation Engineering Studies, North Carolina State, pp 1–117